GEORGIA INSTITUTE OF TECHNOLOGY — OFFICE OF CONTRACT ADMINISTRATION

PROJECT ADMINISTRATION DATA SHEET

[X] ORIGINAL [ ] REVISION NO. ____

Project No. E-20-692 (R6034-0A0) GTRC DATE 9 / 23 / 85

Project Director: Philip Roberts School/ Civil Engineering

Sponsor: U. S. Environmental Protection Agency

Type Agreement: Cooperative Agreement No. CR-812801-01-0

Award Period: From 9/16/85 To ~~5/16/86~~ 10/31/86 (Performance) 5/16/86 (Reports)

Sponsor Amount:	This Change	Total to Date
Estimated:	$ 47,144	$ 47,144
Funded:	$ 47,144	$ 47,144
Cost Sharing Amount:	$ 9,167	Cost Sharing No: E-20-324 (F6034-0A0)

Title: Experiments on Merging Buoyant Jets in a Density-Stratified Current

ADMINISTRATIVE DATA OCA Contact Brian J. Lindberg X4820

1) Sponsor Technical Contact:

Donald J. Baumgartner
Environmental Research Lab/EPA
South Ferry Road
Marrangansett, Rhode Island 02882

2) Sponsor Admin/Contractual Matters:

Sheila Brown (202) 382-5290
Grants Specialist
Grants Administration Division
Environmental Protection Agency
401 M Street, SW (PM-216)
Washington, Dc 20460

Defense Priority Rating: N/A Military Security Classification: N/A

(or) Company/Industrial Proprietary: N/A

RESTRICTIONS

See Attached EPA Supplemental Information Sheet for Additional Requirements.

Travel: Foreign travel must have prior approval – Contact OCA in each case. Domestic travel requires sponsor approval where total will exceed greater of $500 or 125% of approved proposal budget category.

Equipment: Title vests with GIT. Property managment standards included in 40 CFR, part 30 as part of this agreement. Final property report per 40 CFR 40.160-4.

COMMENTS:

EPA budget is 84% of total estimated project costs.

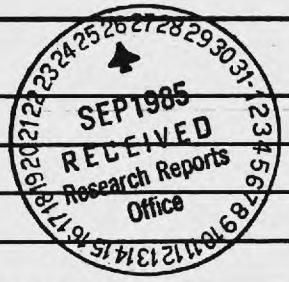

COPIES TO: SPONSOR'S I. D. NO. 02.129.000.85.007

Project Director
Research Administrative Network
Research Property Management
Accounting
Procurement/GTRI Supply Services
Research Security Services
Reports Coordinator (OCA)
Research Communications (2)
GTRC
Library
Project File
Other A. Jones

FORM OCA 85-285

GEORGIA INSTITUTE OF TECHNOLOGY **OFFICE OF CONTRACT ADMINISTRATION**

SPONSORED PROJECT TERMINATION/CLOSEOUT SHEET

Date 9-23-87

Project No. E-20-692 School/~~Lab~~ CE

Includes Subproject No.(s) N/A

Project Director(s) Phillip Roberts GTRC / ~~GIT~~

Sponsor U.S. Environmental Protection Agency

Title Experiments on Merging Buoyant Jets in a Density-Stratified Current

Effective Completion Date: 10-31-86 (Performance) 10-31-86 (Reports)

Grant/Contract Closeout Actions Remaining:

- [ ] None
- [X] Final Invoice or Final Fiscal Report
- [X] Closing Documents
- [ ] Final Report of Inventions -Already submitted
- [X] Govt. Property Inventory & Related Certificate
- [ ] Classified Material Certificate
- [ ] Other _____

Continues Project No. _____ Continued by Project No. _____

COPIES TO:

Project Director
Research Administrative Network
Research Property Management
Accounting
Procurement/GTRI Supply Services
Research Security Services
Reports Coordinator (OCA)
Legal Services

Library
GTRC
Research Communications (2)
Project File
Other _____

FORM OCA 69.285

E-20-692

SR646

Georgia Institute of Technology

A UNIT OF THE UNIVERSITY SYSTEM OF GEORGIA

ATLANTA, GEORGIA 30332

SCHOOL OF
CIVIL ENGINEERING

TELEX: 542507 GTRC OCA ATL

TELEPHONE
(404) 894-

August 28, 1987

Dr. D.J. Baumgartner
U.S. EPA
Hatfield Marine Science Center
Newport, OR 97365

Re: Cooperative Agreement No. CR-812801-01-0
Georgia Tech Project No. E20-692

Dear Don:

Enclose are copies of the three final reports on the above referenced agreement. It has been a pleasure working with you on this interesting project, and I look forward to further collaboration in the future.

Yours sincerely,

Philip J.W. Roberts,
Associate Professor

cc: Pat Heitmuller, OCA

THE SPATIAL EVOLUTION OF SUBMERGED WASTEFIELDS

by

Philip J.W. Roberts,[1] M. ASCE, and W.H. Snyder[2]

ABSTRACT

Some fundamental aspects of the formation and mixing of submerged wastefields caused by ocean outfalls are considered. Dilution was found to increase with distance up to an asymptotic value, and the distance required for this to occur in strong perpendicular currents is predicted by interpreting it as the distance at which the buoyancy-induced turbulence collapses. An expression for lateral spreading in parallel currents is derived which is found to be of the same form as for unstratified currents, except that the rate of spreading in stratified currents is much reduced at the same Froude number. An expression for the rate of spreading in perpendicular currents is derived by assuming results from mixed-region collapse can be applied. An applications example shows that the mixing region can extend for several hundred meters downstream from the discharge. Because of the gravitational spreading a line diffuser will produce a wastefield width of the order of the diffuser length for most oceanic conditions, suggesting that Y or similarly complex diffuser orientations are not necessary to produce a widely dispersed wastefield.

---

[1]Assoc. Prof. of Civil Engrg., Georgia Inst. of Tech., Atlanta, GA 30332
[2]Meteorology and Assessment Division, U.S. Environmental Protection Agency, Research Triangle Park, North Carolina 27711. On assignment from the National Oceanic and Atmospheric Administration, U.S. Dept. of Commerce.

INTRODUCTION

The mixing of buoyant effluent discharged from a submerged multiport diffuser into a flowing, stratified ocean is a complex phenomenon dependent on many parameters. In the previous paper (Roberts, et al., 1987, hereafter referred to as paper I) we presented some of the results from an extensive series of towing tank experiments whose purpose was to investigate the three-dimensional flow fields generated by the discharge of buoyant effluent from a multiport diffuser into a steady, linearly stratified current flowing at an arbitrary direction relative to the diffuser. Results for source conditions approximating a "line plume" were given from which the gross properties of the established wastefield could be predicted at the downstream distance where the asymptotic value of the minimum dilution was achieved. Up to this distance entrainment, turbulent mixing, and dilution due primarily to the source buoyancy takes place, and beyond this distance the wastefield width increases due to gravitational spreading. In this paper we look more closely at these fundamental aspects of wastefield formation and mixing, in particular the distance for the minimum dilution to be achieved and the rate of lateral spreading for parallel and perpendicular currents. Although the discussion is primarily for the line plume (series 3 and 4, see figure 2 of paper I) source conditions, the results presented here were not found to be significantly different for those experiments with higher source momentum fluxes or wider port spacings (series 5 through 11), and these results are also included. The results which are influenced by source conditions are discussed in the third paper of the series.

The experimental procedure is summarized in the next section. General observations derived from shadowgraphs, effluent concentration profiles, and overhead photographs are then presented. The turbulent mixing region for strong perpendicular currents is then analyzed and an expression for the mixing distance is obtained by equating it to the distance at which the buoyancy-induced turbulence collapses under the influence of the stable ambient stratification. Lateral spreading of the wastefield in parallel currents is then analyzed by using results from previous studies of spreading of intrusions into linearly stratified stagnant fluids. Next, the spreading rates for perpendicular currents are analyzed by utilizing previous studies of mixed region or wake collapse.

The results are then applied to the wastefield produced by the West Point outfall of Metropolitan Seattle, whose gross properties were predicted in paper I, to show how mixing distances and wastefield widths can be predicted.

EXPERIMENTS

The experiments were conducted in the towing tank using the same procedures and model multiport diffuser described in paper I. In addition, overhead photographs of the wastefield produced in parallel currents were obtained by use of a 35mm camera and wide-angle lens. Also, shadowgraphs of the flowfields in stagnant and perpendicular currents were obtained by photographing the shadow of the flow produced by a strong parallel light source projected through the flow onto a translucent screen taped to the tank wall. Cross-sectional profiles of effluent concentration and dilution were obtained at various distances by towing the sampling rake downstream of the main carriage.

GENERAL OBSERVATIONS

Shadowgraphs of the line plume case (ℓ_m/ℓ_b = 0.078 and s/ℓ_b = 0.31, series 3) for perpendicular currents with $F = u^3/b$ = 0 (stagnant), 0.1, 1, and 10 are shown in Figure 1. These shadowgraphs correspond to the photographs of figure 4, paper I, except that there is no shadowgraph for F = 100. Also shown on the shadowgraphs are downstream distances expressed in dimensionless form as x/ℓ_b.

The shadowgraphs show a sharp interface between the turbulent wastefield and the ambient fluid. They also give a qualitative indication of the state of the turbulence: active, energetic turbulence has much fine-scale structure, or small eddies, whereas turbulence whose energy has decayed has little fine-scale structure, the smallest eddies having rapidly dissipated. The general nature of the flows considered here is that the turbulence near to the source, as evidenced by its fine-scale structure, is very active; it entrains ambient fluid and dilutes the effluent in a region of intense mixing. Further from the source the turbulent energy decays, as shown by the lack of

fine-scale structure, and the rate of mixing and entrainment substantially reduces. This process is known as turbulence collapse and is considered further in the next section. For the stagnant case, Figure 1a, the mixing region appears to be primarily confined to the rising plume region. This is the "classical" picture of the mechanism by which buoyant jets in stagnant fluids become diluted, although some mixing in the horizontally spreading layer is also indicated. As the current speed is increased the mixing zone is swept downstream by a distance which increases with the current speed. These observations clearly have implications for definitions of the "zone of initial dilution" or "mixing region" allowed for wastewater discharges by regulatory agencies.

Concentration profiles in a vertical plane through the horizontally spreading wastewater layer formed by the line plume case for zero crossflow at various distances from the source are shown in Figure 2. These are plotted with the same axes, and to the same scales, as those shown in figures 5 and 7 of paper I. The sampling distances can be compared to those shown on the corresponding shadowgraph, Figure 1a, and it can be seen that near to the rising plumes, at x/ℓ_b = 1.7, local concentration peaks exist and the wastefield is not quite horizontally homogeneous. The shadowgraph also suggests some active turbulence at this distance. The center portion of the layer has become fairly homogeneous horizontally by x/ℓ_b = 3.2 and no further changes in maximum concentration (or minimum dilution) occur for longer distances. Apparently, some mixing is occurring in the horizontal layer near to the source, indicating that some care is necessary in choosing the locations at which dilutions are measured in laboratory experiments. On the other hand, minimum dilutions computed at x/ℓ_b = 1.7 and 3.2 differ by only about 10%, and the majority of the dilution is effected by the rising plumes.

All of the major characteristics of wastefield formation in a perpendicular crossflow are evident in the concentration profiles shown in Figure 3. These profiles are for the line plume case with F=1, and distances can be compared to the corresponding shadowgraph shown in Figure 1c. Near to the source, at x/ℓ_b = 2.5, the layer is thin, considerable lateral inhomogeneity exists with high concentrations, and turbulent entrainment and mixing are very active. At x/ℓ_b = 4.8 the concentrations are reduced and the layer is thicker due to turbulent entrainment. The layer is also

more uniform laterally, and is completely laterally homogeneous by x/ℓ_b = 9.7. At this distance the maximum concentration (or minimum dilution) have reached their asymptotic values and the turbulence has essentially collapsed, as suggested by the shadowgraph at this distance. Beyond this distance little further entrainment or mixing take place and concentrations or dilution no longer change with distance. Following completion of the mixing process, the wastefield collapses vertically and spreads laterally (compare the width at x/ℓ_b = 18.1 to that at 9.7) under the influence of the ambient stratification in a manner similar to that observed for submarine-wake collapse by Lin and Pao (1979). This process is complicated, however, by the overlap between the active mixing region and lateral spreading region as can be seen by comparing the layer width at x/ℓ_b = 4.8 to that at 9.7.

The smallest values of dilution, S, (corresponding to the highest concentration) at any downstream distance were extracted from the concentration profiles for perpendicular currents and are plotted in Figure 4 in the form suggested by the dimensional analyses of paper I as:

$$\frac{SqN}{b^{2/3}} = f\left[\frac{x}{\ell_b}, F\right] \qquad (1)$$

Results for all of the source conditions studied ($0.078 \leq \ell_m/\ell_b \leq 0.50$ and $0.31 \leq s/\ell_b \leq 1.92$) are plotted as they show little deviation from the line plume results; the symbols showing the different source conditions can be identified from figure 2 of paper I. For each value of the Froude number F the dilution increases monotonically with distance and eventually reaches an asymptotic value at a distance x_a beyond which the dilution remains essentially unchanged. This is consistent with the previous discussions, and it is this asymptotic value of dilution which we have defined as the "minimum dilution" S_m and which was plotted in figure 8 of paper I. Figure 4 allows a quantitative estimation of the distance x_a required for the asymptotic dilution to be achieved, and it is apparent that this distance increases with current speed. The approximate distances are shown by the dashed line drawn through the intersections of x_a with the asymptotic dilution values and are in general agreement with the behavioral transition indicated by the shadowgraphs. Arguments from which x_a can be predicted are given in the next section. As

discussed above, the thickness of the wastefield first increases with distance from the source due to entrainment, then decreases due to gravitational collapse. The values of thickness and rise heights given in figures 10, 11, and 12 of paper I are those computed at the asymptotic dilution distance x_a.

Overhead photographs of wastefield spreading in parallel currents at F = 1 and 10 are shown in Figure 5. Comparison of these photographs to the corresponding sideview photographs (figures 6b and 6c of paper I) shows a complex, three-dimensional flow field. The darkening apparent at the top of the rising plumes in the sideview photographs can be seen to be caused by the lateral spreading which begins immediately at the leading edge of the diffuser. This lateral spreading can cause the width of the wastefield to be quite large, even for this parallel flow case. The width of the wastefield increases linearly with downstream distance, leading to a wedge-shaped wastefield, and the spreading angle decreases as the current speed increases. The same observations were made by Roberts (1979a) for line plumes in an *unstratified* parallel current. A major difference between the spreading in a stratified current, however, compared to an unstratified one is that the rate of spreading is much less in the stratified case at the same value of F. (Compare Figure 5 to the photographs in unstratified currents shown in figure 11 of Roberts, 1979a). This rate of spreading is analyzed in a later section.

The downstream evolution of concentration profiles for line plume conditions in parallel currents at F = 1 and 100 are shown in Figure 6. Features similar to those shown for perpendicular currents are evident: the increase in dilution with distance, increasing lateral homogeneity due to transverse mixing, and vertical collapse accompanied by lateral spreading. The rate of lateral spreading is more rapid than for perpendicular currents, however, and two other features are evident which do not occur for perpendicular currents. First is the occurrence of twin concentration peaks on either side of the centerline. These correspond to the cores of the individual jets which are swept downstream by the ambient current. It should be noted, however, that similar peaks were observed by Roberts (1979a) for unstratified flows in which the source was a line plume issuing from a vertical slot. Apparently, the twin peaks can be caused by a vortex

structure generated by the interaction of the buoyancy flux and the crossflow even in the absence of the high local concentration levels found in the cores of the individual jets. The twin peaks can persist for long distances downstream (see Figure 6b at F = 100), beyond the point at which the turbulence collapses, and their evolution is slow compared to the active turbulence collapse. The second difference between parallel and perpendicular currents is the considerable thickening of the wastefield near the centerline (Figure 6a especially), the reasons for which are not readily apparent. This rather complex structure of the wastefield downstream from the diffuser in a parallel current suggests that considerable difficulties may be encountered in field studies of ocean outfalls under similar conditions.

The variation of the smallest dilution with distance for parallel diffusers is plotted in the form of Eq. 1 in Figure 7. Again, results for all source conditions are shown as they deviate little from the line plume results. As was found for the perpendicular case, dilutions increase monotonically with distance up to their asymptotic values which were plotted in figure 8 of paper I. A comparison of Figures 4 and 7 shows the distance, x_a, for achievement of the asymptotic dilution to be always less for parallel currents than for perpendicular currents at the same value of F.

It is convenient to present at this point a model of the phases of wastefield formation in the forced entrainment regime which will be used to describe the essential features observed. A sketch of the postulated phases of wastefield formation is shown in Figure 8 which can be compared to the similar sketch for unstratified flows given in figure 4 of Roberts (1979a). This model is used below to obtain predictions of x_a and the variations of S_m and z_t with current speed as reported in paper I. We will show that the results are consistent with a model which assumes the turbulence to be initially unaffected by the stratification and in which the plume grows linearly with distance downstream until an internal Froude number of the turbulence falls to some critical value at which point the turbulence collapses. The distance at which the turbulence collapses is the distance at which the asymptotic dilution is reached, and beyond this distance little further entrainment or dilution transpires.

ANALYSIS OF MIXING DISTANCE

There have been many studies reported recently of the conditions under which turbulence can sustain itself in the presence of stable density stratification and of the conditions which lead to turbulence collapse. Lin and Pao (1979) suggested that the turbulent wake of a body moving through a stratified fluid is initially unaffected by stratification but becomes affected when the time scale of the turbulence in the wake approaches the buoyancy period, 1/N. Thorpe (1982) applied the same arguments to explain the effect of stratification on the mean-shear-free turbulence generated by an oscillating grid. The largest eddies are first affected by the stratification, and assuming the time scale of these eddies to be given by ℓ/w' where ℓ is some turbulence macroscale (or largest eddy size) and w' a velocity scale of the largest eddies (approximately the root-mean-square value of the vertical velocity fluctuations), he suggests that stratification begins to affect the turbulence when $\ell/w' \approx 1/N$. This leads to the idea that an internal Froude number of the turbulence, F_i, exists:

$$F_i = \frac{w'}{\ell N} \tag{2}$$

such that for $F_i > F_{ic}$, where F_{ic} is a critical value of F_i, there is little or no effect of stratification. When the value of F_i becomes equal to F_{ic} the turbulence collapses rapidly in a time scale of the order of ℓ/w' and some of the turbulent kinetic energy is radiated away by internal waves. As internal waves of frequencies higher than 1/N cannot be generated in a stratified fluid, there is little coupling between eddies of smaller timescales and the stratification and hence little stratification effect for $F_i > F_{ic}$. Hopfinger (1985) has reviewed many experiments which support this viewpoint and has concluded that $F_{ic} \approx 1$. Roberts and Matthews (1987) applied these ideas to explain the observations of experiments on high momentum-flux jets in a linearly stratified stagnant fluid. They found the results to be consistent with predictions of a model which assumed the turbulence to be completely unaffected by the stratification until $F_{ic} \approx 0.75$ for the largest (entraining) eddies near the edge of the jet and then to abruptly collapse. We now apply these ideas to the present problem to obtain an expression for the turbulence collapse distance

which we identify with the distance x_a required to reach the asymptotic dilution.

A further assumption considerably simplifies the analysis for the forced entrainment regime. It is assumed that the horizontal velocity in the plume is approximately equal to the ambient velocity and that the behavior of the plume at a given distance is approximately equal to that of a buoyant thermal at the same vertical position. For the present case, a buoyant thermal is an instantaneous release of buoyant effluent over a horizontal area. These analogies were first suggested by Scorer (1959) for plumes generated by point sources (e.g. smokestacks) and were applied very successfully to the analysis of vertical buoyant jets in crossflows by Wright (1977, 1984). Cederwall (1971) applied the idea to line plumes in strong perpendicular crossflows and explained the approach as an assumption that the variables b, u, and x were "kinematically" related to each other and merely describe the rate at which buoyancy is added to each element of fluid passing over the source with no longitudinal fluid transfer. The list of independent variables is then reduced to b/u, the buoyancy flux per unit horizontal area, and t, the travel time of a fluid element. Results are then related to distance x by the Galilean transformation x = ut.

For example, the height h of the plume is given by:

$$h = f\left[\frac{b}{u} , t \right] \tag{3}$$

in which N does not appear as we are assuming the plume to be initially unaffected by stratification. A dimensional analysis of Eq. 3 yields:

$$h = C_1 \left[\frac{b}{u} \right]^{1/2} t = C_1 \left[\frac{b}{u} \right]^{1/2} \frac{x}{u} \tag{4}$$

which can be expressed in the present notation as:

$$\frac{h}{x} = C_1 F^{-1/2} \tag{5}$$

where C_1 is an experimental constant. This result was first obtained by Rouse (1947), who called the forced entrainment process gravitational diffusion, and also by Cederwall (1971). Eq. 5 predicts the plume height to grow linearly with distance from the source. The value of C_1 can be estimated

from Rouse's analysis (see eq. 19 of Roberts, 1979a), by taking the height, h, of the plume to be the height where the local concentration is 5% of the maximum to yield $C_1 = 0.75$. The angle of growth of h to the horizontal, ϕ, is then given by $\phi = \tan^{-1}(0.75F^{-1/2})$. The linear growth rate and the predicted angle of this growth are in good agreement with the observed initial behavior of the plumes evident in the shadowgraphs for $F \geq 1$.

Similarly, the average intensity of the vertical turbulent fluctuations in the plume are given by:

$$w' = f\left[\frac{b}{u}, t\right] \tag{6}$$

which becomes, following a dimensional analysis:

$$w' = C_2\left[\frac{b}{u}\right]^{1/2} \tag{7}$$

where C_2 is another experimental constant. Eq. 7 predicts the intensity of these fluctuations to be independent of distance x, but we know of no experiments from which the value of C_2 can be estimated.

The internal Froude number of the turbulence in the plume, F_i (Eq. 2), can now be estimated by combining Eqs. 4 and 7 to yield:

$$F_i = C_3 \frac{u}{xN} \tag{8}$$

where C_3 is an experimental constant and in which we recognize that the largest eddy size is a constant fraction of the plume height h. Thus, F_i decreases with distance x from the source and if we equate F_i to the critical value $F_i \approx 1$ at $x = x_a$ we obtain:

$$x_a = C_3 \frac{u}{N} \tag{9}$$

which can be expressed in the present notation as:

$$\frac{x_a}{l_b} = C_3 F^{1/3} \tag{10}$$

It is interesting to note that Eqs. 9 and 10 predict the collapse, or mixing distance, to be independent of the source buoyancy flux b, and to be directly proportional to the current speed u. The reason for the independence of the result from b can be seen from Eqs. 4 and 7: whereas the intensity of turbulent fluctuations increases in proportion to $b^{1/2}$, the size of the eddies is also proportional to $b^{1/2}$ and the effect on the internal turbulent Froude number is cancelled, Eq. 8.

The distance at which the asymptotic minimum dilution is achieved can be predicted by equating it to the collapse distance. To estimate C_3, values of x_a/ℓ_b were computed from Eq. 10 for F = 1, 10, and 100, and compared with those estimated from Figure 4. A value of 8.5 for C_3 gave reasonable agreement, so Eq. 10 becomes:

$$\frac{x_a}{\ell_b} = 8.5\ F^{1/3} \qquad (11)$$

which is plotted on Figure 4 at the intersection of the value of x_a/ℓ_b calculated from Eq. 11 with the asymptotic value of dilution at that value of F. It can be seen that this equation predicts the asymptotic dilution distances quite well. For F=1 and 10 the values of x_a/ℓ_b calculated from Eq. 11 are 8.5 and 18.3 respectively. The shadowgraph of Figure 1c does suggest a transition in turbulence behavior for F=1 around x_a/ℓ_b = 8.5 and is consistent with the concentration profiles of Figure 3. For F=10 (Figure 1d) x_a/ℓ_b = 18.3 is beyond the view of the shadowgraph which shows active turbulence at least up to x_a/ℓ_b = 12.

These concepts can also be applied to predict the observed variations of asymptotic dilution and rise height with current speed in the forced entrainment regime reported in paper I. Assuming the top of the wastefield, z_t, to be equal to the height h of the plume at the collapse distance, i.e. z_t = h at x = x_a we obtain, on combining Eqs. 5 and 10 and writing the result in the present notation:

$$\frac{z_t}{\ell_b} = C_4\ F^{-1/6} \qquad \text{for } F \gg 1 \qquad (12)$$

where C_4 is an experimental constant. This is the same equation obtained by Roberts (1979b) using

quite different arguments (quoted as eq. 13a in paper I) and which was found to predict the results closely over the range $1 \leq F \leq 100$ with $C_4 = 2.5$ (see eq. 17 and figure 10 of paper I).

Dilution can be estimated by recognizing that it is proportional to the ratio of the ambient volume flux per unit width, q_t, passing through the height z_t to the source volume flux per unit length, q, i.e.:

$$S_m \alpha \frac{q_t}{q} \tag{13}$$

but $q_t = uz_t$ and substituting z_t from Eq. 12 we obtain, after some manipulation:

$$\frac{S_m qN}{b^{2/3}} = C_5 F^{1/6} \quad \text{for } F \gg 1 \tag{14}$$

where C_5 is an experimental constant. Again, this is the same form as predicted by Roberts (1979b) and which was found, with suitable choice of the coefficients, to describe the results well over the range $0.1 \leq F \leq 100$ (see eq. 14 and figure 8 of paper I).

Direct combination of Eqs. 11 and 5 with $C_1 = 0.75$ yields $C_4 = 6.4$, a value much higher than the experimentally deduced value of 2.5. The reason for this discrepancy is that the collapsing turbulence has a more complex structure than the simple model proposed here. The shadowgraphs show that turbulence collapse begins at the plume edge and progresses to the middle of the layer. The asymptotic dilution point, which presumably occurs when all the turbulence has collapsed, is thus downstream of the point where the stratification effect begins. This is the same as assumed by Roberts and Matthews (1987) for a horizontal pure jet, but the more detailed arguments used there cannot be applied here due to our lack of knowledge of the variation of turbulence properties across the layer. When the eddies at the plume top begin to be affected by stratification, the plume height grows more slowly than the initial linear growth rate, and extrapolation of the initial growth rate to the point at which all of the turbulence collapses leads to the noted overestimation of rise height. Nevertheless, the simplified model predicts the collapse distance quite well, and correctly predicts the observed power law relationships, Eqs. 12 and 14, and so is a useful model

until more detailed turbulence measurements are available.

GRAVITATIONAL SPREADING FOR PARALLEL CURRENTS

In this section we analyze and obtain an expression for the lateral spreading rate for parallel currents as shown, for example, in the photographs of Figure 5. This is done by applying a Galilean transformation to previous observations of the spreading rate of a similar layer into an otherwise stagnant ambient.

The experiments of Manins (1976) are applicable. He measured the spreading rate of the horizontal layer resulting from a continuous release of homogeneous fluid from a slot into a linearly stratified ambient fluid at its level of neutral buoyancy. He found that after a brief adjustment stage a quasi-steady state was reached in which there is a balance between inertia and buoyancy forces. In this stage the layer thickness h_a and frontal velocity u_s are constant and are given by:

$$u_s = q_o^{1/2} N^{1/2} \quad \text{and} \quad h_a = 2q_o^{1/2} N^{-1/2} \qquad (15a,b)$$

where q_o is the source volume flux per unit width. The Froude number of the spreading layer, F_s, can then be calculated as:

$$F_s = \frac{u_s}{h_a N} = \frac{1}{2} \qquad (16)$$

Therefore, the layer Froude number adjusts itself to a constant value of order unity. Koh (1983) and Buhler (1986) have suggested that this result would apply to the spreading layer resulting from a submerged diffuser.

We first apply Eqs. 15a and 15b to see if they predict the layer thicknesses reported in paper I for stagnant currents. The volume flux q_o in the horizontally spreading layer is given by $q_o = S_a q/2$, where S_a is the flux-averaged dilution and the factor 2 arises because the surface layer splits into two halves. The results of paper I suggest $S_a \approx 2S_m$, therefore $q_o = S_m q$ and as the minimum dilution is given by eq. 12 of paper I:

$$\frac{S_m q N}{b^{2/3}} = 0.97 \qquad (17)$$

we find: $$q_o = 0.97\, b^{2/3} N^{-1} \qquad (18)$$

and combining Eq. 18 with Eqs. 15a and 15b we obtain:

$$u_s = b^{1/3} \quad \text{and} \quad h_a = 2\ell_b \qquad (19a,b)$$

Equation 19b is very close to the experimentally observed value $h_a = 1.8\ \ell_b$ (eq. 16b of paper I). An interesting feature of Eq. 19a is that the frontal spreading velocity is predicted to be independent of N and therefore independent of the rise height. Roberts (1979c) reported the same finding for unstratified ambients.

We now apply Eq. 19a to predict the spreading layer for parallel currents by means of the Galilean transformation x = ut as was done for unstratified currents by Fischer et al. (1979) and Roberts (1979a). The width, w, at time t of the unsteady spreading layer is given by $w = 2u_s t$ which becomes, when applied to the steady spreading of the layer in a parallel current and using Eq. 19a:

$$w = 2\, b^{1/3}\, \frac{x}{u} \qquad (20)$$

or in the present notation:

$$\frac{w}{L} F^{1/3} = 2\,\frac{x}{L} \qquad (21)$$

The widths, w, of the spreading layers were estimated from the downstream concentration profiles (at the position where the concentration is 5% of the maximum) and from the photographs. The results for all source conditions are plotted in Figure 9 using linear scales of the form $wF^{1/3}/L = f(x/L)$, as suggested by Eq. 21. Although there is considerable scatter this form of data reduction correlates the results quite well, particularly considering the very wide range of current speeds ($1 \le F \le 100$) and source parameters ($0.078 \le \ell_m/\ell_b \le 0.50$ and $0.31 \le s/\ell_b \le 1.92$) represented by Figure 9. In part the scatter is due to experimental error caused by the large rake

spacing near the plume edge, as measurement of the plume width was not a primary focus of the present experiments. This experimental error is about ±20% which is comparable to the scatter of the data.

The spreading is reasonably well predicted by Eq. 21 except that a better fit to the data is given by:

$$\frac{w}{L} F^{1/3} = 0.70 \frac{x}{L} \quad \text{or} \quad \frac{w}{L} = 0.70 \frac{x}{L} F^{-1/3} \tag{22}$$

Possible reasons for the differences in the constant between Eqs. 21 and 22 are the presence of a counterflowing bottom layer for the present situation and the vertical variation in concentration over the spreading layer compared to that in Manins' experiment in which the spreading layer was uniformly mixed. We note that, except for the value of the constant, Eq. 22 is the same as that derived for spreading in unstratified parallel currents by Fischer, et al. (1979) (eq. 10.14) and Roberts (1979a) (eq. 22). The value of the constant for unstratified flows is about 1.2, i.e. the spreading rate in unstratified flows is much more rapid than in stratified flows.

The analysis given above predicts a linear growth rate and is only valid to the end of the diffuser, i.e. $x \leq L$. As will be discussed below, a different analysis is expected for $x > L$ with a slower, non-linear growth rate more like $w \sim x^{1/2}$. The photographs of Figure 5 (for which the diffuser occupies about 1/2 of the total length shown) and the results of Figure 9 clearly show, however, that the wastefield continues to grow linearly with distance beyond the end of the diffuser and at the same rate as for $x \leq L$. Why is this so? A possible explanation is given by the observations of Maxworthy (1980) on the spreading rate of a mixed region. He finds that trains of nonlinear internal waves are produced by this situation and that mixed fluid can be trapped in leading solitary waves which move at constant velocity. The mixed fluid is eventually ejected rearwards by the wave. While it is only speculation that this mechanism occurs here, transport by a constant velocity internal wave generated by the spreading layer for $x \leq L$ and persisting for $x > L$ would explain the continuing linear growth law beyond the end of the diffuser.

GRAVITATIONAL SPREADING FOR PERPENDICULAR CURRENTS

Downstream from the point where the internal turbulence ceases to be active, the wastefield collapses vertically and spreads horizontally. This process, which can be seen in the concentration profiles of Figures 2 and 3, is similar to the collapse of submarine wakes discussed by Lin and Pao (1979) and of mixed region collapse studied originally by Wu (1969). Wu found that after a brief initial period there was a principal stage of spreading governed approximately by $w \sim t^{1/2}$, and that the Richardson number at the spreading layer edge is large enough that no instability or entrainment of ambient fluid would be expected. Kao (1976) also obtained $w \sim t^{1/2}$ and showed by conservation of volume that Eq. 16 also applies to the mixed region collapse, i.e. the Froude number of the front is a constant. The difference between the spreading of the continuous source and the mixed region is that u_s and h are constant in the former case, whereas $u_s \sim t^{1/2}$ and $h \sim t^{-1/2}$ in the latter. Kao obtains:

$$\frac{w}{w_o} = \left[\frac{\pi}{2} (Nt - 0.57) \right]^{1/2} \tag{23}$$

for the principal stage, where w_o is the radius of the initially cylindrical mixed region. Assuming that Eq. 23 can be applied to the present case by means of the Galilean transformation $x = ut$ suggests a scaling in the present notation:

$$\frac{w}{L} = f\left[\frac{x}{L_b} F^{-1/3} \right] \tag{24}$$

with an asymptotic solution $w \sim x^{1/2}$.

The widths w of the spreading layers were estimated from the concentration profiles (at the position where the concentration is 5% of the maximum) and are plotted in Figure 10 using linear axes suggested by Eq. 24. The results are fitted with the semi-empirical equation of the form suggested above:

$$\frac{w}{L} = 1 + 0.17\left[\frac{x}{L_b} F^{-1/3} \right]^{1/2} \tag{25}$$

We also note that from the previous discussions that turbulence is expected to cease to be active at $x\ F^{-1/3}/\ell_b = 8.5$, and this point is marked on Figure 10. There is considerable scatter in the data when plotted in this way, but as for the parallel currents the experimental uncertainty of these measurements is large, about ±20%. Thus, the results cannot be taken as confirmation of the $w \sim x^{1/2}$ growth law implied by Eqs. 23 or 25 and attempts to deduce the growth law by plotting the results on logarithmic scales were thwarted due to the large data scatter. We also note that Amen and Maxworthy (1980) suggest a more complex spreading process than predicted by Eq. 23 with growth laws dependent on the initial geometry.

Nevertheless, considering the very wide range of current speeds ($0.1 \leq F \leq 100$) and source conditions ($0.078 \leq \ell_m/\ell_b \leq 0.50$ and $0.31 \leq s/\ell_b \leq 1.92$) represented on Figure 10 the correlation of Eq. 24 is quite good and the results show no systematic dependency on F, ℓ_m/ℓ_b, or s/ℓ_b. Eq. 25 can be used to predict any of the results with an expected maximum error of about ±20%, which is comparable to the experimental error. This equation predicts the width of the wastefield to grow as $w \sim x^{1/2}$ for stratified flows compared to the more rapid spreading in unstratified flows which was found to be $w \sim x$ initially (Roberts, 1979a) and $w \sim x^{2/3}$ farther downstream (Larsen and Sorensen, 1968).

APPLICATIONS

We continue with the example of the wastefield produced by the West Point outfall of Metropolitan Seattle whose gross properties were predicted in table 1, paper I. The length of the mixing region x_a can be predicted from Eq. 11 for perpendicular currents. For example, at u = 10 cm/s, we have F = 0.13 and ℓ_b = 12.6 m, so that $x_a = 8.5\ \ell_b\ F^{1/3}$ = 54 m. The width of the wastefield for a parallel current can be estimated from Eq. 22. For example, 500 m downstream at u = 10 cm/s, $w = 0.70 \times F^{-1/3}$ = 691 m. The width for a perpendicular current can be estimated from Eq. 25. For example, 500 m downstream at u = 10 cm/s, L = 183 m, $w = [1 + 0.17\ (x/F^{1/3}\ell_b)^{1/2}]L$ = 458 m. Results for other current speeds are summarized in Table 1.

The mixing region can extend for several hundred meters downstream. These mixing distances are upper limits for the values at other current directions at the same speeds, as perpendicular currents are expected to cause the longest mixing lengths (see Figures 4 and 7). Within this distance dilutions will be lower than the asymptotic values given in table 1 of paper I.

The lateral growth of the wastefield due to gravitational spreading can be quite rapid, especially at low parallel current speeds. For higher parallel current speeds the rate of spreading is reduced and will result in wastefield widths less than the diffuser length at the end of the diffuser for current speeds above some critical value. This value can be estimated from Eq. 22 by substituting $w/L = 1$ at $x/L = 1$ (the end of the diffuser) to yield $F = 0.34$. Thus, the wastefield width at the end of the diffuser will be greater than the diffuser length when $F < 0.34$ and less than the diffuser length when $F > 0.34$. This corresponds to a current speed of about 14 cm/s for the West Point outfall, a value comparable to the standard deviation of the local currents. As the wastefield continues to spread beyond the end of the diffuser, and because the wastefield width is greater for other current directions, we can conclude that line diffusers will produce a wastefield width comparable to the diffuser length most of the time under typical oceanic conditions. The results of paper I showed that dilutions are not reduced even for strong parallel currents. Thus, as was implied for unstratified currents by Roberts (1979a), Y or similar complex diffuser configurations are not needed to produce a widely dispersed wastefield.

SUMMARY AND CONCLUSIONS

Some fundamental aspects of the formation and mixing of wastefields resulting from the discharge of buoyant effluent from a submerged multiport diffuser into a linearly stratified steady current of arbitrary speed and direction are analyzed. We consider in particular the mixing distance for strong perpendicular currents and the rate of lateral gravitational spreading of the wastefield for parallel and perpendicular currents.

Regions of fine-scale turbulence structure seen in the shadowgraphs, Figure 1, indicate where the buoyancy-induced turbulence is actively entraining ambient fluid and diluting the effluent. For

stagnant ambients the mixing region is confined primarily to the rising plumes, but for higher current speeds the mixing region can be swept far downstream. Within the mixing region the layer thickness and dilution increase due to entrainment as can be seen from Figures 2 and 3. At the end of the mixing region the wastefield is horizontally homogeneous and dilution no longer increases with distance beyond this point (Figure 4). This asymptotic value of the smallest dilution at the end of the mixing zone is termed the "minimum dilution." Expressions for the length of the mixing zone are obtained by equating it to the distance at which the buoyancy-induced turbulence collapses under the influence of the ambient stratification. It was assumed that the turbulence is completely unaffected by ambient stratification near the source and collapses when an internal Froude number of the turbulence falls to a critical value. This leads to Eq. 11 for the collapse distance, a result in good agreement with measurements of the distance required for the asymptotic value of dilution to be reached, and consistent with observations of the collapse of turbulence inferred from the shadowgraphs. This model is also found to correctly predict the form of the observed variation of rise height and dilution with current speed for strong perpendicular currents, Eqs. 12 and 14.

For parallel currents the wastefield spreads linearly with distance up to and beyond the end of the diffuser as shown in the overhead photographs of Figure 5. Twin peaks in the concentration profiles are observed which can persist for long distances downstream (Figures 6a and 6b). The distance required for the asymptotic dilution to be achieved for parallel currents (Figure 7) is always less than for perpendicular currents under otherwise similar conditions.

The rate of spreading in parallel currents is analyzed by applying a Galilean transformation to the results of previous observations of the spreading of a continuous release of effluent from a slot source into a linearly stratified fluid at its level of neutral buoyancy. An expression is derived (Eq. 22) which describes the results for a wide range of conditions within experimental error (Figure 9). The experimental error and data scatter are large (about 20%), however, and Eq. 22 can only be used with these limitations in mind. The expression for the rate of spreading in stratified currents has the same form as that found for unstratified currents, except that the effect of the

stratification is to considerably reduce the rate of spreading.

The wastefield collapses vertically and spreads horizontally for perpendicular currents beyond the mixing region, as can be seen in Figure 3. It is argued that this process is analogous to the collapse of submarine wakes or mixed regions and the spreading rate is analyzed by applying a Galilean transformation to the results of previously published studies of this problem. This suggests a scaling of the form of Eq. 24 with an asymptotic growth law of the form $w \sim x^{1/2}$. The results, plotted in Figure 10, correlate the wide range of observed results reasonably well, albeit with considerable scatter. As for parallel currents the experimental error is quite large (about 20%) and the precision of the experiments is insufficient to confirm the predicted growth laws. An empirical growth law (Eq. 25) is proposed which can be used to predict the observed results with an uncertainty of about 20%.

The results were applied to predict the properties of the wastefield resulting from the West Point outfall of Metropolitan Seattle. The predictions, Table 1, show that the mixing region can extend for several hundred meters downstream. Because of the gravitational spreading, a line diffuser will result in a wastefield width of the order of the diffuser length for most typical oceanic conditions and it is argued that Y or similar complex diffuser configurations are not necessary to produce a widely dispersed wastefield.

All of the results presented in this paper - the variation of dilution with distance and rate of lateral spreading - show no systematic dependence on the source momentum flux or port spacing over the range of conditions tested. For this range ($0.078 \leq \ell_m/\ell_b \leq 0.50$ and $0.31 \leq s/\ell_b \leq 1.92$) these properties are primarily determined by the source buoyancy flux per unit length, b. This provides further confirmation of the importance of the "line plume" approximation for ocean outfalls over a fairly wide range of typical discharge and oceanic conditions.

ACKNOWLEDGMENTS

We are indebted to Gary Briggs for pointing out to us some of the dimensional arguments used in this paper.

APPENDIX I - REFERENCES

Amen, R., and Maxworthy, T. (1980). "The Gravitational Collapse of a Mixed Region into a Linearly Stratified Fluid," J. Fluid Mech., Vol. 96, Part 1, pp. 65-80.

Buhler, J. (1986). Discussion of "Spreading Layer of a Two-Dimensional Buoyant Jet," J. Hydr. Engrg., ASCE, Vol. 112, No. 10, pp. 992-994.

Cedarwall, K. (1971). "Buoyant Slot Jets Into Stagnant or Flowing Environments," W.M. Keck Laboratory of Hydraulics and Water Resources, California Inst. of Technology, Rept. No. KH-R-25.

Hopfinger, E.J. (1985). "Turbulence Collapse in Stratified Fluids," Proc. IUTAM Symposium on Mixing in Stratified Fluids, Margaret River, Australia, 25-29 August.

Kao, T.W. (1986). "Principal Stage of Wake Collapse in a Stratified Fluid: Two-Dimensional Theory," Phys. Fluids, Vol. 19, No. 8, pp. 1071-1074.

Koh, R.C.Y. (1983). "Wastewater Field Thickness and Initial Dilution," J. Hydr. Engrg., ASCE, Vol. 109, No. 9, pp. 1232-1240.

Larsen, J., and Sorensen, T. (1968). "Buoyancy Spread of Wastewater in Coastal Regions," Eleventh Conference on Coastal Engineering, London, England, Vol. 2, pp. 1397-1402.

Lin, J.T., and Pao, Y.H. (1979). "Wakes in Stratified Fluids," Ann. Rev. Fluid Mech., Vol. 11, pp. 317-338.

Manins, P.C. (1976), "Intrusion into a Stratified Fluid," J. Fluid Mech., Vol. 74, part 3, pp. 547-560.

Maxworthy, T. (1980). "On the Formation of Nonlinear Internal Waves from the Gravitational Collapse of Mixed Regions in Two and Three Dimensions," J. Fluid Mech., Vol. 96, Part 1, pp. 47-64.

Roberts, P.J.W. (1979a). "Line Plume and Ocean Outfall Dispersion," J. Hydr. Div., ASCE, Vol. 105, No. HY4, pp. 313-331.

Roberts, P.J.W. (1979b). "A Mathematical Model of Initial Dilution for Deepwater Ocean Outfalls," Proc. of Specialty Conf. on Conservation and Utilization of Water and Energy Resources, San Francisco, Aug. 8-11, pp. 218-225.

Roberts, P.J.W. (1979c). "Two-Dimensional Flow Field of Multiport Diffuser," J. Hydr. Div., ASCE, Vol. 105, No. HY5, pp. 605-611.

Roberts, P.J.W., and Matthews, P.R. (1987). "Behavior of Low Buoyancy Jets in a Linearly Stratified Fluid," to be published in J. of Hydr. Res.

Roberts, P.J.W., Snyder, W.H., and Baumgartner, D.J. (1987). "Submerged Wastefield Formation by Ocean Outfalls," Submitted to J. Hydr. Engrg., ASCE.

Rouse, H. (1947). "Gravitational Diffusion From a Boundary Source in Two-Dimensional Flow," Journal of Applied Mechanics, American Society of Mechanical Engineers, pp. A225-A228.

Scorer, R.S. (1959). "The Behavior of Chimney Plumes," Int. J. Air Poll., Vol. 1, pp. 198-220.

Thorpe, S.A. (1982). "On the Layers Produced by Rapidly Oscillating a Vertical Grid in a Uniformly Stratified Fluid," J. Fluid Mech., Vol. 124, pp. 391-409.

Wright, S.J. (1977). "Effects of Ambient Crossflows and Density Stratification on the Characteristic Behavior of Round Turbulent Buoyant Jets," W.M. Keck Laboratory of Hydraulics and Water Resources, California Institute of Technology, Rept. No. KH-R-36.

Wright, S.J. (1984). "Buoyant Jets in Density-Stratified Crossflow," J. Hydr. Engrg., ASCE, Vol. 110, No. 5, pp. 643-656.

Wu, J. (1969). "Mixed Region Collapse with Internal Wave Generation in a Density-Stratified Medium," J. Fluid Mech., Vol. 35, part 3, pp. 531-544.

APPENDIX II - NOTATION

The following symbols are used in this paper:

b = total source buoyancy flux per unit diffuser length;

c = ratio of local dye concentration to effluent dye concentration;

$C_1 ... C_5$ = experimental constants;

F = Froude number, u^3/b;

F_i = internal Froude number of turbulence, $w'/\ell N$;

F_{ic} = critical value of F_i;

F_s = internal Froude number of spreading layer, $u_s/h_a N$;

h = height of plume;

h_a = thickness of horizontally spreading layer;

ℓ = length scale (size) of largest buoyancy-induced turbulent eddies;

L = diffuser length;

ℓ_b, ℓ_m = length scales (see Eq. 4, paper I);

N = buoyancy frequency (see Eq. 1, paper I);

q = total volume flux per unit diffuser length (see Eq. 1, paper I);

q_o = volume flux per unit width in horizontally spreading layer;

q_t = volume flux per unit length due to ambient current up to top of plume;

s = port spacing (see Figure 1, paper I)

S = smallest value of dilution in any vertical plane downstream from the diffuser;

S_a = flux-averaged dilution;

S_m = minimum dilution;

t = Lagrangian travel time;

u = ambient current speed;

u_s = spreading velocity of horizontal layer;

w = wastefield width;

w_o = initial wastefield width;

w' = intensity of vertical buoyancy-induced turbulent velocity fluctuations;

x = distance downstream from diffuser;

x_a = mixing distance: distance at which asymptotic dilution is achieved.

Table 1. Results for Applications Example: Metropolitan Seattle Outfall at West Point

Current speed, u (cm/s) (1)	Froude number, $F = \frac{u^3}{b}$ (2)	Mixing distance, x_a (m) (3)	Wastefield width at x=500m, parallel current, w (m) (4)	Wastefield width at x=500m, perpendicular current, w (m) (5)
0	0	25	--	--
10	0.13	54	691	458
20	1.05	109	344	377
30	3.53	163	328	342
40	8.37	217	172	321
50	16.3	272	138	306

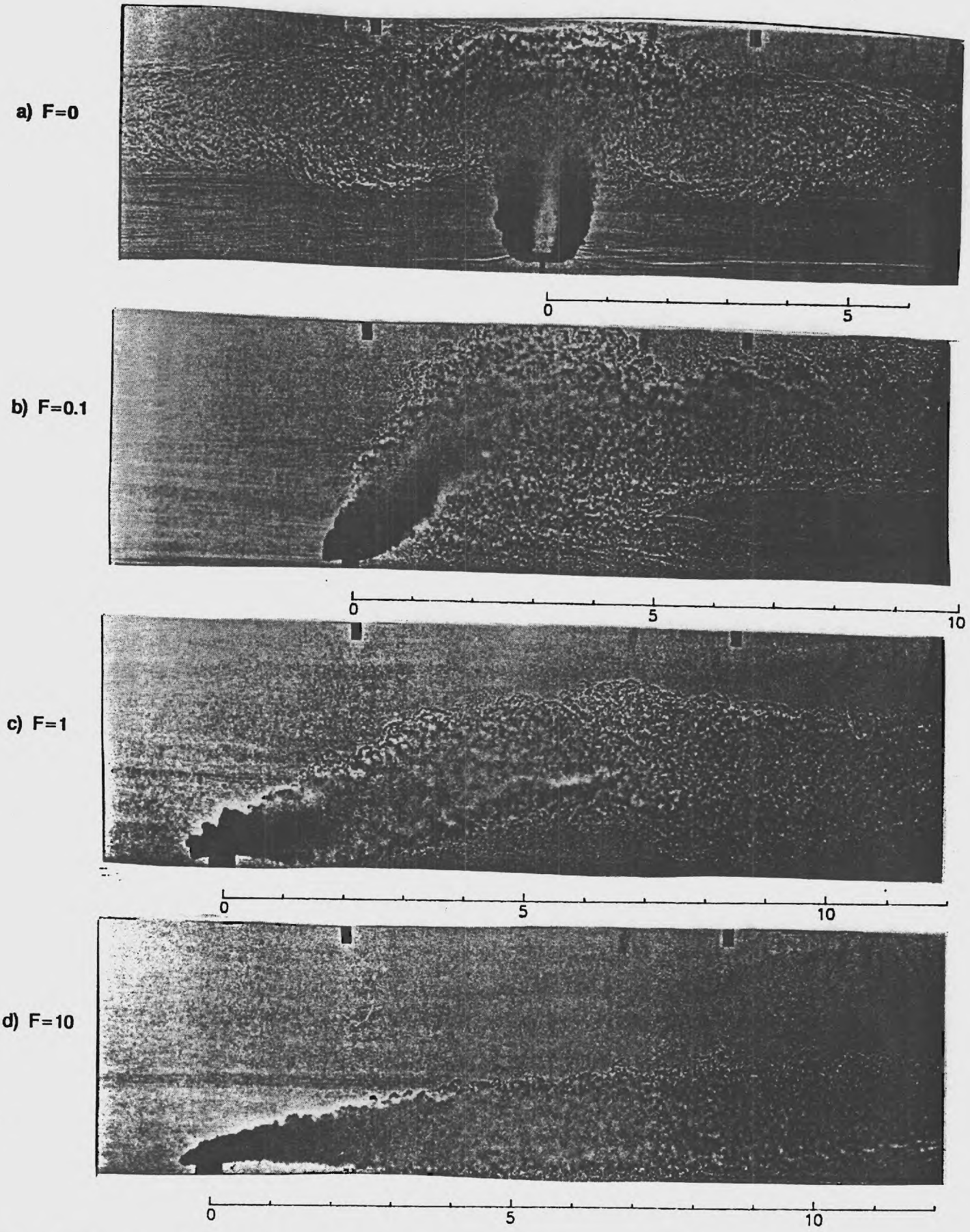

Figure 1. Shadowgraphs of Line Plume Conditions (Series 3) in Perpendicular Currents. The Scale is x/l_b.

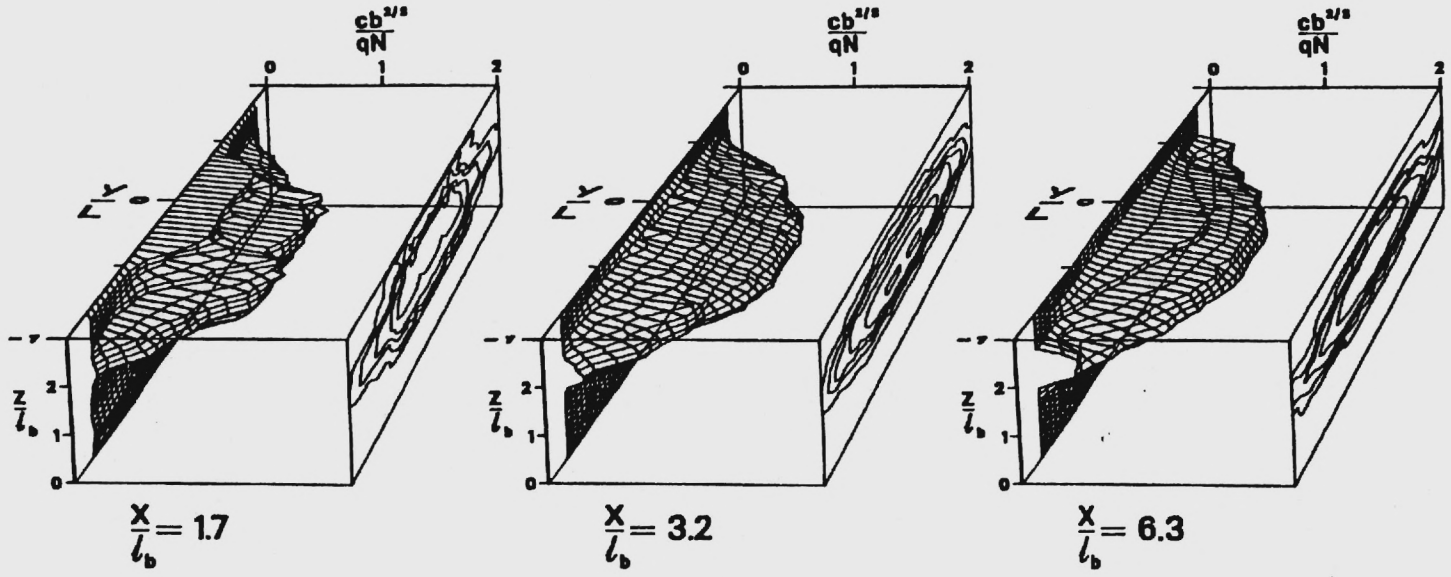

Figure 2. Normalized Concentration Profiles at Various Downstream Distances for Line Plume Conditions (Series 3), Stagnant Ambient

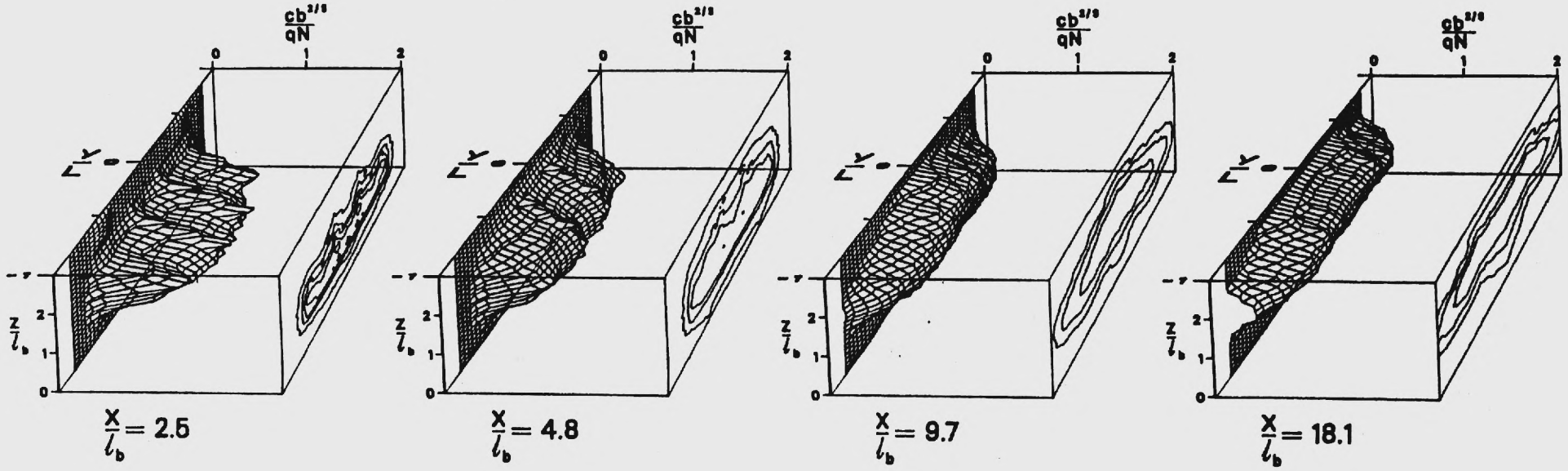

Figure 3. Normalized Concentration Profiles at Various Downstream Distances for Line Plume Conditions (Series 3), Perpendicular Current at F = 1.

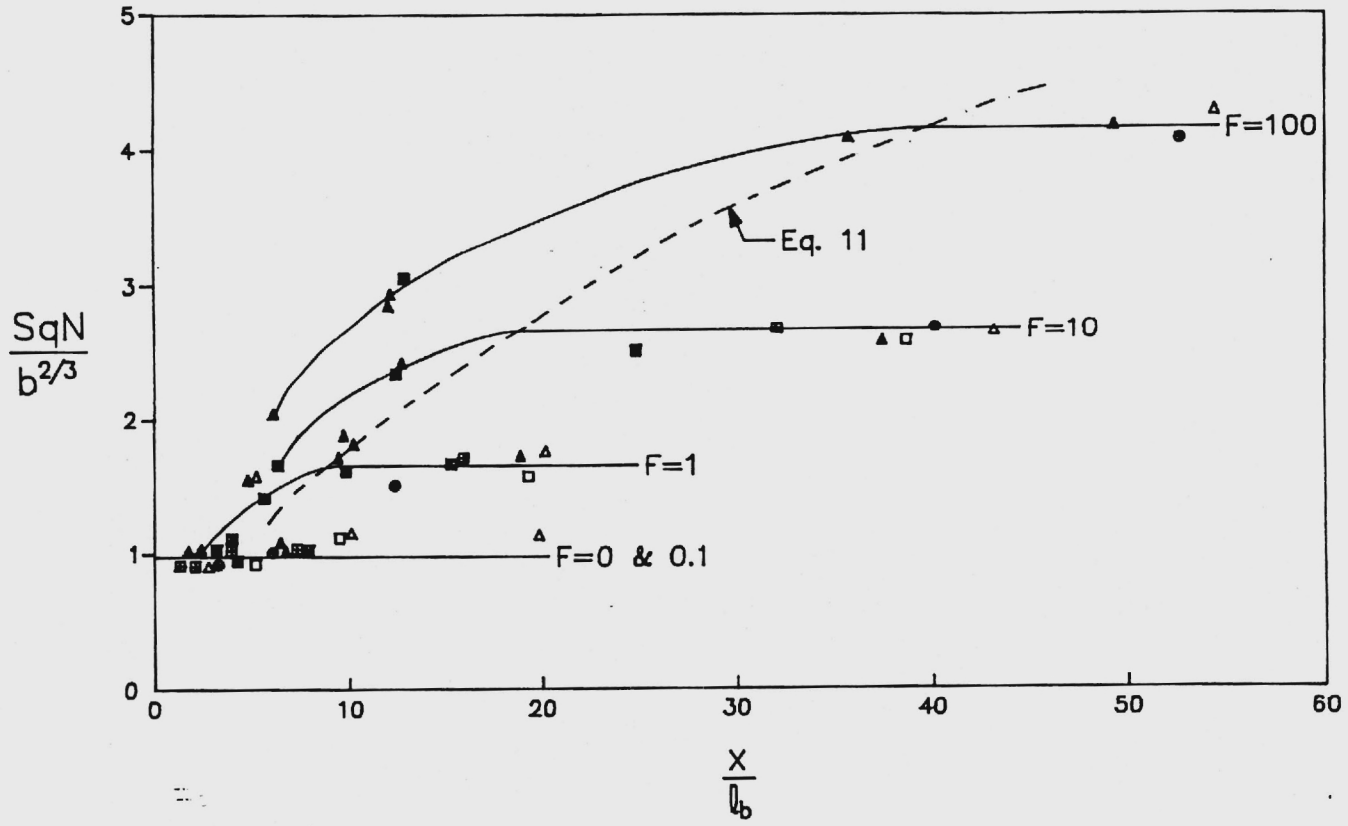

Figure 4. Variation of Dilution with Downstream Distance for Perpendicular Currents, all Experiments

a) F=1

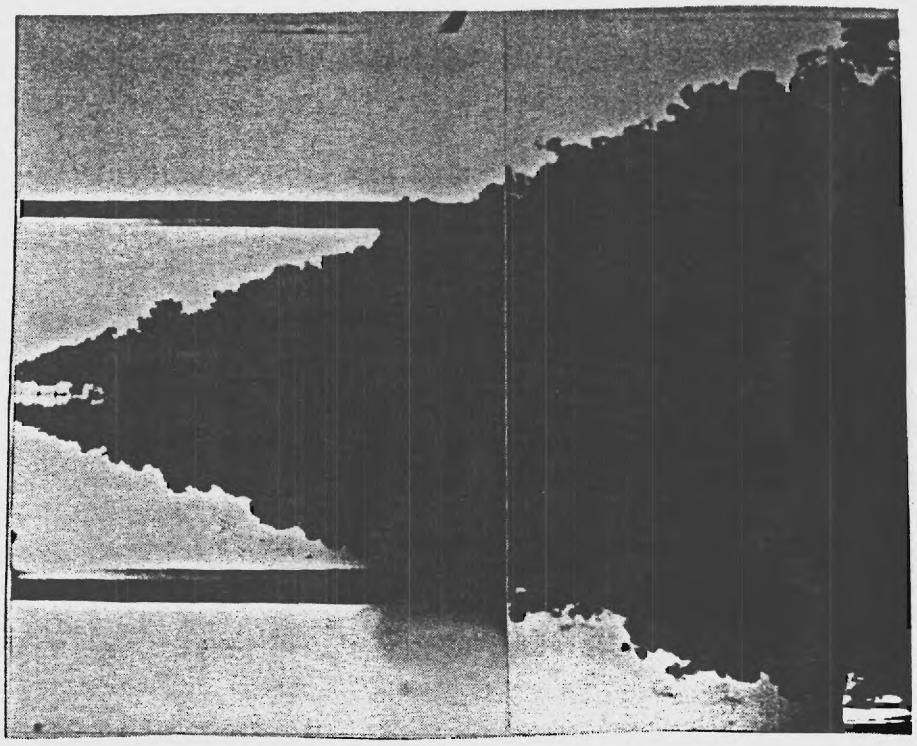

b) F=10

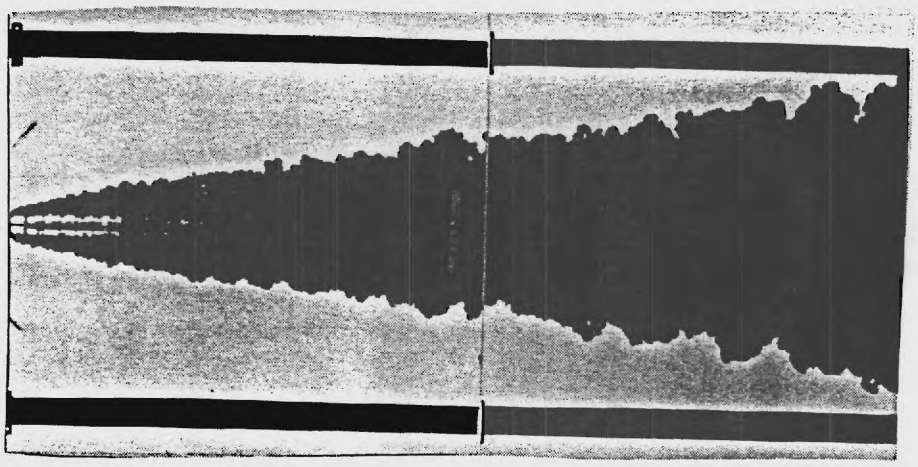

Figure 5. Overhead Photographs of Wastefield Formation for Line Plume Conditions (Series 3 and 4) in Parallel Currents

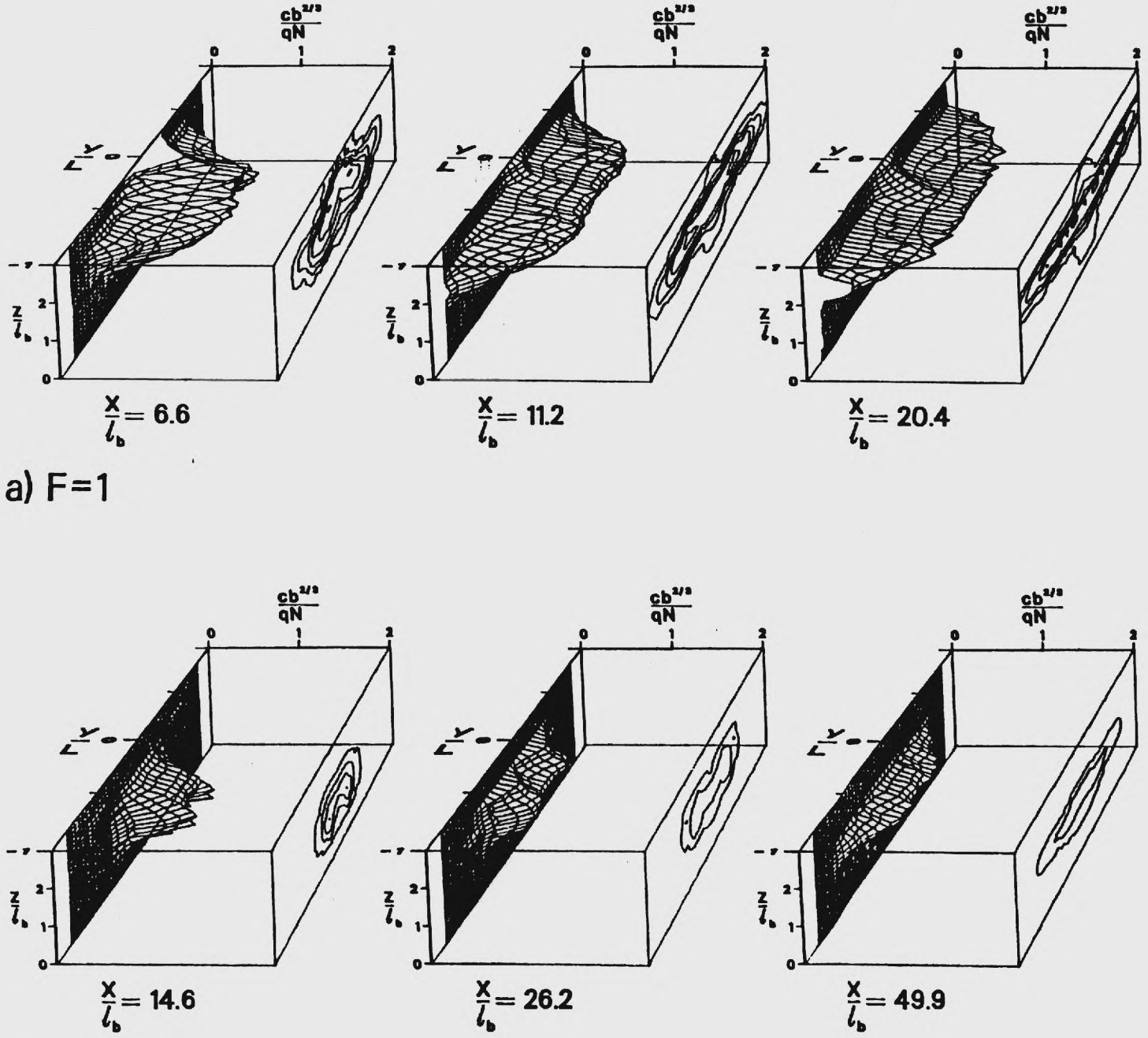

Figure 6. Normalized Concentration Profiles at Various Downstream Distances for Line Plume Conditions (Series 3 and 4), Parallel Currents.

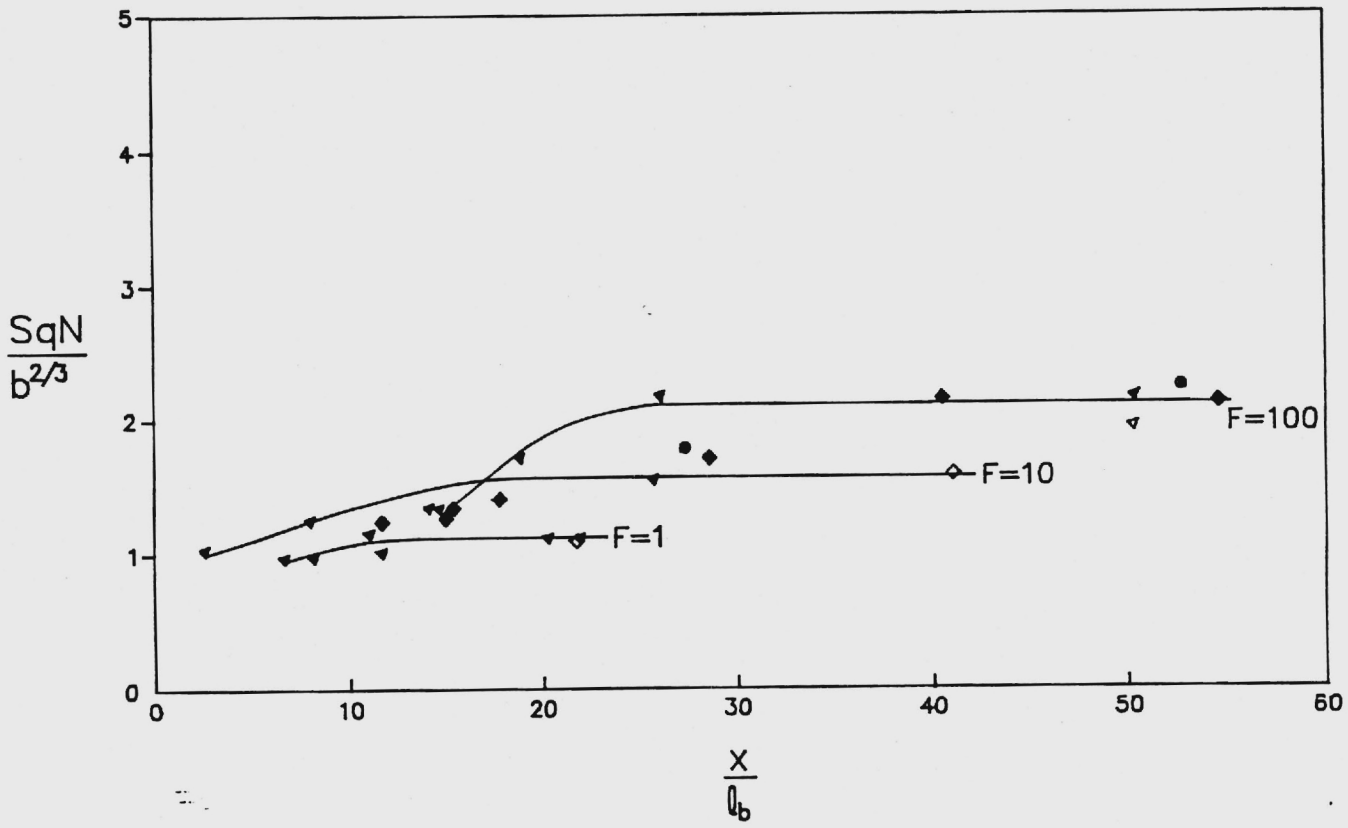

Figure 7. Variation of Dilution with Downstream Distance for Parallel Currents, all Experiments

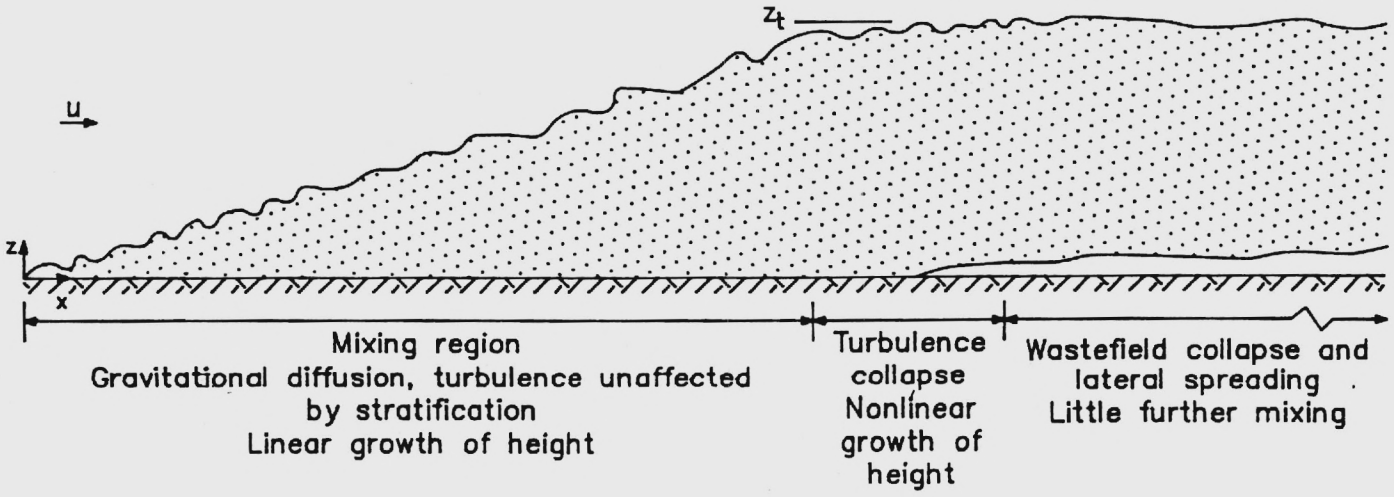

Figure 8. Schematic Depiction of Wastefield Formation in Strong Perpendicular Currents.

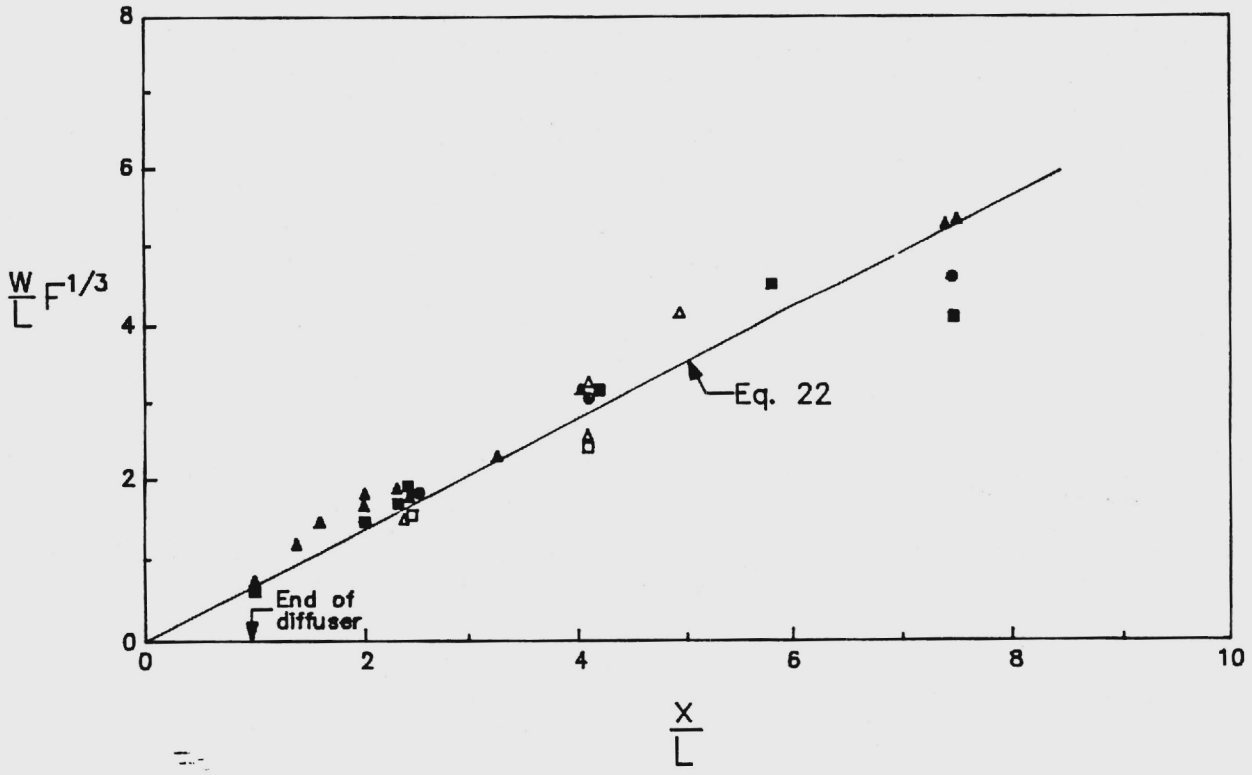

Figure 9. Variation of Wastefield Width with Downstream Distance for Parallel Currents, all Experiments

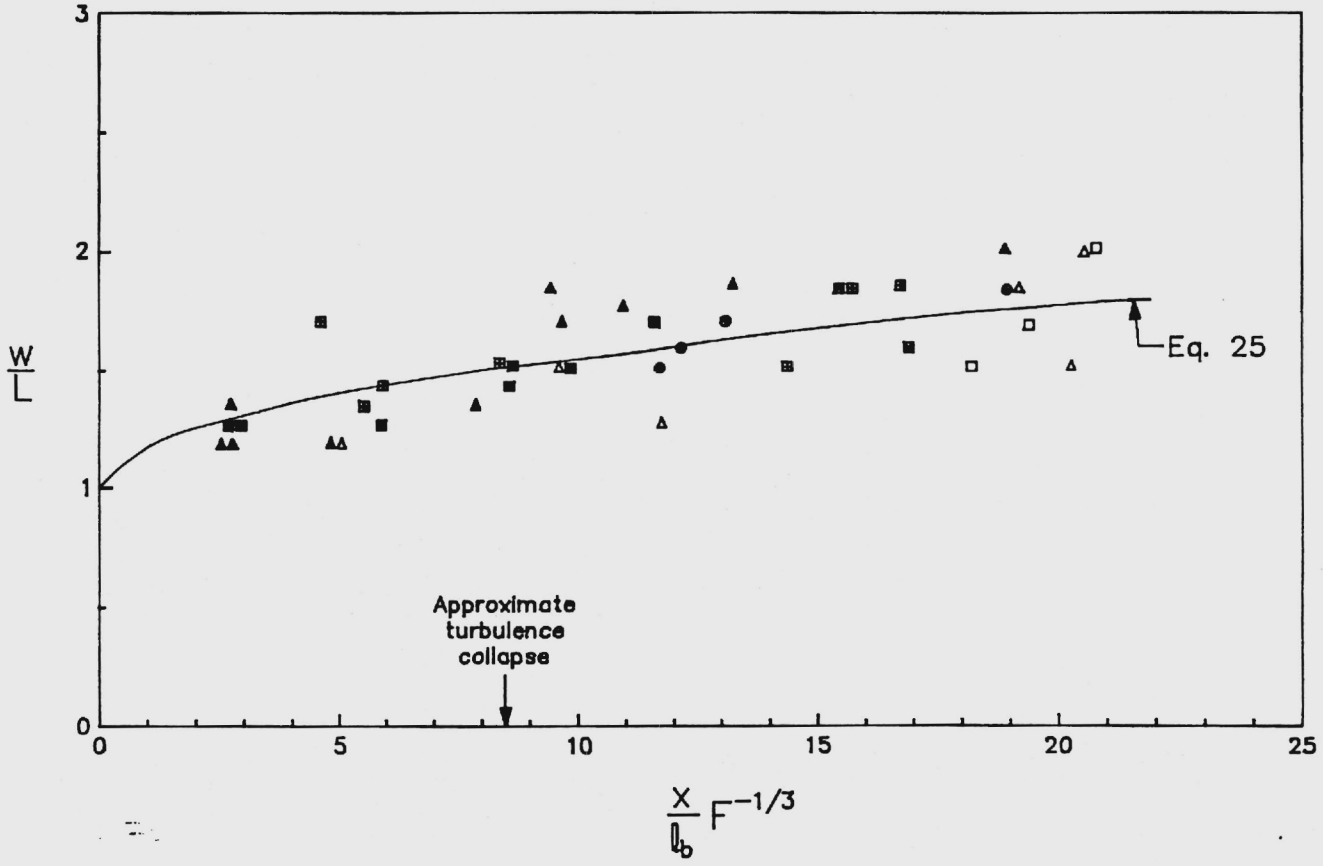

Figure 10. Variation of Wastefield Width with Downstream Distance for Perpendicular Currents, all Experiments

EFFECT OF DIFFUSER DESIGN ON SUBMERGED WASTEFIELDS

by

Philip J.W. Roberts,[1] M. ASCE and W.H. Snyder[2]

ABSTRACT

The effects of port spacing and jet momentum flux on the characteristics of submerged wastefields produced by multiport ocean outfalls in linearly stratified currents was investigated experimentally. Within the parameter range studied the primary effect of these variables is on the rise height and thickness of the wastefield and dilution is closely approximated by line plume results. Point plume results did not reliably predict properties in flowing currents due to rapid plume merging. Increased momentum flux causes a reduction in rise height at low current speeds while leaving the total entrainment path, and hence dilution, fairly constant, but exerts little influence at higher current speeds. Results are presented in graphical and tabular form from which rise heights and thicknesses can be estimated for outfalls which do not approximate line plumes, and an example is given for a proposed design of the Boston MDC outfall.

---

[1]Assoc. Prof. of Civil Engrg., Georgia Inst. of Tech., Atlanta, GA 30332

[2]Meteorology and Assessment Division, U.S. Environmental Protection Agency, Research Triangle Park, North Carolina 27711. On assignment from the National Oceanic and Atmospheric Administration.

INTRODUCTION

In designing ocean outfalls, it is necessary to understand the way in which the parameters under the control of the designer affect effluent mixing. In the previous two papers (Roberts et al. 1987 and Roberts and Snyder 1987, hereafter referred to as papers I and II) we reported the results of experiments to study the mixing and formation of submerged wastefields caused by the discharge of buoyant effluent from multiport diffusers into steady, linearly stratified currents. The primary design variables are the port spacing, s, and the fluxes of buoyancy, b, and momentum, m, per unit diffuser length. The relative importance of these variables is characterized by the length scale ratios ℓ_m/ℓ_b and s/ℓ_b, and the range of these ratios studied (shown in figure 2 of paper I) was chosen to be representative of ocean outfalls. The results given in papers I and II were primarily for the "line plume" condition, i.e. closely spaced jets of low momentum flux with $\ell_m/\ell_b \leq 0.20$ and $s/\ell_b \leq 0.31$. The results in paper I were for gross flow properties - dilution, rise height, and wastefield thickness - and in paper II for mixing distance and the rate of lateral gravitational spreading. Some of these results (particularly dilution and lateral spreading) were found to be insensitive to ℓ_m/ℓ_b and s/ℓ_b over the whole range of parameters tested, not just for $\ell_m/\ell_b < 0.20$ and $s/\ell_b < 0.31$, and these results have already been presented. Some wastefield characteristics are affected by port spacing and momentum flux, however, and in this paper we discuss these effects, particularly the way in which they cause deviations from results expected for line plumes.

We follow the general format of the previous two papers. The experiments are discussed in the following section and the experimental parameters summarized. General observations derived from photographs and concentration profiles are then presented, followed by a section containing the quantitative results. In these sections we first describe the effect of increasing the port spacing parameter s/ℓ_b while maintaining ℓ_m/ℓ_b constant at its line plume value (series 6 and 9, see figure 2 of paper I), then the effect of increasing the source momentum flux parameter ℓ_m/ℓ_b while maintaining s/ℓ_b at its line plume value (series 5), and finally the effect of increasing s/ℓ_b and ℓ_m/ℓ_b (series 8 and 11). The results are then applied to a proposed design of the Boston MDC

outfall to show how to estimate the effects of port spacing and momentum flux. Finally, the results of this paper are summarized and conclusions presented.

EXPERIMENTS

The experiments were conducted in the towing tank using the same multiport diffuser and procedures as described in paper I. The remaining experimental parameters for high momentum flux and/or wide port spacings (series 5, 6, 8, 9, and 11) are summarized in Appendix III.

A few comments concerning the way in which the parameters were varied are warranted. Increasing ℓ_m/ℓ_b while maintaining s/ℓ_b constant (e.g. series 3 to 4 to 5) results from increasing the momentum flux, m, while holding the port spacing, s, buoyancy flux, b, and stratification parameter N constant. This was achieved by increasing the source volume flux q while decreasing the density difference $\rho_a - \rho_o$ between the effluent and receiving water, causing an increase in the densimetric Froude number $F_j = u_j/\sqrt{(g_o'd)}$. For constant ℓ_m/ℓ_b, the value of F_j is constant and the nominal values are: $F_j \approx 5$ (series 3, 6, and 9); $F_j \approx 10$ (series 4); and $F_j \approx 20$ (series 5, 8, and 11). For an ocean outfall, increasing ℓ_m/ℓ_b while maintaining s/ℓ_b constant results from decreasing the port diameter while holding the discharge per unit length and port spacing constant. Increasing s/ℓ_b while maintaining ℓ_m/ℓ_b constant, for example series 3 to 6 to 9, results from moving the same jets further apart so that F_j remains constant. This was accomplished by pinching off the supply lines to some of the Tee's while keeping the effluent density constant and decreasing the total flow rate to maintain the same discharge per port. The port spacings were: $s = 5$ cm (series 3,4, and 5); $s = 10$ cm (series 6 and 8); and $s = 20$ cm (series 9 and 11).

GENERAL OBSERVATIONS

Effect of Port Spacing. - Sideview photographs of widely spaced jets of low momentum flux (series 9, $s = 20$ cm) are shown for stagnant and parallel flowing currents in Figure 1. For the stagnant case, although the plumes do not merge prior to entering the established layer, horizontal spreading in this layer causes it to be laterally homogeneous, despite the very wide port spacing. This is

clearly shown in the concentration profile, Figure 2a, which corresponds to the photograph shown in Figure 1a and was obtained in a vertical plane parallel to the diffuser axis quite close to the rising plumes (x/ℓ_b = 2.8 corresponds to x = 28 cm, a distance less than the rise height). Note that the range of the vertical z/ℓ_b axis has been changed from the profiles previously shown to accommodate the increased normalized rise height which occurs for more widely spaced plumes.

The gradual merging of the individual plumes for this same case in a perpendicular current is shown in rather striking fashion in Figure 2b. Near to the diffuser, at x/ℓ_b = 5.2, the contour plot shows individual plume cores. These cores are not apparent farther downstream, at x/ℓ_b = 10.2, and the wastefield has become very homogeneous laterally by x/ℓ_b = 20.3. The profiles suggest that the distance for the asymptotic dilution to be reached is about x/ℓ_b = 10, very close to that predicted for the line plume shown in figure 4 of paper II and so the two-dimensional length scale ℓ_b is still appropriate even for these very widely spaced jets due to their merging. It has often been assumed that wastefield behavior resulting from diffusers with widely spaced ports can be predicted using results obtained for individual jets, i.e. completely neglecting plume interference and merging. The observations discussed above suggest this assumption is only valid for very widely spaced jets, separated farther than the widest spacing studied here (s/ℓ_b = 1.92), and possibly farther than encountered in normal outfall designs.

The contour plot of Figure 2b at x/ℓ_b = 5.2 shows cores of five individual plumes, although the wastefield results from 14 jets issuing from seven Tees as shown in Figure 1a. Apparently, the upstream jets are quickly swept downstream by the current to merge with the downstream jet from the same riser forming a single plume from each Tee. This would form 7 plumes, but the outer pair are "entrained" inward by mutual attraction to their neighboring plumes and merge with them, forming the five cores. This effect is also apparent in the stagnant case photograph, Figure 1a, in which the outer plumes can be seen bending inward.

Merging in parallel currents (Figures 1b, c and d) is even more rapid, due to direct impingement of the upstream plumes on those downstream. This is probably caused by shielding of the downstream plumes from the current due to entrainment of the ambient flow and also by the

wake caused by the upstream plumes. As would be expected the concentration profiles for these flows (not shown) contain no evidence of the individual jets which produced them and are similar to those for line plumes (figure 7 of paper I and figure 6 of paper II) except that the twin concentration peaks are less well defined and are sometimes completely absent, and the peak concentrations usually occur on the centerline.

Effect of Source Momentum Flux - Concentration profiles for closely-spaced jets of high momentum flux (series 5) for perpendicular currents of various speeds are shown in Figure 3. These are for the same overall Froude numbers, F, as those shown for the line plume case in figure 5 of paper I and are plotted with the same axes and scales as in that figure. In comparing these sets of figures it should be kept in mind that the buoyancy flux, b, and port spacing, s, are the same for both sets and the only difference is that the momentum flux (or the jet densimetric Froude number F_j) is increased compared to those shown in figure 5 of paper I. As previously discussed, this was achieved by increasing q and decreasing ρ_a-ρ_o for fixed port spacing s; for an ocean outfall this would result from decreasing the port diameter d while holding the discharge and port spacing constant. Comparisons of these sets of figures (particularly the contour plots) helps clarify the role of the momentum flux. At low current speeds (F = 0.1) the rise height is reduced by the increased momentum flux with the bottom of the wastefield now extending down to near the port level. The normalized dilutions are hardly changed, however, and are close to the line plume values. This effect is still evident at F = 1, but for $F \geq 10$ there is no longer any evidence of a momentum effect, the profiles of Figure 3 being very similar in all respects to their line-plume counterparts. That the normalized dilution is relatively unaffected by momentum was already inherent in figure 8 of paper I which included this high momentum case.

The primary effect of increasing momentum flux is thus to decrease rise height at low current speeds with the effect decreasing as the current speed increases; the normalized dilution remains unaffected by momentum flux at any current speed. Although we do not have photographs for this case, the photographs of more widely spaced jets at the same ratio of ℓ_m/ℓ_b (and the same jet

Froude number F_j) shown in Figure 4 illustrate why this is so. The stagnant situation, Figure 4a, can be compared to the line plume case, figure 4a of paper I, from which it can be seen that the high momentum jets follow a more shallow trajectory. This causes the jets to entrain more deeper, heavier water from near the port level, resulting in them reaching their level of neutral buoyancy more deeply and reducing the rise height. The total jet path length, however, is not significantly changed, resulting in fairly constant dilution. The flowing current (Figures 4b and 4c) cause even these high momentum flux jets to be rapidly swept downstream. Mixing continues for some distance downstream, as discussed in paper II, and as the momentum effect is confined to the region near the nozzles the mixing again becomes ultimately dominated by the buoyancy flux, with the rise height approaching the line plume result. A comparison of Figure 4b to the corresponding line plume case (figure 4c of paper I, keeping in mind that s/ℓ_b is different) shows that the details of the flow near the diffuser differ; for example, the pronounced wave which occurs for the line plume is not evident for the high momentum case. The flows become similar farther downstream, however. The differences at F = 10 for the two corresponding flows are even less pronounced.

Similar trends were observed for parallel currents. The rise height is reduced at low current speeds with the effect decreasing as F increases. Dilution is relatively unaffected, as was shown in figure 8 of paper I, and the concentration profiles (not shown) are similar to those for line plumes with twin concentration peaks evident. The profiles differed from the corresponding line plume profiles, however, in that they were somewhat wider near the source due to the considerable lateral momentum flux of the jets.

Effect of Increased Port Spacing and Momentum Flux. - Photographs of the high-momentum-flux, widely-spaced jet experiments (series 8 and 11) in perpendicular currents were shown in Figure 4. The upstream jets are quickly swept downstream by the current and the primary momentum-flux effect is to decrease the rise height at low current speeds from that expected for lower momentum flux jets at the same ratio of s/ℓ_b. Concentration profiles (not shown) for perpendicular currents are quite laterally uniform for intermediate spacing (series 8, s = 10 cm, s/ℓ_b = 0.78) but show

some variation for very wide spacing (series 11, s = 20 cm, s/ℓ_b = 1.92). Even in this latter case, however, they are closely uniform for stagnant and fast (F = 10) currents, and for intermediate currents (F = 0.1 and 1) the lateral concentration variation is within 15% of the mean value. This deviation could have resulted from sampling too near to the diffuser, as only one tow was done for these cases, and it is probable that the wastefield becomes more laterally homogeneous farther downstream.

Concentration profiles in parallel currents show no surprises with twin peaks being observed on either side of the centerline.

QUANTITATIVE RESULTS

Introduction. - It was shown by dimensional analysis in paper I that results can be expressed as:

$$\frac{S_m q N}{b^{2/3}}, \quad \frac{z_t}{\ell_b}, \quad \frac{h_a}{\ell_b}, \quad \frac{z_a}{\ell_b} = f\left[\frac{\ell_m}{\ell_b}, \quad \frac{s}{\ell_b}, \quad F, \quad \theta\right] \qquad (1)$$

The normalized dilution showed little dependency on ℓ_m/ℓ_b and s/ℓ_b over the whole range of parameters tested and these results were presented in figure 8 of paper I. The normalized results for z_t, h_a, and z_a for the line plume case ($\ell_m/\ell_b \leq 0.20$ and $s/\ell_b \leq 0.31$), are also independent of ℓ_m/ℓ_b and s/ℓ_b and these results were presented in figures 10, 11, and 12 of paper I. Increasing the value of ℓ_m/ℓ_b and s/ℓ_b does change the rise height and thickness, however, making it difficult to present the results in a compact form.

The high momentum flux and wide port spacing experiments were conducted for: perpendicular and parallel current directions; F = 0, 0.1, 1, 10, and 100; ℓ_m/ℓ_b = 0.078, 0.2 and 0.5; and s/ℓ_b = 0.31, 0.78 and 1.92. The experimental results for ℓ_m/ℓ_b = 0.2 (series 4 only) were already given in paper I and do not differ significantly from those for ℓ_m/ℓ_b = 0.078. Thus, we can present the results for z_t/ℓ_b with perpendicular currents in two graphs, one for the low momentum case ($\ell_m/\ell_b \leq 0.2$) and one for the high momentum case (ℓ_m/ℓ_b = 0.5) with contours of constant values of s/ℓ_b to show the port spacing effect; two more graphs would be required for parallel

currents for a total of four. Similarly, presentation of h_a and z_a results would require 8 more graphs for a total of 12. As this seems rather excessive, we present only the results for z_t/ℓ_b as this parameter represents the wastefield rise height and is probably the most important of these parameters for outfall design. To show the results for h_a and z_a we use the fact that the ratios h_a/z_t and z_a/z_t do not vary widely and summarize them in tabular form. Until mathematical models which reliably predict these results are developed, the graphs and tables can be used with interpolation to predict properties for many outfalls.

The results for z_a/z_t and h_a/z_t for all experiments are summarized in Table 1. The ratio z_a/z_t is fairly constant at 0.66 for all conditions, but h_a/z_t varies systematically with current speed and direction. These ratios can be used with the following results for z_t to predict z_a and h_a to within a maximum error of about ±20%.

Effect of Port Spacing. - The results for low momentum flux jets (ℓ_m/ℓ_b = 0.078, series 3, 6 and 9) are shown for perpendicular currents in Figure 5 and for parallel currents in Figure 6. Smooth contours have been drawn through the data for each value of s/ℓ_b and the line plume results from paper I are also shown for comparison. The line plume result for a stagnant current (eq. 16a of paper I) is:

$$\frac{z_t}{\ell_b} = 2.5 \qquad (2)$$

The perpendicular current results (Figure 5) show that the normalized rise height increases as s/ℓ_b increases, a result already implied by the concentration profiles in Figure 2. The actual rise height z_t, does not change greatly, however, and the increase in z_t/ℓ_b is caused primarily by the decrease in ℓ_b which results from increasing s/ℓ_b while ℓ_m/ℓ_b is held constant. Nevertheless, rise heights for $s/\ell_b > 0.31$ could be considerably overestimated by direct application of the line plume results, and Figure 5 should be used for $s/\ell_b \leq 1.92$ and $\ell_m/\ell_b \leq 0.2$. This is not true for the parallel case, however, as Figure 6 shows little deviation from the line plume results for $0.31 < s/\ell_b \leq 1.92$.

It has been suggested (Muellenhof et al., 1985, Koh 1982) that the dilution and rise height of effluent issuing from diffusers with very widely spaced ports can be estimated by applying results obtained from single, isolated plumes. So it is of interest to see whether these methods can predict the results obtained here.

For isolated buoyant jets issuing from a round nozzle into a linearly stratified, stagnant fluid, similar dimensional and length scale arguments to those used in paper I can be applied. This has been done by Wong (1985) who obtains the following results in the plume regime:

$$\frac{S_m Q_j N^{5/4}}{B^{3/4}} = 0.80 \; ; \quad \frac{z_t}{\ell_B} = 4.0 \; ; \quad \frac{h_a}{\ell_B} = 1.6 \qquad (3a,b,c)$$

where Q_j is the jet discharge and B the buoyancy flux equal to $g_o' Q_j$. Wong found that Eqs. 3a, b, and c apply for $\ell_M/\ell_B \leq 0.6$ where ℓ_B and ℓ_M are length scales defined as:

$$\ell_B = \frac{B^{1/4}}{N^{3/4}} \quad \text{and} \quad \ell_M = \frac{M^{3/4}}{B^{1/2}} \qquad (4a,b)$$

where M is the jet momentum flux equal to $u_j Q_j$. For series 3, 6, and 9 experiments ($\ell_m/\ell_b = 0.078$), we find $\ell_M/\ell_B \approx 0.15$, well into the point plume regime as we would expect. These experiments thus show the effects of gradually moving point plumes closer together until they approach the line plume condition. The experimental results for stagnant currents are shown in Table 2 along with predictions for point plumes from Eqs. 3a, b, and c, and for dilution for line plumes from eq. 12 of paper I:

$$\frac{S_m q N}{b^{2/3}} = 0.97 \qquad (5)$$

A number of interesting observations can be deduced from this Table. As the plumes are moved closer together the dilution gradually decreases from 103 at s = 20 cm, a value very closely predicted by the point plume formula, to 76 at s = 5 cm, a value very closely predicted by the line plume formula. The rise heights z_t are closely predicted by the point plume formula, but the

thickness is not, being underestimated by 20% even for the widely spaced plumes. This latter effect is expected due to the rapid lateral spreading at collapse (Figures 1a and 2a), leading to a field thicker than that resulting from single plumes even when the plumes do not merge before entering the horizontal layer. The layer thickness increases further as the plumes are brought together up to the line plume limit at s = 5 cm. These results suggest that point plume formulae could be used for dilution and rise height for stagnant fluids for $s/\ell_b \geq 1.92$. The line plume formula also predicts dilutions quite well in this range, however, overestimating the dilution at $s/\ell_b = 1.92$ by about 13%. This is unexpected, as the numerical predictions of Wright et al. (1982), replotted in figure 2 of paper I, suggest that normalized dilution would be overestimated by about 60% by use of the line plume formula at $s/\ell_b = 1.92$. We conclude that point jet formulae should be used for dilution for $s/\ell_b \geq 1.92$ and the plume regime curve ($\ell_m/\ell_b = 0.078$ in figure 2 of paper I) should be shifted to the right with deviations from the line plume result occurring at $s/\ell_b \approx 1$, rather than 0.3 as suggested by Wright et al. Thus, the point plume formula is valid for $s/\ell_b = 1.92$, a fact somewhat obscured by the use of two-dimensional parameters in figure 8 of paper I in which the $s/\ell_b = 1.92$ data point appears low but within the experimental scatter. The conclusion that the line plume relations for dilution apply within the parameter range studied remains valid, however, even though the rise heights and wastefield thicknesses do not always approximate those due to line plumes.

We now compare the observed results for widely spaced, low momentum flux jets in perpendicular currents with predictions based on results for point plumes, despite the early warning of Figure 2b that plume merging might render such a technique invalid.

Wright (1984) has presented the results of extensive studies of vertical buoyant jets discharging into steady, linearly stratified currents and has shown that the results for buoyancy dominated flows can be expressed as:

$$\frac{S_o Q_j}{u\,\ell_u^2} = C_1\left[\frac{z_m}{\ell_u}\right]^2; \quad \frac{z_m}{\ell_u} = 2.3\left[\frac{\ell_a}{\ell_u}\right]^{2/3}; \quad \frac{z_a}{\ell_u} = 1.8\left[\frac{\ell_a}{\ell_u}\right]^{2/3} \qquad (6a,b,c)$$

where ℓ_u and ℓ_a are length scales defined by:

$$\ell_u = \frac{B}{u^3} \quad \text{and} \quad \ell_a = \frac{u}{N} \tag{7a,b}$$

and S_o is smallest centerline dilution in the plume and z_m the maximum rise height. C_1 is an experimental constant which Wright's data suggest has a value of about 0.7. The minimum dilution S_m occurs off the centerline for point plumes in flowing currents and Chu (1979) suggests $S_m \approx 0.60\ S_o$. Combining these coefficients and substituting the rise height from Eq. 6b into Eq. 6a we obtain for the minimum dilution:

$$\frac{S_m Q_j}{u\ \ell_u^2} = 2.2 \left[\frac{\ell_a}{\ell_u} \right]^{4/3} \tag{8}$$

The observed results for widely spaced plumes (series 9) are shown in Table 3 along with the predicted values for point plumes (Eqs. 6c and 8) and for line plumes using eq. 14 of paper I:

$$\frac{S_m q N}{b^{2/3}} = 2.19 F^{1/6} - 0.52 \tag{9}$$

and the graphical results shown in figure 12 of paper I. The line plume formula predicts dilution much more closely than does the point plume formula. Neither the line- nor point-plume formulae predict the rise heights well, and graphical solutions based on Figure 5 should be used. That the line plume approximation would closely predict dilutions was already inherent in figure 8 of paper I in which these widely spaced results were included, and also from the merging of the jets to a flow approximating that from a line source as shown in Figure 2b.

Further comments concerning the point plume results can be made. First, if coefficients appropriate to centerline dilutions were used, the predicted dilutions in Table 2 would be much higher than observed. Second, the upstream plumes were observed to be rapidly swept downstream by the current and to merge with their downstream counterparts from the same Tee before merging with their neighbors. This suggests that each Tee produces a single plume and that B in the point plume formula should be replaced by 2B. This would increase the predicted rise heights by about

60%, leading to considerable overestimation of z_a, and decrease predicted dilutions. Even if such gyrations are followed and coefficients adjusted, it is apparent that the point plume formula (which predicts $S_m \propto u^{1/3}$) cannot predict the observed trend in the data (which is $S_m \propto u^{1/2}$), even though the point plume formula was applicable for the same discharge conditions in a *stagnant* current. Thus, the line plume formula is a good approximation even for widely spaced jets up to $s/\ell_b = 1.92$, the maximum spacing studied here. The point plume formulae do not work well for flowing perpendicular currents within the parameter range tested, and as plume merging is even more rapid for other current directions, they may not be applicable for most conditions typical of ocean outfalls.

Effect of Momentum Flux. - The measured values of z_t/ℓ_b for the high momentum flux jets ($\ell_m/\ell_b = 0.50$) of various spacings are shown in Figure 7 for perpendicular currents and in Figure 8 for parallel currents. Again, smooth contours are drawn through the data for each value of s/ℓ_b and the line plume results are also shown. It can be seen that the primary effect of the increased momentum flux on the closely-spaced jets ($s/\ell_b = 0.31$) in perpendicular currents is to decrease the rise height at low current speeds with the rise height tending to the line plume result for $F \geq 10$ as was already apparent from the concentration profiles for this case shown in Figure 3. As s/ℓ_b increases the normalized rise height z_t/ℓ_b increases (as was found for the low momentum case). And for the widely spaced jets ($s/\ell_b = 1.92$) this increase is offset by the decrease caused by the increased momentum flux leading to results close to that for a line plume for $F \leq 1$.

From the numerical predictions of Wright et al. (1982), plotted in figure 2 of paper I we would expect the increased momentum flux to increase normalized dilution by almost 20% for stagnant currents. The experimental results, figure 8 of paper I, show less effect than this and are affected by momentum by an amount less than the experimental error of about 10%. Thus, we can that over the whole parameter range studied, $s/\ell_b \leq 1.92$ and $\ell_m/\ell_b \leq 0.50$, dilutions can be predicted by the line plume results to within about 10%.

APPLICATIONS

In order to illustrate the use of these results for outfalls whose port spacings and momentum fluxes exceed those in the line plume regime, we apply them to the design proposed for the Boston MDC outfall by Alam, Harleman, and Colonell (1982). This application is of particular interest because several mathematical models were used whose predictions generated considerable controversy (Abraham and others, 1983) and because Alam et al. have stated strongly that jet momentum plays a substantial role in determining initial dilution for this outfall.

The proposed outfall has a total length, L, of 2324 m, consisting of a total number of ports, n, of 700, each having a nominal diameter, d, of 6 inches (0.152 m), spaced a distance, s, of 22 ft (6.71 m) apart. Alam et al. presented predictions for March (unstratified) and August (stratified) conditions. As we are here primarily concerned with stratified flows, we use only the August conditions when the total discharge rate, Q, was 24.3 m^3/s and the density stratification profile is shown in their figure 4. This profile is reasonably linear over the bottom 15 m with a density change of about 1.1 σ_t units yielding a buoyancy frequency $N = \sqrt{(-g/\rho_a)(d\rho/dz)} = 2.65 \times 10^{-2}\ s^{-1}$, where the ambient density at the diffuser depth, ρ_a, is taken to be 1.0248 g/cc.

The source fluxes, length scales, and length scale ratios can be computed from these data. The volume flux per unit length $q = Q/L = 1.05 \times 10^{-2}\ m^2/s$, and the buoyancy flux per unit length $b = qg(\rho_a-\rho_o)/\rho_a = 2.59 \times 10^{-3}\ m^3/s^3$ where the effluent density ρ_o is taken as 0.999 g/cc. The jet velocity $u_j = 4Q/n\pi d^2 = 1.91$ m/s yielding a source momentum flux $m = u_j q = 2.01 \times 10^{-2}\ m^2/s^4$. The length scales are $\ell_b = b^{1/3}/N = 5.18$ m and $\ell_m = m/b^{2/3} = 1.07$ m, and length scale ratios are $\ell_m/\ell_b = 0.21$ and $s/\ell_b = 1.30$. These fall within the range studied here and we can immediately conclude from the previous discussions (and figure 2 of paper I) that source momentum flux will play little role in dilution but that the rather wide port spacing will probably result in no merging of the plumes before entering the horizontal layer under stagnant conditions but will result in merging for flowing currents.

Dilution predictions for this outfall were presented in Alam et al. and also Roberts (1983) for four current speeds: zero, 10th percentile (0.027 m/s); 50th percentile (0.078 m/s); and 90th

percentile (0.146 m/s). The length scale ratios ℓ_m/ℓ_b and s/ℓ_b fall within the range at which dilutions can be estimated from the line plume results, figure 8 of paper I. Following Roberts (1983) we estimate dilutions for perpendicular currents only. For example, at u = 0.146 m/s, $F = u^3/b = 1.20$, for which figure 8 (or eq. 14) of paper I yields $S_m qN/b^{2/3} = 1.74$ hence $S_m = 1.74b^{2/3}/qN = 118$. The concentration profiles for this case would be similar to those shown in Figure 2b except that the plume merging would be even more rapid than shown due to the smaller value of s/ℓ_b and the staggered ports of the proposed outfall. Calculation of the flux-averaged dilution S_a, which would be desirable for comparison with the predictions of Alam et al. and Roberts (1983), presents a problem, however, as we do not know the ratio S_a/S_m with great precision. As discussed in paper I this ratio should lie between $\sqrt{2}$, for a stagnant line plume, and 1.9, which is the *spatial* average dilution ratio at this current speed as shown in figure 9 of paper I; the ratio for nonmerged point plumes in stagnant flows is about 1.73. Thus the average dilution is predicted to lie between 165 and 222. The variation of minimum dilution with distance would be expected to follow the line plume results and so can be predicted from figure 4 of paper II. From this figure (or eq. 11 of paper II) we estimate the mixing distance, the distance to achieve asymptotic dilution, is $x_a = 8.5\ell_b F^{1/3} = 47$ m; slower current speeds will result in smaller values of x_a. As discussed previously, the primary effect of increased port spacing is to increase z_t/ℓ_b, and at $s/\ell_b = 1.30$ and F = 1.20, Figure 5 yields $z_t/\ell_b \approx 3.0$ or $z_t = 3.0\ell_b = 15.5$ m. From Table 4 we find $z_a/z_t \approx 0.66$ and $h_a/z_t = 0.89$, so $z_a = 0.66z_t = 10.2$ m and $h_a = 0.89z_t = 13.8$ m. Results for the other current speeds were calculated in similar fashion and are summarized in Table 4.

Although the primary objective of this section is to demonstrate use of the present results, a few comments comparing the estimates of Table 4 with those of table 16 in Roberts (1983) are warranted. The new estimates of dilution are higher than those given using Roberts (1979) model and given in column 5 of table 16. The reasons for this difference were discussed in paper I where it was shown that direct application of *unstratified* results to the *stratified* case, which was the basis of Roberts (1979) model, results in an underestimation of dilution even though the line plume

approximation is valid and the trend of the predictions is correct. Due to these differences we no longer advocate use of the original model, but rather recommend use of the new results as presented in these papers. Thus, although the predictions using Roberts' (1979) model were low, the strong assertion of Alam et al. that this was caused by neglect of momentum effects and that momentum plays a significant role in increasing dilution must be definitely rejected, and the primary reason for their very low estimates using Roberts' model was their incorrect use of minimum rather then average dilution. As concluded by Roberts (1983) the other estimates of dilution presented by Alam et al. are too high, and this remains true even with the increased estimates of dilution given here. In using Abraham's and Roberts' models, Alam et al. assumed that the plumes rose to the thermocline, a distance of 17.8 m. The present results predict a smaller rise height and show that even a seemingly weak stratification below the thermocline can reduce rise height and dilution, especially at high current speeds.

The effect of increasing jet momentum can be demonstrated by decreasing the port size to 4 inches (0.102 m) from the original nominal design value of 6 inches (0.152 m) while holding the total discharge and port spacing constant. The densimetric jet Froude number F_j is about 10 for the original design, somewhat lower than typical designs, and about 27 for the 4 inch nozzle, somewhat higher than typical. The jet velocity u_j increases to 4.25 m/s, the momentum flux m (which is directly proportional to u_j for fixed q) increases to 4.46×10^{-2} m^2/s^4, and ℓ_m increases to 2.38 m. Then $\ell_m/\ell_b = 0.46$ and s/ℓ_b remains unchanged at 1.30. This value of 0.46 is approaching the upper limit of that studied here ($\ell_m/\ell_b = 0.50$) but is still within the range at which dilution can be estimated by the line plume results, and the dilution predictions of Table 4 still apply. The rise height is affected, however, and Figure 7 gives $z_t/\ell_b \approx 2.5$ at $s/\ell_b = 1.30$ and $F = 0$. (For intermediate values of ℓ_m/ℓ_b, interpolation between Figures 5 and 7 can be used to estimate z_t/ℓ_b). Thus, $z_t = 2.5\ell_b = 13.0$ m, considerably lower than the 16.2 m estimated for the original design. Rise heights at other current speeds can also be estimated from Figure 7.

It should be noted that the effect of source momentum flux depends on the shape of the ambient density profile. For linear profiles, as studied here, increasing momentum flux causes a

reduced rise height at low current speeds but leaves the dilution relatively constant. For profiles which are uniform over some depth, e.g. up to the thermocline, the plume will always rise to the same height regardless of current or source conditions. In this case, increased momentum flux can result in a longer entrainment path and increased dilution. Whether this will occur depends on the ratio ℓ_m/H (or ℓ_M/H) where H is the rise height. If $\ell_m/H << 1$ the momentum effect is negligible and dilution will be buoyancy dominated; if $\ell_m/H >> 1$ dilution will be increased by the momentum flux.

SUMMARY AND CONCLUSIONS

Results were presented to show the effects of port spacing and source momentum flux on submerged wastefield characteristics, particularly the way in which they cause deviations from the line plume results. Within the range of parameters tested ($\ell_m/\ell_b \leq 0.50$ and $s/\ell_b \leq 1.92$) dilutions are closely approximated by the line plume results and the primary effect of increasing port spacing and momentum flux is on the wastefield rise height and thickness. For $\ell_m/\ell_b \leq 0.2$ and $s/\ell_b \leq 0.31$ the flows approximate those due to line plumes and the results of paper I can be used to predict wastefield characteristics. For $0.31 \leq \ell_m/\ell_b < 0.50$ and $0.31 \leq s/\ell_b < 1.92$ dilution can still be estimated from the line plume results to within about 10% but rise height and thickness should be estimated from the graphical and tabular results (Figures 5 through 8 and Table 1) with interpolation where necessary.

For widely spaced ports ($s/\ell_b = 1.92$) under stagnant conditions, the individual plumes do not merge prior to entering the horizontal layer (Figure 1a). The rapid spreading of the plumes at collapse, however, causes a horizontally homogeneous wastefield to form (Figure 2a). Dilution for this case can be estimated from point plume results although the line plume approximation also yields close estimates. Rise height can also be estimated from point plume relations but wastefield thickness cannot be due to plume merging after collapse.

For a flowing perpendicular current the plumes merge prior to turbulence collapse forming a very laterally uniform wastefield, Figure 2b, and for parallel currents they merge by direct

impingement, Figures 1b, c, and d. Thus, point plume results are not applicable for flowing currents for $s/\ell_b \leq 1.92$ and plume merging must be considered.

The primary effect of increasing momentum flux is to decrease rise height at low current speeds. For narrowly spaced jets ($s/\ell_b \leq 0.31$) and perpendicular currents with $F \geq 10$ the effect of the momentum flux (at least up to $\ell_m/\ell_b = 0.50$) becomes negligible (Figures 3 and 7) and the discharge is again buoyancy dominated. This is because the jets are rapidly swept downstream by the current and the momentum flux effect is confined to a fairly short region near the nozzles. At low or stagnant current speeds the lowered rise height caused by the increased momentum flux results in a fairly constant entrainment path length of the jets compared to pure plumes and therefore little change in dilution.

An example showing application of the results to a previously proposed design for the Boston MDC outfall is given. Predictions are summarized in Table 4 and it is concluded that jet momentum plays little role in the mixing process but the wide port spacing will cause some deviations in rise height from line plume results. The port diameter is then decreased from 6 to 4 inches and it is shown how the results can be used to predict the effect of the increased momentum flux. It is found that the effect is to decrease the rise height while leaving dilution unaffected.

The dominant diffuser design parameters which determine dilution are the source buoyancy flux b and diffuser orientation θ over the range of parameters studied. Because $b = qg(\rho_a-\rho_o)/\rho_a$ and as g, ρ_a and ρ_o are essentially constant for all municipal sewage discharges into coastal waters, the dominant source parameter is the discharge per unit length, q. As the total discharge Q is presumably specified, that leaves only the diffuser length L as the primary design variable with the diffuser details, i.e. port spacing and diameter, exerting little influence on effluent dilution for a fairly wide range of typical outfall conditions.

APPENDIX I - REFERENCES

Abraham, G., Frick, W.E., Ludwig, R.G., and Roberts, P.J.W. (1983). Discussion of "Evaluation of Selected Initial Dilution Models," J. Environ. Engrg. ASCE, Vol. 109, No. 5, pp. 1213-1222.

Alam, A.M.Z., Harleman, D.R.F., and Colonell, J.M. (1982). "Evaluation of Selected Initial Dilution Models," J. Environ. Engrg. Div., ASCE, Vol. 108, No. EE1, pp. 159-186 and closure to discussion (1984) Vol. 110, No. 4, pp. 857-860.

Chu, V.H. (1979). "L.N. Fan's Data on Buoyant Jets in Crossflow," J. Hydraul. Div., ASCE, Vol. 105, No. HY5, pp. 612-617.

Koh, R.C.Y. (1982), "Initial Sedimentation of Waste Particles Discharged From Ocean Outfalls." Environ. Sci. Technol., Vol. 16, No. 11, pp. 757-763.

Muellenhoff, W.P., Soldate, A.M., Baumgartner, D.J., Schuldt, M.D., Davis, L.R., and Frick, W.E. (1985). "Initial Mixing Characteristics of Municipal Ocean Discharges," U.S. Environ. Prot. Agency, Rept. No. EPA-600/3-85-073a.

Roberts, P.J.W. (1979). "A Mathematical Model of Initial Dilution for Deepwater Ocean Outfalls." Proc. of Specialty Conf. on Conservation and Utilization of Water and Energy Resources, San Francisco, Aug. 8-11, pp. 218-225.

Roberts, P.J.W. (1983). Discussion of "Evaluation of Selected Initial Dilution Models," J. Environ. Engrg., ASCE, Vol. 109, No. 5, pp. 1218-1222.

Roberts, P.J.W., Snyder, W.H., and Baumgartner, D.J. (1987). "Submerged Wastefield Formation by Ocean Outfalls," Submitted to J. Hydr. Engrg., ASCE.

Roberts, P.J.W. and Snyder, W.H. (1987). "The Spatial Evolution of Submerged Wastefields," submitted to J. Hydr. Engrg., ASCE.

Wong, D.R. (1985). "Buoyant Jet Entrainment in Stratified Fluids," Dept. of Civil Engrg., Univ. of Michigan, Ann Arbor, Rept. No. UMCE 85-9.

Wright, S.J., et al. (1982). "Outfall Diffuser Behavior in Stratified Ambient Fluid," J. Hydraulics Div., ASCE, Vol. 108, No. HY4, pp. 483-501.

Wright, S.J. (1984). "Buoyant Jets in Density-Stratified Crossflow," J. Hydr. Engrg., ASCE, Vol. 110, No. 5, pp. 643-656.

APPENDIX II - NOTATION

The following symbols were used in this paper:

b = total source buoyancy flux per unit diffuser length, $g_o'q$;

B = buoyancy flux of a round jet, $g_o'Q_j$;

d = port diameter;

F = Froude number, u^3/b;

F_j = jet Froude number, $u_j/\sqrt{(g_o'd)}$;

g = acceleration due to gravity;

g_o' = modified acceleration due to gravity, $g(\rho_a-\rho_o)/\rho_a$;

h_a = wastefield thickness;

H = wastefield rise height in unstratified ambient;

L = diffuser length;

ℓ_a = length scale for round jet, u/N;

ℓ_b = two-dimensional length scale; $b^{1/3}/N$;

ℓ_B = length scale for round jet; $B^{1/4}/N^{3/4}$;

ℓ_m = two-dimensional length scale, $m/b^{2/3}$;

ℓ_M = length scale for round jet, $M^{3/4}/B^{1/2}$;

ℓ_u = length scale for round jet, B/u^3;

M = total source momentum flux per unit diffuser length, u_jq;

M = source momentum flux of round jet, u_jQ_j;

n = total number of diffuser ports;

N = buoyancy frequency, $\sqrt{(-gd\rho/\rho_a dz)}$

q = total discharge per unit diffuser length; Q/L;

Q = total discharge from multiport diffuser;

Q_j = discharge of round jet;

s = port spacing;

S_a = flux-averaged dilution;

S_m = minimum dilution;

S_o = centerline dilution of round jet;

u = speed of ambient current;

u_j = jet exist velocity;

x_a = distance from diffuser at which asymptotic minimum dilution is reached;

z_a = height to level of minimum dilution at x_a;

z_m = maximum rise height of round jet;

z_t = height to top of wastefield at x_a;

θ = angle of ambient current to diffuser;

ρ = ambient density;

ρ_a = ambient density at level of ports;

ρ_o = effluent density.

Table 1. Ratios of layer thickness and minimum dilution heights to rise height.

Ratio (1)	Current direction, θ (degrees) (2)	Froude number, $F = u^3/b$ (3)	Mean value (4)	Standard deviation (5)	Range (6)
$\frac{z_a}{z_t}$	All	All	0.66	0.07	0.53 - 0.77
$\frac{h_a}{z_t}$	90	≥10	0.94	0.08	0.79 - 1.00
$\frac{h_a}{z_t}$	90	0.1-10	0.89	0.11	0.65 - 1.00
$\frac{h_a}{z_t}$	90	≤0.1	0.75	0.12	0.50 - 0.93
$\frac{h_a}{z_t}$	0	≥0.1	0.82	0.07	0.64 - 0.96

Table 2. Results for low momentum flux jets in stagnant flow and comparison of predictions with line- and point-plume results

Test number	Port Spacing s, (cm)	Rise height, z_t (cm)		Layer thickness, h_a (cm)		Minimum dilution, S_m		
		Observed	Calculated from point plume formula, Eq. 3b	Observed	Calculated from point plume formula, Eq. 3c	Observed	Calculated from point plume formula, Eq. 3a	Calculated from line plume formula, Eq. 3~~5~~
(1)	(2)	(3)	(4)	(5)	(6)	(7)	(8)	(9)
3-11-4	5	43	40	30	16	76	102	76
6-11-2	10	44	42	27	17	87	101	93
9-11-2	20	40	39	20	16	103	100	116

Table 3. Results for low momentum flux, widely spaced jets in perpendicular currents and comparison with predictions of line- and point-plume results

Test number	Froude number, $F = u^3/b$	Minimum dilution, S_m			Height to S_m, z_a (cm)		
		Observed	Calculated from point plume formula, Eq. 8	Calculated from line plume formula, Eq. 9	Observed	Calculated from point plume formula, Eq. 6c	Calculated from line plume results,
(1)	(2)	(3)	(4)	(5)	(6)	(7)	(8)
9-12-2	0.112	131	218	120	24	23	19
9-13-1	1.16	214	289	211	23	17	17
9-14-1	9.68	287	316	290	15	13	9
9-15-1	99.5	469	411	461	12	10	6

Table 4. Application of Results to Proposed Boston MDC Outfall

Ambient current	Froude number, $F=u^3/b$	Rise height to top of wastefield z_t (m)	Wastefield thickness, h_a (m)	Height to level of minimum dilution, z_a (m)	Minimum dilution, S_m	Average dilution, S_a
(1)	(2)	(3)	(4)	(5)	(6)	(7)
zero current	0	16.2	12.2	10.7	59	83-112
10th percentile	0.007	16.2	12.2	10.7	59	83-112
50th percentile	0.176	15.6	13.9	10.3	72	102-137
90th percentile	1.160	15.5	13.8	10.2	117	165-222

APPENDIX III - Summary of Experimental Parameters, Series 5 to 11.

Test no.	Current direction	Current speed	Port spacing	Discharge per port	Modified acceleration due to gravity	Sample distance	Buoyancy frequency	Height to top of wastefield	Wastefield thickness	Height to minimum dilution	Minimum dilution	Average dilution	Reynolds number
		u	s	Q_j	g_o'	x	N	z_t	h_a	z_a	S_m	S_a	Re
	(degrees)	(cm/s)	(cm)	(cm^3/s)	(cm/s^2)	(cm)	(s^{-1})	(cm)	(cm)	(cm)			
(1)	(2)	(3)	(4)	(5)	(6)	(7)	(8)	(9)	(10)	(11)	(12)	(13)	(14)
5-11-1	90	0	5	5.83	46.2	52	0.295	35	30	23	29.5	63.6	2312
5-12-1	90	2.3	5	5.77	46.1	102	0.295	37	34	23	32.1	61.0	2289
5-13-1	90	4.9	5	5.78	46.1	202	0.295	31	31	19	47.7	87.4	2291
5-14-1	90	10.3	5	5.57	49.5	602	0.324	25	25	14	83.8	174.0	2211
5-15-1	90	22.2	5	5.78	49.5	802	0.324	18	18	10	126.4	-	2296
5-23-1	0	4.8	5	5.67	49.5	233	0.324	38	34	26	50.2	98.4	2248
5-24-1	0	10.3	5	5.75	46.4	433	0.305	35	31	24	56.4	133.3	2280
5-25-1	0	22.2	5	5.72	46.4	833	0.305	28	27	20	70.4	183.5	2270
6-11-1	90	0	10	2.85	115.4	17	0.295	47	30	36	82.2	161.4	1128
6-11-2	90	0	10	2.72	115.4	52	0.295	44	27	32	87.1	159.2	1079
6-12-1	90	1.8	10	2.55	115.4	28	0.295	44	34	30	85.7	182.6	1009
6-12-2	90	1.8	10	2.67	115.4	102	0.295	43	31	32	97.7	184.7	1057
6-12-3	90	1.8	10	2.55	115.4	52	0.295	41	32	24	97.0	178.0	1011
6-13-1	90	3.9	10	2.30	114.3	202	0.302	33	29	22	165.7	343.5	910
6-13-2	90	3.9	10	2.70	114.3	77	0.302	36	31	26	129.3	277.7	1070
6-14-1	90	8.4	10	2.18	114.3	202	0.302	30	30	18	66.6	126.5	866
6-14-2	90	8.4	10	2.52	114.3	152	0.302	30	29	16	262.8	543.1	995
8-11-1	90	0	10	5.87	48.8	52	0.300	31	25	22	44.8	91.4	2327
8-12-1	90	1.8	10	5.80	48.8	52	0.300	34	32	22	38.6	75.2	2297
8-12-2	90	1.8	10	5.77	47.8	102	0.300	34	28	22	41.5	-	2288
8-13-1	90	3.9	10	5.90	47.8	202	0.300	30	30	18	66.6	126.5	2340
8-23-1	0	3.9	10	5.72	47.8	233	0.300	30	24	18	56.1	109.3	2267
9-11-1	90	0	20	2.27	114.2	28	0.306	39	20	28	103.2	-	898
9-12-1	90	1.5	20	2.28	114.2	102	0.306	34	22	24	133.2	210.5	907
9-12-2	90	1.5	20	2.27	114.2	202	0.306	35	25	24	131.8	-	897
9-13-1	90	3.2	20	2.13	114.2	202	0.306	31	20	23	214.5	-	845
9-13-2	90	3.2	20	2.13	114.2	102	0.306	31	23	23	217.8	400.9	847
9-13-3	90	3.2	20	2.17	114.2	52	0.306	35	26	27	185.7	401.6	857
9-14-1	90	6.8	20	2.35	118.6	402	0.343	28	22	15	286.8	-	932
9-15-1	90	14.6	20	2.27	118.6	502	0.343	22	21	12	469.3	-	897
9-23-1	0	3.2	20	2.48	115.3	233	0.306	27	20	20	127.8	268.2	983
9-24-1	0	6.8	20	2.47	115.3	433	0.306	27	19	20	126.7	294.4	976
9-24-2	0	6.8	20	2.23	117.6	433	0.301	26	22	16	144.0	381.8	884
9-25-1	0	14.6	20	2.50	115.3	533	0.306	24	20	16	223.1	-	989
11-11-1	90	0	20	5.72	46.4	52	0.307	27	18	16	43.1	83.1	2269
11-12-1	90	1.5	20	5.97	46.4	102	0.307	29	27	20	51.3	102.5	2364
11-13-1	90	3.2	20	6.08	46.4	202	0.307	26	23	20	72.8	-	2413
11-14-1	90	6.8	20	6.08	46.4	402	0.307	21	20	15	121.2	256.6	2410
11-23-1	0	3.2	20	6.45	46.4	233	0.307	20	17	10	50.1	104.0	2560
11-24-1	0	6.8	20	6.28	46.4	433	0.307	21	18	15	73.2	172.3	2491

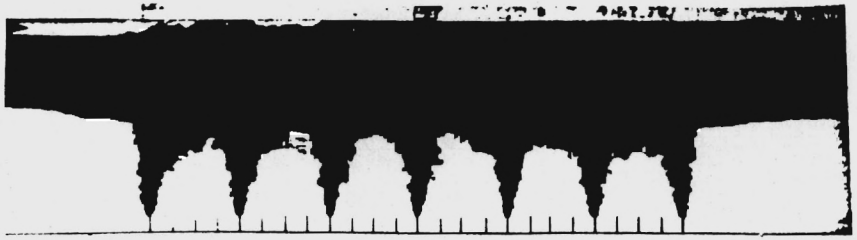

a) F=0

b) F=1

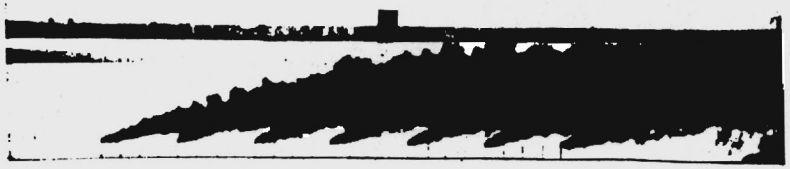

c) F=10

d) F=100

Figure 1. Sideview Photographs of Widely Spaced Jets of Low Momentum Flux (Series 9) in Stagnant and Parallel Currents.

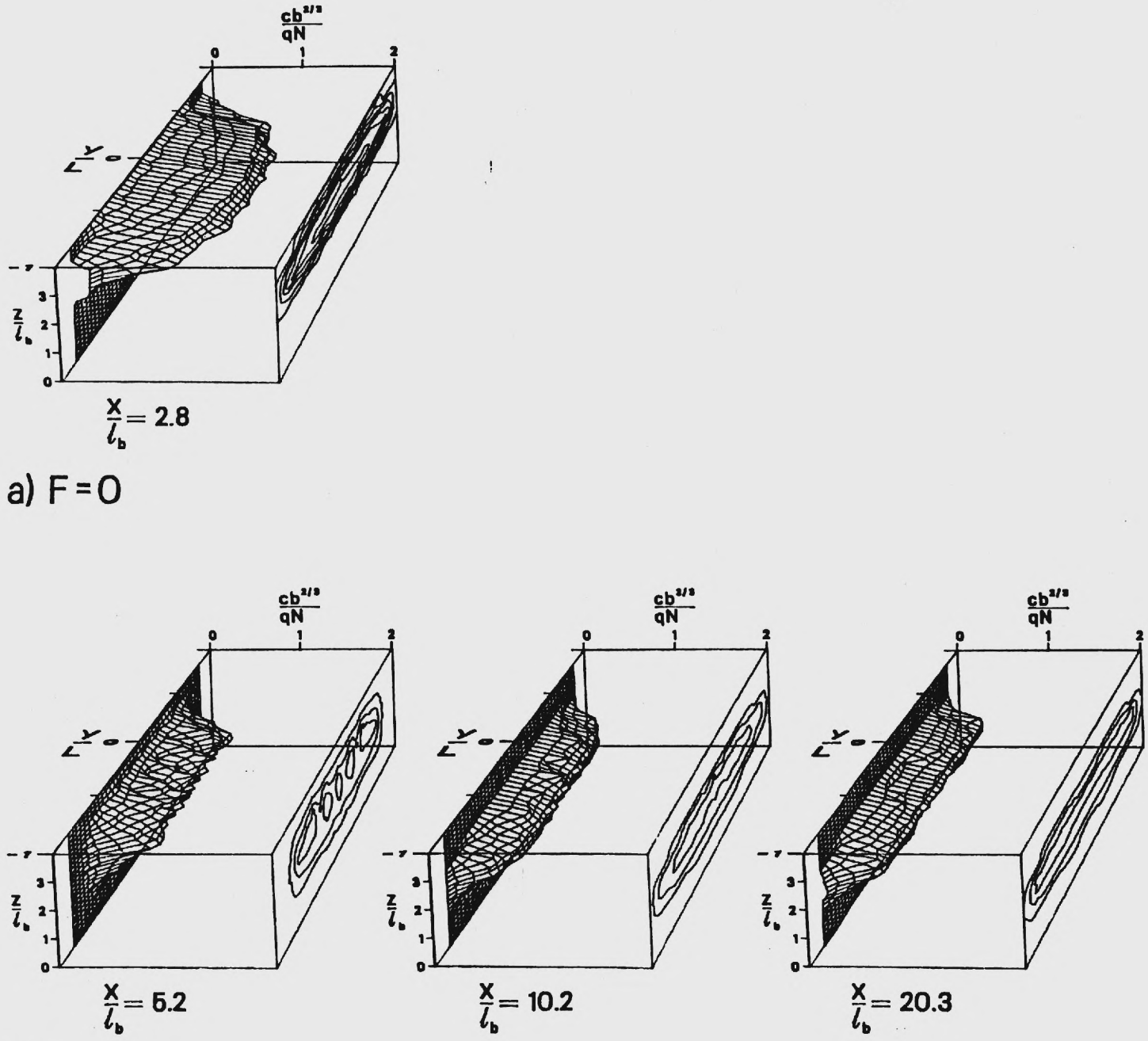

Figure 2. **Normalized Concentration Profiles of Widely Spaced Jets of Low Momentum Flux (Series 9) in a Stagnant and a Perpendicular Current.**

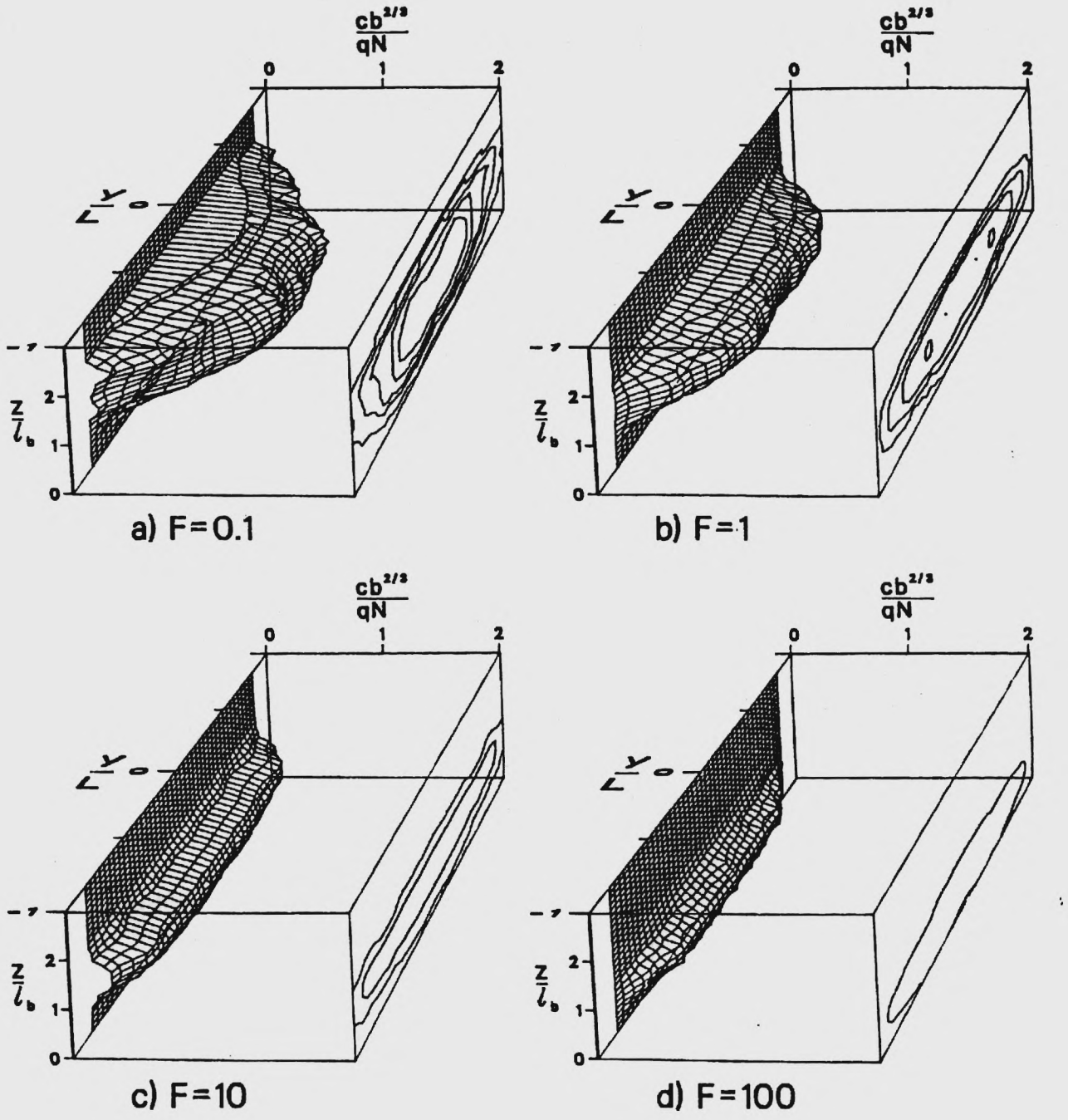

Figure 3. Normalized Concentration Profiles for Narrowly Spaced Jets of High Momentum Flux (Series 5) in Perpendicular Currents.

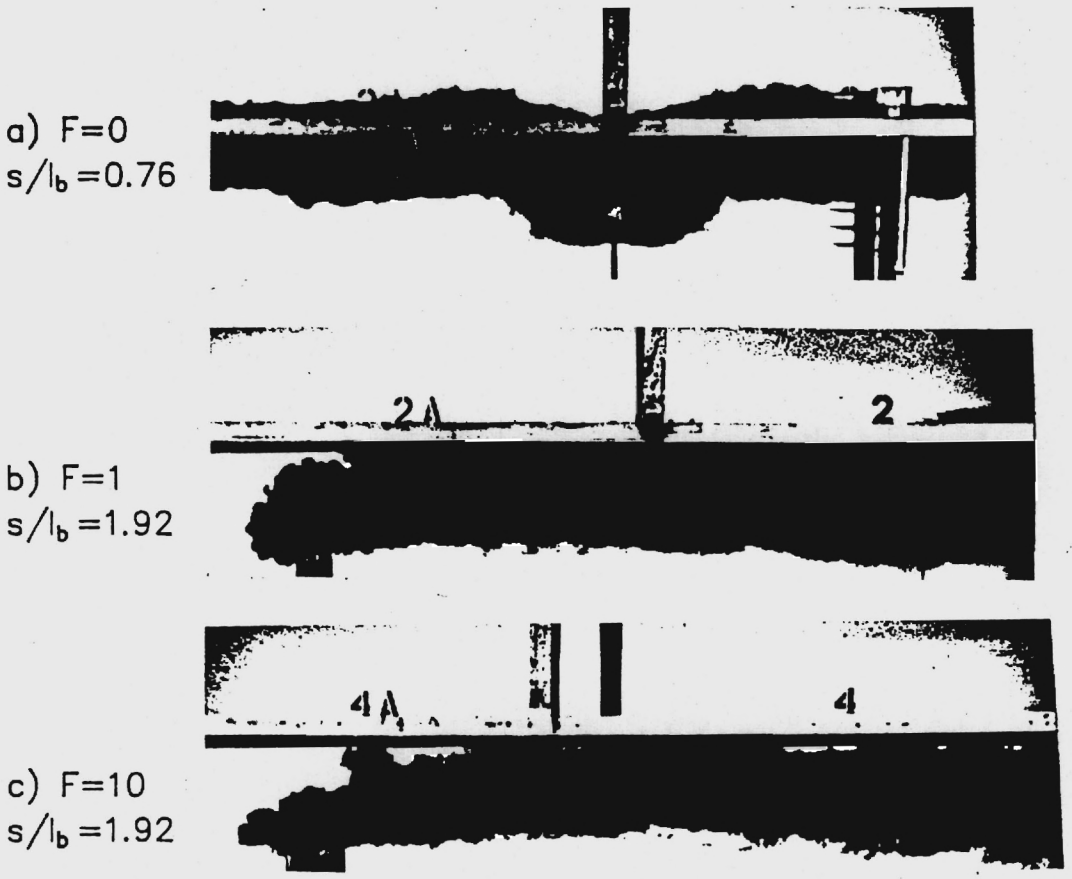

Figure 4. Photographs of High Momentum Flux Jets (Series 8 and 11) in Stagnant and Perpendicular Currents.

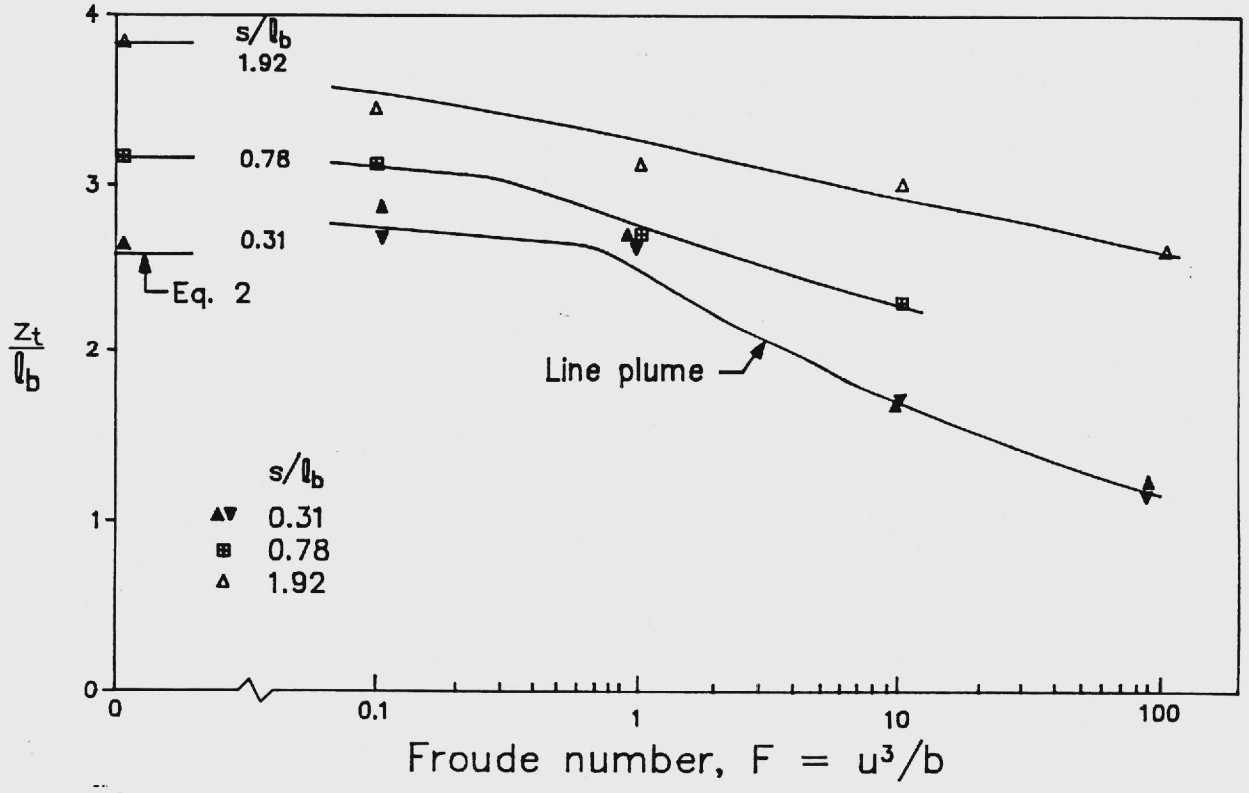

Figure 5. Height to Top of Wastefield for Low Momentum Flux Jets (l_m/l_b = 0.078) in Perpendicular Currents.

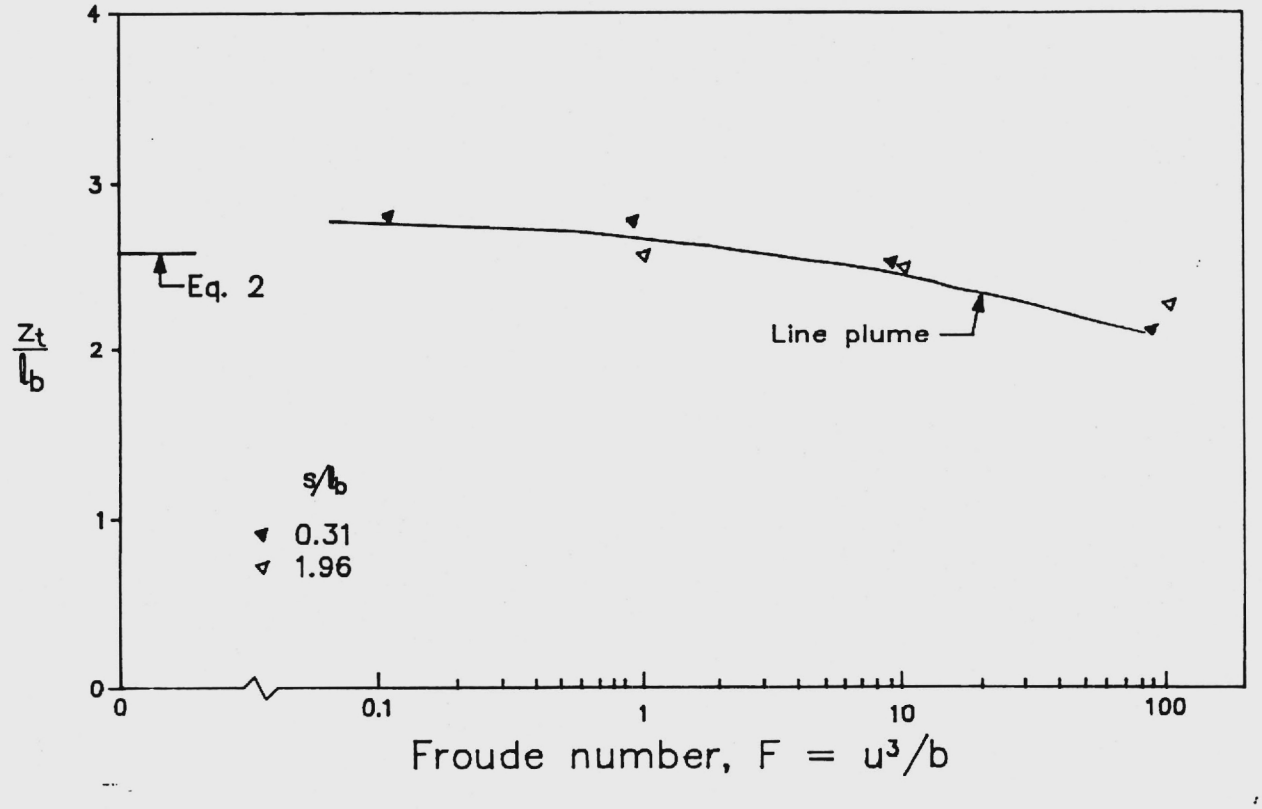

Figure 6. Height to Top of Wastefield for Low Momentum Flux Jets (l_m/l_b = 0.078) in Parallel Currents.

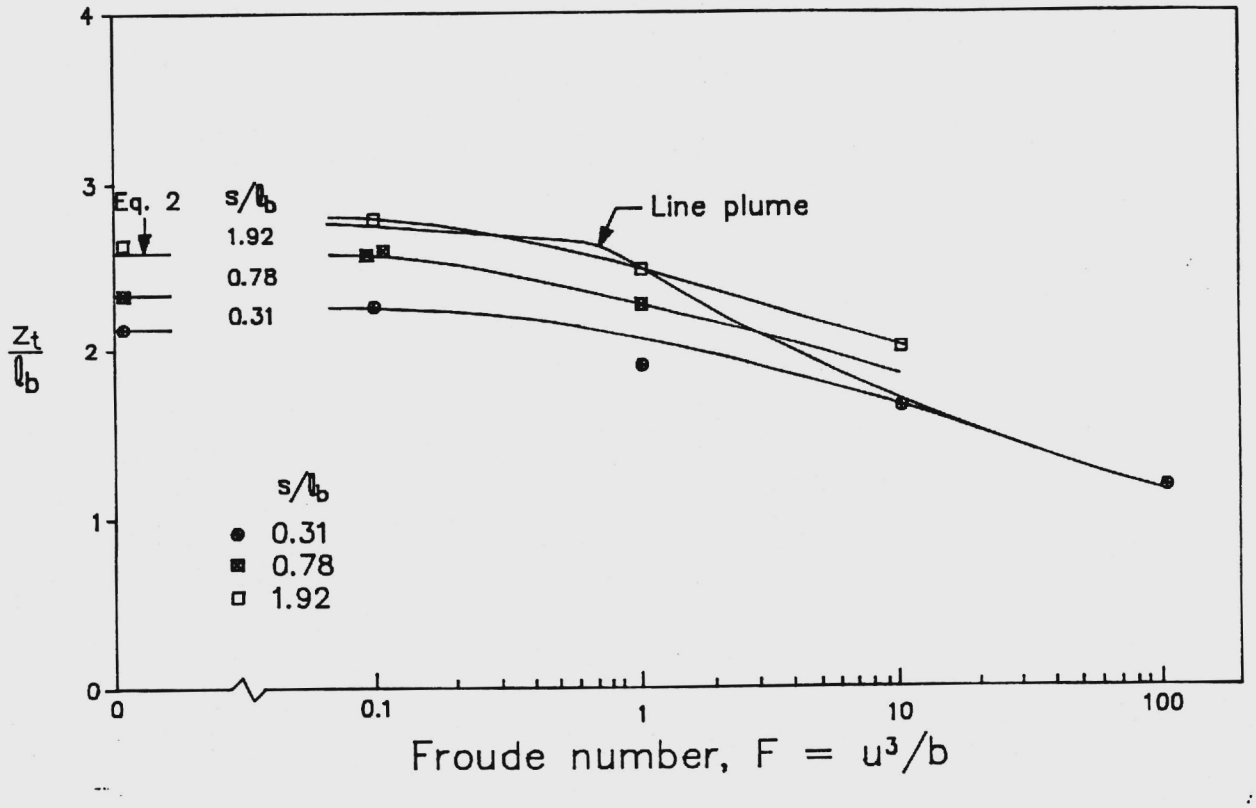

Figure 7. Height to Top of Wastefield for High Momentum Flux Jets (l_m/l_b = 0.50) in Perpendicular Currents.

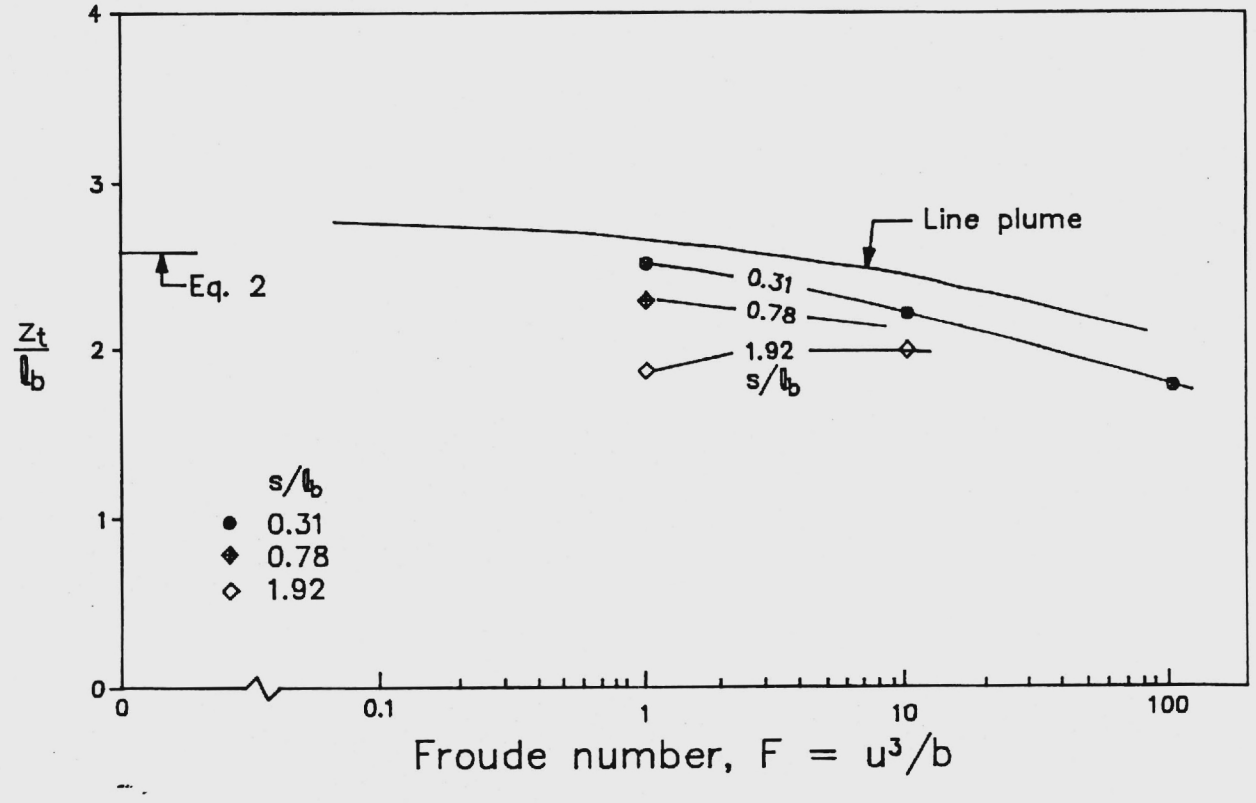

Figure 8. Height to Top of Wastefield for High Momentum Flux Jets (l_m/l_b = 0.50) in Parallel Currents.

SUBMERGED WASTEFIELD FORMATION BY OCEAN OUTFALLS

by

Philip J.W. Roberts[1], M. ASCE, W.H. Snyder[2] and D.J. Baumgartner[3]

ABSTRACT

The results of experiments to study the dilution and formation of wastefields caused by discharge from a diffuser into a linearly density-stratified steady current of arbitrary speed and direction are presented. Experiments were conducted using a model multiport diffuser for a range of parameters typical of ocean outfalls. In this paper, gross results for "line plume" source conditions are given. In general, the wastefield rise height and thickness decrease and dilution increases with current speed. Diffusers perpendicular to the current result in higher dilutions than when parallel, but even parallel diffusers show dilutions which increase with current speed and which are always higher than under stagnant conditions. Effluent concentration profiles for perpendicular currents show little horizontal structure as the individual plumes rapidly merge. The results for dilution show no dependency on port spacing or source momentum flux over the parameter range tested, and the dominant source parameter is the buoyancy flux per unit length. The results confirm the value of the "line plume" approximation for predicting dilutions for deepwater ocean outfalls over a fairly wide parameter range.

---

[1]Assoc. Prof. of Civil Engrg., Georgia Inst. of Tech., Atlanta, Ga. 30332

[2]Meteorology and Assessment Division, U.S. Environmental Protection Agency, Research Triangle Park, North Carolina 27711. On assignment from the National Oceanic and Atmospheric Administration, U.S. Dept. of Commerce

[3]Director, Pacific Division, Environmental Research Laboratory, Hatfield Marine Science Center, Newport, OR. 97365.

INTRODUCTION

It is common practice to design ocean outfall diffusers so that the natural density stratification present in the ocean is utilized to produce a submerged wastefield. In order to design the outfalls and to assess the environmental impact of the discharge it is necessary to predict the characteristics of the wastefield formed, particularly the depth of submergence, wastefield thickness, and dilution. Prediction of these characteristics is a difficult task, however, due to the many variables involved which include ambient parameters such as stratification and currents, and design variables such as port spacing and diameter and jet efflux velocity. Although numerical models to predict dilution and rise height have been developed, there are few experimental data available to verify these models, particularly for flowing density-stratified currents.

An extensive series of experiments was performed in a large density-stratified towing tank in order to study the dynamics of merging buoyant jets and the formation of wastefields in density-stratified currents of arbitrary speed and direction, and to obtain results for the verification and testing of mathematical models of initial dilution. Roberts (1979a) has shown that the effects of finite diffuser length are important, even for very long diffusers perpendicular to the current, and in the present experiments the tank used was wide enough to accommodate long diffusers which are shorter then the tank width, so that end effects will be generated. Almost 100 experiments were conducted, some of which involved replicate conditions sampled at different downstream distances so that about 50 different combinations of port spacing, jet velocity, effluent density, and current speed and direction were studied. Because of the large amount of data generated, the wide variety of conditions studied, and the many aspects of the problem considered, we have divided presentation of the results into three papers. In this paper we describe the overall experimental program and experimental procedures, explain the rationale for the range of parameters investigated, and present gross results of the experiments conducted under conditions such that the effect of port spacing and source momentum flux (or jet densimetric Froude number) are negligible. The flow for this case approximates a line plume, and this paper is analogous to that of Roberts

(1979a) who studied line plumes in an unstratified current. In that study, however, a line plume issuing from a slot source was used; in the present study a model multiport diffuser was used with the effluent issuing from a row of ports contained in Tee-shaped risers. The second paper (paper II) is also primarily concerned with line plume results, but discusses some of the more basic fluid mechanical aspects of wastefield formation, in particular the variation of dilution with distance, collapse of buoyancy induced turbulence, and lateral gravitational spreading. Finally, in the third paper (paper III) the effects of increased port spacing and source momentum flux (or jet Froude number) are discussed, and the results compared to those obtained for the line plume condition.

In this paper we first define the problem to be studied and then derive the dominant dimensionless groups which describe it. Values of these dimensionless groups are computed for typical operating outfalls and the parameter range chosen for the present experiments is explained. The experimental setup is described, and results presented for the line plume case. These results are the gross properties of interest in outfall design: dilution, rise height, and wastefield thickness. The basic flowfields are described and an application of the results is given.

ANALYSIS

The basic flow situation under consideration is shown in Figure 1. Buoyant effluent of density ρ_o issues horizontally at a velocity u_j from a round port of diameter d. The ports are paired in Tee risers which are spaced a distance s apart. The ambient density, ρ, decreases linearly with height, z, and has a value of ρ_a at the port level; a uniform ambient current flows at a speed u with an angle θ to the diffuser axis. Effluent dilution increases with distance from the diffuser until it reaches an asymptotic value at a distance denoted by x_a. At this distance, the thickness of the wastefield is h_a, the height to the level of maximum concentration is z_a, and the height to the top of the established wastefield is z_t.

The discharge can be characterized by the source fluxes per unit length of volume, q, momentum, m, and buoyancy, b:

$$q = \frac{Q}{L} , \quad m = u_j q , \quad b = g_o' q \tag{1}$$

where Q is the total discharge, L the diffuser length, and $g_o' = g(\rho_a - \rho_o)/\rho_a$ is the modified acceleration due to gravity. Following the notation of the literature on density stratified flows we characterize the ambient stratification by the buoyancy frequency, N:

$$N = \sqrt{-\frac{g}{\rho_a}\frac{d\rho}{dz}} \tag{2}$$

Any property, Φ, can then be expressed as:

$$\Phi = f(q, b, m, s, u, N, \theta) \tag{3}$$

In which we have assumed the flow to be fully turbulent and independent of molecular viscosity and Reynolds number effects. Following Wright et al. (1982) we define three length scales:

$$\ell_q = \frac{q^2}{m}, \quad \ell_b = \frac{b^{1/3}}{N}, \quad \ell_m = \frac{m}{b^{2/3}} \tag{4}$$

Note, however, that Wright et al. base their length scales on the fluxes from each side of the diffuser, whereas our length scales are based on the total fluxes. A dimensional analysis of Eq. 3 yields, when expressed in terms of the length scales of Eq. 4:

$$\Phi = f\left[\frac{\ell_q}{\ell_b}, \frac{\ell_m}{\ell_b}, \frac{s}{\ell_b}, \frac{u^3}{b}, \theta \right] \tag{5}$$

For the range of conditions typical of ocean outfalls, ℓ_q/ℓ_b is much less than one and can be neglected as the source volume flux, q, has little dynamic effect in determining plume behavior except very near to the ports (Brooks 1980, Wright et al. 1982). The ratio u^3/b is a type of Froude number, denoted by F, used by Roberts (1979a) to describe the results of line plume experiments. Thus Eq. 5 becomes:

$$\Phi = f\left[\frac{\ell_m}{\ell_b}, \frac{s}{\ell_b}, F, \theta \right]. \tag{6}$$

For example, the geometrical properties defined in Figure 1 can be expressed in terms of length scale ratios:

$$\frac{z_t}{\ell_b}, \frac{h_a}{\ell_b}, \frac{z_a}{\ell_b} = f\left[\frac{\ell_m}{\ell_b}, \frac{s}{\ell_b}, F, \theta\right] \tag{7}$$

The corresponding normalized expression for dilution has been given many times (Fischer et al. 1979, Roberts 1979b, Brooks 1980) and is, in the present notation:

$$\frac{S_m q N}{b^{2/3}} = f\left[\frac{\ell_m}{\ell_b}, \frac{s}{\ell_b}, F, \theta\right] \tag{8}$$

where S_m is the minimum dilution, defined as the smallest value of dilution observed in a vertical plane through the wastefield at the distance x_a.

RANGE OF PRESENT EXPERIMENTS

For zero crossflow, Eqs. 7 and 8 become:

$$\frac{S_m q N}{b^{2/3}}, \frac{z_t}{\ell_b}, \frac{h_a}{\ell_b}, \frac{z_a}{\ell_b} = f\left[\frac{\ell_m}{\ell_b}, \frac{s}{\ell_b}\right] \tag{9}$$

A limiting case of Eq. 9 is when ℓ_m/ℓ_b and s/ℓ_b both tend to zero, that is, closely spaced jets of small momentum flux. This is the "line plume" situation in which the effects of port spacing and jet momentum flux are negligible, and the flow behaves like one generated from a source of buoyancy flux only. Eq. 9 then becomes:

$$\frac{S_m q N}{b^{2/3}}, \frac{z_t}{\ell_b}, \frac{h_a}{\ell_b}, \frac{z_a}{\ell_b} = C_1, C_2, C_3, C_4 \tag{10}$$

where C_1 through C_4 are experimental constants.

The functional form of Eq. 9 can be predicted from mathematical models. For example, the dilution and terminal rise height of merging buoyant jets in a stratified, stagnant ambient have been modeled by Koh and Fan (1970), Wright, et al. (1982), Muellenhoff, et al. (1985) and others. Wright et al. have presented curves showing the dependency of S_m, z_t, z_a, and h_a on the length scale ratios. Their results for dilution are shown in Figure 2 which suggests that dilution becomes

independent of ℓ_m/ℓ_b and s/ℓ_b for $\ell_m/\ell_b < 0.1$ and $s/\ell_b < 0.3$.

The purpose of the present experiments was to obtain results representative of typical ocean outfalls. In order to decide the range of parameters to study, length scale ratios were computed for several major operating outfalls using typical density stratifications and design parameters given in Fischer et al. (1979), table 10.1. The results, plotted on Figure 2, suggest that most of these outfalls operate such that the source momentum flux exerts little influence on dilution. The diffusers with very widely spaced ports ($s/\ell_b > 3$) are those of the Cities of Los Angeles and San Diego, both of which were placed into operation before 1964; the trend in outfall design since then has been to use more ports which are more closely spaced. Based on these considerations, it was decided to perform experiments covering the cross-hatched range shown in Figure 2. Tests were conducted for ℓ_m/ℓ_b = 0.078, 0.20, and 0.50, and s/ℓ_b = 0.31, 0.78, and 1.92, corresponding to model port spacings, s, of 5, 10, and 20 cm, and nominal jet Froude numbers, $F_j = u_j/\sqrt{g_o'd}$, of 5, 10, and 20. Tests were run for most of these source conditions at $F = u^3/b$ = 0, 0.1, 1, 10, and 100, and with diffusers oriented perpendicular, at 45°, and parallel to the current to cover the same range as for the *unstratified* line plume experiments of Roberts (1979a). The large number of conditions tested poses a problem in identifying them in the graphical presentations of results. We attempt to solve this by marking each source condition with a symbol and "series number" as shown in Figure 2. In subsequent plots, the symbols shown are used for perpendicular currents, for parallel currents they are rotated 45° clockwise, and for 45° currents (series 3 only) they are rotated 180°. In subsequent tables, the first digit of the test number is the series number.

EXPERIMENTS

The experiments were conducted in the stratified towing tank of the U.S. EPA Fluid Modeling Facility in North Carolina. This large tank is 120 cm deep, 240 cm wide, and 25 m long, and is equipped with a carriage which allows models to be towed the length of the tank at speeds from 2 to 50 cm/s. The tank has an aluminum framework, and the sides and bottom are lined with acrylic plastic for viewing and photography; for more details of the tank, see Thompson and Snyder

(1976). The tank can be filled with salt water to an arbitrary stable stratification, but for the present series of experiments only linear density profiles were used. Ambient densities were measured by drawing water samples from various depths and measuring the weight of an object suspended in the sample with a Mettler PL200 electronic balance. Effluent densities were measured similarly, and the absolute error in specific gravity was estimated to be less than 0.0005. A nominal buoyancy frequency, N, of 0.3 s^{-1} and a multiport model diffuser 120 cm long were used in all experiments. This diffuser length is half the tank width so that three-dimensional flows were generated for all diffuser orientations. The risers were spaced 5 cm apart and larger port spacings were achieved by blocking off some of the feeder lines. The risers were approximately 30 cm long, 0.395 cm outside diameter, with a nozzle size of 0.318 cm. Each riser was fed separately by a line attached to a manifold box which was fed by a positive displacement pump and care was taken to ensure that each feeder line was similar and of the same length to achieve a uniform flow distribution among the ports.

The general configuration of the experiments, shown in Figure 3, is similar to that used by Isaacson et al. (1983) and others. A negatively buoyant effluent is discharged near the water surface and falls downward; the current is simulated by towing the diffuser at a constant speed. Blue dye was added to the effluent for flow visualization as well as quantitative dilution measurements which were obtained by drawing water samples by vacuum through a sampling array towed behind the diffuser. The array was in the shape of a 10x10 rectangular matrix, for a total of 100 sampling probes. The probe spacings were varied to match the expected results, but were usually non-uniform in the horizontal with a closer spacing near the diffuser centerline. The probes were connected to a sampling chamber by Tygon tubing, and approximately 50 cc of sample was drawn through each probe. The dye concentration of each sample was measured with a Brinkman Probe Colorimeter model PC/600 which had been calibrated with a set of 11 dye standards. The voltage output from the colorimeter was digitized on a PDP 11/40 minicomputer and the dye concentrations recorded for later analyses. The error in dilution calculated from dye concentrations is estimated to be less than 3%.

The usual experimental procedure was as follows. Ambient density profiles and effluent densities were measured and the tow speed and discharge rates calculated to match the desired parameter values. The sampling rake was purged of water by flushing with air and the effluent pump was started and allowed to run for a short time to enable the flow to establish. The towing carriage was started and, after a steady-state condition was established, sampling was begun. Sideview photographs were obtained with a 35mm camera equipped with a 100 mm lens to minimize parallax. Samples were obtained for 30 to 45 seconds after which the effluent pump was turned off and the towing carriage stopped. The test tubes, tow speed, probe locations, etc., were changed and the next test immediately run. In this way we were able to run several tests in rapid succession with no interference from previous tests. The effluent flowrate was measured with an error of less than 1% by timing the drop in the liquid level in the reservoir and the tow speed was measured by timing the passage of the carriage between two fixed points; it's error is also less than 1%.

In this paper we are concerned with properties of flows approximating those due to line plume discharges (series 3). None of the normalized results for series 4 experiments were found to differ significantly from those of series 3, however, and so series 3 and 4 experiments are summarized together in Appendix III as being representative of the "line-plume" results. The remaining experiments, in which deviations from the line plume results were observed, are summarized in paper III in which these effects are discussed. Also given in Appendix III are the nozzle Reynolds numbers, $Re = u_j d/\nu$, where ν is the kinematic viscosity.

GENERAL OBSERVATIONS

The following observation apply to the "line plume" source case (ℓ_m/ℓ_b = 0.078 and s/ℓ_b = 0.31, series 3). Bars visible in photographs are part of the external tank framework, and in no cases did the plume impact the water surface or the tank bottom.

Sideview photographs showing the effect of current speed on perpendicular diffusers are shown in Figure 4. The flowfield in a stagnant environment (Figure 4a) is similar to that described by

Wright et al. (1982). The two plumes from each side of the diffuser do not rapidly merge; they overshoot their equilibrium rise height before collapsing back to form a layer which is thick compared to the total rise height. As the current speed is increased only slightly to F = 0.1 (Figure 4b) the upstream layer is expelled and all of the flow is swept downstream. At F = 1 (Figure 4c) the plumes from the opposite sides of the diffuser rapidly merge forming a flow which is more appropriately described as resulting from a single plume. Another interesting feature of this case is the wave-like form of the wastefield; this pronounced wave does not appear at smaller or larger values of F. For F > 1 (Figures 4d and 4e), the plume bottom stays at the nozzle level and the rise height and thickness of the wastefield decrease rapidly with increasing current speed.

These photographs show similarities to the flow regimes found for unstratified crossflows by Cederwall (1971) and Roberts (1979a). At low current speeds, Figure 4b at F = 0.1, the flow has the normal plume-like pattern with the plume bent downstream by the current. As the current speed is increased, Figure 4d at F = 100, the plume cannot entrain all of the oncoming flow while maintaining the free plume pattern and becomes attached to the lower boundary. For unstratified flows, Cederwall predicted this transition to occur at F = 0.2 and denoted it as the forced entrainment regime and also predicted that an upstream wedge would form for 0.2 < F < 1 which was swept downstream when F > 1. The stratified flow regimes are somewhat different from this in that the upstream wedge is swept downstream by slower currents, at least for F > 0.1. Apparently, surfacing fields with residual buoyancy spread more rapidly in the lateral direction than submerged fields, as investigated further in the following paper. Also, the flow at F = 1, which resembles a large internal wave, has characteristics of both the free plume and forced entrainment regimes. The forced entrainment regime does not become fully established until the Froude number becomes greater than a value which lies somewhere between 1 and 10.

Concentration profiles across the plume for perpendicular currents at the asymptotic dilution distance x_a are shown in Figure 5. The profiles are expressed as:

$$\frac{cb^{2/3}}{qN} = f\left[\frac{z}{\ell_b}, \frac{y}{L}\right] \qquad (11)$$

in which c is the ratio of the local dye concentration to that in the discharge (i.e. the reciprocal of dilution) and the normalized expression for concentration is the reciprocal of the dilution expression, Eq. 8. The concentration profiles are shown as three-dimensional representations with two-dimensional contour plots projected onto the end plane; the outer contour level is 0.05 and the contour interval is 0.2. The profiles generally show little horizontal structure, the individual plumes having fully merged due to gravitational collapse, as was also observed by Isaacson et al. (1983). End effects can be seen due to the diffuser being shorter than the tank width. As these profiles are all plotted to the same scale it can be seen that as the current speed increases, the rise height and thickness decrease, and the minimum dilution increases.

The formation and dilution of wastefields in parallel currents are shown in the sideview photographs of Figure 6 and the concentration profiles of Figure 7. The individual Tee risers can be seen in these photographs and it is apparent that the individual plumes rapidly merge. As was observed for the perpendicular case, no upstream flow occurs for $F \geq 0.1$. The dark leading edge of the wastefield is caused by lateral spreading which begins at the front edge of the diffuser. The concentration profiles are not as horizontally homogenous as for perpendicular currents and the maxima do not usually occur on the centerline but as twin peaks on either side. The same behavior was found by Roberts (1979a) in his unstratified experiments. The wastefield thickness is not laterally uniform, being thicker in the center. As the current speed increases, the minimum dilution increases and the rise height and wastefield thickness decrease, as was observed for perpendicular currents.

Profiles were also obtained for the 45^{o} current experiments, but are not shown in order to save space. The profiles were found to be laterally nonuniform, with the maximum concentration occurring off the centerline and with a lateral tilt to the whole field.

QUANTITATIVE RESULTS

In this paper we concentrate on results for closely spaced jets which rapidly merge together. The parameters for these cases are: ℓ_m/ℓ_b = 0.078 and 0.20, and s/ℓ_b = 0.31 (series 3 and 4), which

correspond to $F_j \cong 5$ and 10 and $s = 5$ cm; the effect of wider port spacing and higher source momentum flux will be discussed in paper III.

Measurements of minimum dilution are plotted in the form of Eq. 8 in Figure 8. Although we are here concentrating on line plume conditions, the results for all tested source conditions are shown as they deviate little from those for line plumes. Thus, over the range tested ($0.078 < \ell_m/\ell_b < 0.5$ and $0.31 < s/\ell_b < 1.92$) the source momentum flux and port spacing do not significantly affect normalized dilution. We note that this observation contradicts the numerical results of Wright et al. (1982) for stagnant flows reproduced in Figure 2 which predict a fairly substantial effect of port spacing and momentum flux over this parameter range; the reasons for this lack of sensitivity to s/ℓ_b and ℓ_m/ℓ_b are discussed in paper III. As was found for the unstratified case by Roberts (1979a), dilution is unaffected by the current for $F \leq 0.1$ and for this case the results asymptote to:

$$\frac{S_m q N}{b^{2/3}} = 0.97 \qquad (12)$$

In comparison, Fischer, et al. (1979), Roberts (1979b), Wright, et al. (1982) predict the value of the constant to be 0.88, 0.73, and 0.96, respectively, and Wallace and Wright (1984) find experimentally a value of 0.88 for a single plume released from a slot source. The results of Fischer, et al. and Roberts implicitly assume that the plumes from the opposing sides of the diffuser have merged together to form a single plume. The present results suggest (see Figure 4a) that this will not normally be the case, and the plumes should be considered as two distinct ones under stagnant conditions. Dilution increases with current speed when $F > 0.1$ and is highest for a diffuser perpendicular to the current and lowest for one parallel. Even the parallel case, however, shows an increase in dilution with current speed and in no case is it lower than in the stagnant case. This is consistent with the findings of Roberts (1979a) for an unstratified current.

A numerical model of line plumes in stratified currents was developed by Roberts (1979b) using the experimental results for unstratified currents of Roberts (1979a). The model predicts that the

dilution for a diffuser perpendicular to the current at F = 100 is about twice that when parallel, in contrast to the unstratified case when the ratio is about four. This is very close to the observed results (Figure 8). The reason for the difference between stratified and unstratified currents lies in the relationship between rise height and dilution. In the unstratified case the wastefield always reaches the surface, whereas in the stratified case the rise height is reduced and is dependent on current speed and direction. A perpendicular current causes a lower rise height than one parallel at the same current speed, resulting in an attenuated effect of current on dilution. Analytical expressions which predict the effect of a perpendicular current on rise height and dilution in the forced entrainment regime were also given in Roberts (1979b). The relationships are his equations 18 and 17 which become, in the present notation:

$$\frac{z_t}{\ell_b} = 1.86F^{-1/6} \; ; \quad \frac{S_m q N}{b^{2/3}} = 1.08F^{1/6} \qquad (13a,b)$$

Eq. 13b underestimates the measured dilutions by 24 to 45%, and a fit to the data in the forced entrainment regime ($F \geq 10$) yields a value of the constant of about 1.9. It is useful to fit an equation over the whole region for which the current increases the dilution, however, and we obtain the following semi-empirical equation for the range $0.1 < F < 100$:

$$\frac{S_m q N}{b^{2/3}} = 2.19F^{1/6} - 0.52 \qquad (14)$$

and which is plotted on Figure 8. This equation predicts the results closely over this range of F, and thus, although Roberts' model correctly predicts the trend of the results, modifications are necessary to account for the differences in mixing mechanisms between stratified and unstratified conditions. Note that Eqs 13b and 14 predict that in the forced entrainment regime $S_m \propto u^{1/2}$ whereas in the unstratified case, when the effluent is mixed over the whole depth, $S_m \propto u$ (Roberts, 1979a). Again, these results show the lessened sensitivity of dilution to current speed in a stratified current compared to an unstratified one.

For constant discharge and oceanic stratification, Figure 8 can be considered as showing the

effect of varying current speed and direction on dilution. As F would not normally exceed 100 this figure indicates that dilution will vary by a factor of less than five times higher than that expected under stagnant conditions.

The U.S. Environmental Protection Agency usually specifies dilution in terms of its average value, S_a. Definitions of dilution have been discussed by N.H. Brooks in Isaacson et al. (1978) and, in general, average refers to the flux-averaged value. In order to compute this average, detailed knowledge of the velocity distribution across the wastefield is required, and, as we did not measure velocities, it is impossible to calculate here. Nevertheless, it is instructive to compute a spatial average dilution S_a defined as:

$$S_a = \frac{1}{c_a} \quad \text{where} \quad c_a = \frac{1}{A}\int_A c\,dA \tag{15}$$

where c_a is the spatial average concentration over the plume area A. We defined the limits of the integration in Eq. 15 as the area over which the concentration is greater than 5% of the maximum. Other limits, for example 1% or 10%, change the calculated values by less than 10%. The results are plotted in Figure 9 as the ratio of average to minimum dilution at the asymptotic dilution distance. For perpendicular and 45^o currents the ratio is about 2 ± 0.2 for $0 < F < 100$ and for parallel currents the ratio increases for $F > 1$ as the flow becomes narrower and more three-dimensional (Figure 7). In comparison, the ratios of flux-averaged to minimum dilutions for free round and line plumes range between about 1.4 and 1.8 (Fischer et al., 1979). Because we would expect velocities in the horizontal spreading layer to be correlated with c and to be highest where c is highest, Eq. 15 will yield an upper estimate of the flux-averaged dilution. The difference between flux-averaged and spatial-averaged dilutions is mostly important at low currents speeds; at higher speeds where the velocity across the layer is fairly uniform and equal to the ambient current speed, the difference will be small.

Measurements of the wastefield's geometrical properties of rise height, thickness, and height to level of minimum dilution as defined in Figure 1 are shown in Figures 10, 11, and 12. The height to the top of the wastefield and the thickness are defined by the heights where the

concentration is 5% of the maximum. Results are shown for ℓ_m/ℓ_b = 0.078 and 0.2, both with s/ℓ_b = 0.31. The first combination is the line plume condition, but none of the results for the second combination (which results from doubling the nozzle Froude number from 5 to 10) differ significantly. Larger port spacings and/or larger source momentum fluxes do cause deviations from these results, and their effects are discussed in paper III. The results for 45^o currents do not differ significantly from those for perpendicular currents, and smooth lines are drawn through the data for F > 0.1.

For zero crossflow Eq. 10 applies, and Figures 10, 11, and 12 suggest:

$$\frac{z_t}{\ell_b} = 2.5 \; ; \quad \frac{h_a}{\ell_b} = 1.8 \; ; \quad \frac{z_a}{\ell_b} = 1.7 \qquad (16a,b,c)$$

These are close to the results of Wright, et al. (1982) who found h_a/ℓ_b = 2.0 and z_a/ℓ_b = 2.0 for the line plume condition. The rise height and thickness increase slightly as the current speed is increased to F = 0.1 for reasons which can be seen from the photographs of Figures 4a and 4b. The portion of the wastefield which spreads to the left at F = 0 is completely swept downstream by even the slow current corresponding to F = 0.1. The wastefield which was previously upstream is "folded" into the downstream layer which, having to now accommodate twice the flow at F = 0, compensates by thickening slightly and rising slightly higher. The rise height and thickness remain fairly constant between F = 0.1 and 1 and thereafter decrease rapidly with increasing current speed in the forced entrainment regime. The equation suggested by Roberts (1979b) to predict rise heights in this regime (Eq. 13a) yields predictions which lie in between the observed results for z_t (the top of the wastefield) and z_a (the height of minimum dilution). This discrepancy would be expected as in the unstratified case the minimum dilution always occurs at the surface and the plume always rises to the surface, whereas in the stratified case the minimum dilution is below the wastefield top. Roberts' model equates the rise height in the stratified case to the water depth in the unstratified case and assumes the dilutions to be the same, but it is not apparent whether rise height should refer to the level of minimum dilution or the wastefield top. By modifying the constant of Eq. 13a we obtain:

$$\frac{z_t}{\ell_b} = 2.5F^{-1/6} \qquad (17)$$

which fits the data very closely over the range $1 \leq F \leq 100$. In the forced entrainment regime, the bottom of the wastefield is at the port level and so h_a and z_t are the same and Eq. 17 predicts the observed values of h_a for $F \geq 10$ (see Figure 11). The height to the level of minimum dilution also follows an $F^{-1/6}$ power law for $F >> 1$ and the results can be predicted by:

$$\frac{z_a}{\ell_b} = 1.5F^{-1/6} \qquad (18)$$

for $F \geq 5$. These power law relationships for dilution and rise height are also derived in the following paper by using different arguments.

It is sometimes suggested that numerical models of merging buoyant jets derived for perpendicular currents can be applied to other current angles by taking the component of the current perpendicular to the diffuser or the projected diffuser length, or both. We note that, although the results for dilution for 45^o currents could be reasonably predicted by taking u as the component perpendicular to the diffuser, the rise heights and thicknesses would not be as closely predicted.

EXPERIMENTAL ERRORS

Errors in the computation of dimensionless parameters presented in this paper arise from random errors in the measurement of effluent flowrate, tow speed, ambient and effluent densities, dilution, and deviation of the ambient density profiles from their assumed linear form. Considerable effort was made to minimize these errors and to ensure repeatability of the results. In all cases, the density profiles were closely linear, and the slope of the profile, and hence N, was calculated by a least squares fit to the observed data. Combining the estimated measurement errors given previously suggests a maximum error in the computation of $S_m qN/b^{2/3}$ of about 8%. We found the results to be repeatable to about 5%. Similarly, the dimensionless rise heights are expected to be

accurate to about 5%, with most of the error due to interpolation in the vertical space between the probes.

Of seemingly greater concern than measurement errors are systematic errors resulting from the low nozzle Reynolds numbers which ranged from 910 to 2600. The effect of low jet Reynolds numbers on buoyant plumes has been discussed by Isaacson, et al. (1982) and Snyder (1981). Results quoted by Snyder suggest that buoyant plume rise from vertical stacks is independent of Reynolds number for Re > 300. We observed, as did Isaacson, et al., that initially laminar plumes became turbulent soon after they entered the tank. The effect of the initial laminar portion is to reduce entrainment near to the nozzle, causing a slightly lowered final dilution and increased rise height. To quantify this effect, we performed three tests on single jets at nozzle Reynolds numbers of 456, 1073, and 1481, while keeping the ratio of the momentum to buoyancy length scales constant. The results showed no systematic Reynolds number effect, and the scatter in the rise height results from the mean value was 6%.

APPLICATIONS

As an example of the application of these results, consider the outfall of Metropolitan Seattle at West Point for which design parameters are given in Fischer, et al. (1979), table 10.1. The design average flow is 194 ft^3/s (5.49 m^3/s), the diffuser length is 600 ft (183 m), the port spacing, s, on each side of the diffuser is 6 ft (1.83 m), and the port sizes range from 4.5 to 5.75 inches (114 to 146 mm). Density stratifications at nearby Alki Point vary between 0.002 and 0.025 σ_t-units per m (Roberts, 1986), and assuming a typical nozzle size of 5 inches (127 mm) and the strongest stratification yields, when substituted into Eqs. 1 and 2: u_j = 2.17 m/s; m = 0.0651 m^3/s^2; b = 0.00765 m^3/s^3; and N = 0.0157 s^{-1}. The length scales, calculated from Eq. 4, are ℓ_m = 1.68 m and ℓ_b = 12.6 m, and the length scale ratios are ℓ_m/ℓ_b = 0.13 and s/ℓ_b = 0.15. Based on Figure 2 and the present results we would expect the behavior of the discharge to be well within the line plume regime in which the effects of source momentum and port spacing are negligible. The wastefield characteristics can then be computed from Figures 8 through 12.

Puget Sound at West Point is subject to strong, reversing tidal currents with peak speeds of about 0.50 m/s which yields $0 < F < 20$. For stagnant currents, Eqs 12 and 16 apply and for flowing currents we must use the results shown in Figures 8 through 12 or the semi-empirical Eqs. 14, 17, and 18 where applicable. In a stagnant current, for example, Eq. 12 gives $Sm = 0.97b^{2/3}/qN = 80$ and Eq. 16a gives $z_t = 2.5\ell_b = 31.5$ m; other results for currents varying over a typical tidal range are given in Table 1. As the current speed increases from zero to 0.50 m/s, the minimum dilution increases from 80 to 245, the height to the top of the wastefield varies from 31.5 m to 19.8 m, the height of minimum dilution varies from 21.4 m to 11.8 m, and the thickness varies from 22.7 to 19.8 m. Note that the maximum rise height occurs at a current speed of 10 cm/s, but as the water depth is about 70 m over the diffuser the wastefield is always quite deeply submerged. This wide variation in rise height will result in "injection" of the effluent into different layers and a very thick average wastefield. Similar wide variations in predicted dilutions and rise heights for outfalls operating under the influence of strong tidal currents were reported for San Francisco by Roberts (1980).

SUMMARY AND CONCLUSIONS

A series of experiments to study the dilution and formation of wastefields caused by sewage discharged from submerged outfalls with multi-port diffusers into stratified currents was conducted. The receiving water is linearly density-stratified and flows at an arbitrary speed and direction relative to the diffuser. The experiments were conducted in a large stratified towing tank with a model multiport diffuser covering a range of parameters typical of modern ocean outfalls. In this paper we describe the overall experimental program and present results for conditions such that the effect of port spacing and jet momentum flux are negligible. These are the "line plume" results in which the dominant source parameter is the buoyancy flux per unit length. We present "gross results" of interest to outfall designers: wastefield thickness, rise height, and dilution. Details of the mixing process and the effects of higher source momentum fluxes and larger port spacings are discussed in two subsequent papers.

Experiments were conducted for Froude numbers, $F = u^3/b$, of 0, 0.1, 1, 10, and 100 with diffusers perpendicular, at 45^o, and parallel to the current. Photographs of flow fields are shown in Figures 4 and 6, and in general they show that the rise height and thickness decrease as the current speed increases. For a perpendicular current, even a very slow speed ($F \geq 0.1$) will cause the upstream wedge to be swept downstream. Effluent concentrations, and hence dilutions, were measured with a rake of sampling probes towed downstream of the diffuser, and typical concentration profiles for perpendicular and parallel diffusers are shown in Figures 5 and 7. The concentration profiles for perpendicular diffusers show little horizontal structure as the individual plumes rapidly merge together, but the profiles for parallel diffusers are more complex with twin peaks lying away from the diffuser centerline.

Quantitative results for minimum and average dilution, height to top of wastefield, height to level of maximum concentration, and wastefield thickness are shown in Figures 8 through 12. Because the results for dilution show little dependency on the port spacing or source momentum flux over the range tested, all of the dilution results are shown in Figure 8. The rise height and thickness are dependent on these parameters, however, and Figures 10 through 12 show only those results for the line plume condition.

Dilution is unaffected by the current for $F < 0.1$, and thereafter increases with current speed. For $F > 0.1$ a perpendicular diffuser obtains a higher dilution than one parallel, although dilutions in flowing currents are always higher than in the stagnant case. The same observations were made by Roberts (1979a) for diffusers discharging into unstratified currents, although the difference between perpendicular and parallel currents is less in the stratified case compared to the unstratified case. The reason for this lessened effect is that in the unstratified case the wastefield always reaches the surface, regardless of current direction. In the stratified case, however, the rise height depends on current direction (see Figures 10 and 12), with perpendicular currents resulting in lower rise heights than parallel. As dilution is related to rise height, the effect of stratification is to attenuate the effect of current direction. Spatial average dilutions are about twice the minimum dilutions and provide an upper limit to the true flux-averaged dilutions.

The experimental results are compared to the numerical predictions of Roberts (1979b) which were based on an extrapolation of his unstratified experiments to the stratified case. This model predicts that, at F = 100, dilution for a perpendicular current is twice that when parallel, and for strong perpendicular currents the rise height is proportional to $F^{-1/6}$ and dilution is proportional to $F^{1/6}$ (Eqs. 13a,b). Although the measured data do follow these trends and power laws, direct application of this model results in an underestimation of the measured dilutions. Modification of the coefficients in Roberts' equations results in Eqs. 14, 17, and 18, for perpendicular currents. These equations describe the results closely over their specified ranges, as shown in Figures 8 through 12. For stagnant currents, dilution and rise height can be calculated from Eqs. 12 and 16.

An applications example is given for the discharge from Metropolitan Seattle at West Point, which shows the dilution, rise height, and wastefield thickness to vary considerably over a tidal cycle (Table 1). This variation in rise heights results in "injection" of the wastefield into layers of different heights through the tidal cycle and a thick average layer.

It is remarkable that the results for dilution are so independent of port spacings and source momentum flux over the range tested and are so dependent on the buoyancy flux per unit length. The results are a strong confirmation of the value of the "line plume" approximation for ocean outfalls first used by Brooks and Koh (1965) and further investigated by Roberts (1979a) and others.

ACKNOWLEDGMENTS

The assistance of Paul Bookman, Northrop Services, Inc., in constructing the multiport diffuser and associated apparatus is gratefully acknowledged as is the untiring support provided by Leonard Marsh and Roy Carlson, Northrop Services, Inc., and of Bob Lawson, EPA, during the conduct of the experiments. We also wish to thank Mike Shipman, Northrop Services, Inc., for his technical support in developing computer programs to reduce and plot the data collected. We appreciate the financial support of the U.S Environmental Protection Agency, Pacific Division, Newport, Oregon.

APPENDIX I - REFERENCES

Brooks, N.H. (1980). "Synthesis of Stratified Flow Phenomena for Design of Ocean Outfalls," Second Intl. Symp. on Strat. Flows, Trondheim, Norway, 24-27 June, pp. 809-831.

Brooks, N.H., and Koh, R.C.Y. (1965). "Discharge of Sewage Effluent from a Line Source into a Stratified Ocean," XI Congress, Intl. Assoc. for Hydraul. Res., Paper No. 2.19, Leningrad.

Cederwall, K. (1971). "Buoyant Slot Jets into Stagnant or Flowing Environments." W.M. Keck Laboratory of Hydraulics and Water Resources, California Institute of Technology, Rept. No. KH-R-25.

Fischer, H.B. et al. (1979). "Mixing in Inland and Coastal Waters," Academic Press.

Isaacson, M.S., Koh, R.C.Y., and Brooks, N.H. (1978). "Sectional Hydraulic Modeling Study of Plume Behavior: San Francisco Southwest Ocean Outfall Project," W.M. Keck Laboratory of Hydraulics and Water Resources, California Institute of Technology, Tech. Memo. 78-2.

Isaacson, M.S., Koh, R.C.Y., and Brooks, N.H. (1983). "Plume Dilution for Diffusers with Multiple Risers," J. Hydraulic Engrg, ASCE, Vol. 109., No. 2, pp. 199-220.

Koh, R.C.Y., and Fan, L.N. (1970). "Mathematical Models for the Prediction of Temperature Distributions Resulting From the Discharge of Heated Water Into Large Bodies of Water," U.S. Environmental Protection Agency Water Pollution Control Research Series, Rep. No. 16130DW010/70.

Muellenhoff, W.P., et al. (1985). "Initial Mixing Characteristics of Municipal Ocean Discharges," U.S, Environmental Protection Agency, EPA/600/3-85/073a.

Roberts, P.J.W. (1979a). "Line Plume and Ocean Outfall Dispersion," J. Hydraulics Div., ASCE, Vol. 105, No. HY4, pp. 313-330.

Roberts, P.J.W. (1979b). "A Mathematical Model of Initial Dilution for Deepwater Ocean Outfalls," Proc. of Specialty Conf. on Conservation and Utilization of Water and Energy Resources, San Francisco, Aug 8-11, pp. 218-225.

Roberts, P.J.W. (1980). "Ocean Outfall Dilution: Effects of Currents," J. Hydraulics Div., ASCE, Vol. 106, No. HY5, pp. 769-782.

Roberts, P.J.W. (1986). "Engineering of Ocean Outfalls," The Role of the Oceans as a Waste Disposal Option, G. Kullenberg, ed., NATO ASI Series C, Vol. 172, pp 73-109.

Snyder, W.H. (1981). "Guideline for Fluid Modeling of Atmospheric Diffusion," Rept. No. EPA-600/8/81/009, U.S. Environmental Protection Agency, Res. Triangle Park, NC.

Thompson, R.S., and Snyder, W.H. (1976). "EPA Fluid Modeling Facility," Proc. Conf. on Environmental Modeling and Simulation, Cincinnati, Ohio. U.S. Environmental Protection Agency Rept. No. EPA-600/9-76-016.

Wallace, R.B., and Wright, S.J. (1984). "Spreading Layer of Two-Dimensional Buoyant Jet." J. Hydraulic Eng., ASCE, Vol. 110, No. 6, pp. 813-828.

Wright, S.J., et al. (1982). "Outfall Diffuser Behavior in Stratified Ambient Fluid," J. Hydraulics Div., ASCE, Vol. 108, No HY4, pp. 483-501.

APPENDIX II - Notation

The following symbols are used in this paper:

A = plume cross-sectional area;

b = total source buoyancy flux per unit diffuser length, Eq. 1;

c = ratio of local dye concentration to effluent dye concentration, $1/S$;

c_a = spatial average dilution;

$C_1 ... C_4$ = experimental constants;

d = port diameter, Figure 1;

F = Froude number, u^3/b;

F_j = Nozzle Froude number, $u_j/\sqrt{g_o' d}$;

g = acceleration due to gravity;

g_o' = modified acceleration due to gravity, $g(\rho_a - \rho_o)/\rho_a$;

h_a = wastefield thickness at x_a, Figure 1;

ℓ_q, ℓ_b, ℓ_m = length scales, Eq. 4;

L = diffuser length;

m = total source momentum flux per unit diffuser length, Eq. 1;

N = buoyancy frequency, Eq. 3;

q = discharge per unit diffuser length, Eq. 1;

Q = total discharge;

Re = nozzle Reynolds number, $u_j d/\nu$;

s = port spacing, Figure 1;

S = dilution;

S_a = spatial average dilution;

S_m = minimum dilution;

u = ambient current speed;

u_j = jet exit velocity

x, y, z = coordinates, Figure 1

x_a = distance from diffuser at which minimum dilution is reached;

z_a = height to level of minimum dilution at x_a, Figure 1;

z_t = height to top of wastefield at x_a, Figure 1;

θ = angle of ambient current to diffuser, Figure 1;

ν = kinematic viscosity;

ρ = ambient density;

ρ_a = ambient density at the level of the ports;

ρ_o = effluent density.

APPENDIX III - Summary of Experimental Parameters, Series 3 and 4.

Test no.	Current direction	Current speed	Port spacing	Discharge per port	Modified acceleration due to gravity	Sample distance	Buoyancy frequency	Height to top of wastefield	Wastefield thickness	Height to minimum dilution	Minimum dilution	Average dilution	Reynolds number
		u	s	Q_j	g_o'	x	N	z_t	h_a	z_a	S_m	S_a	Re
	(degrees)	(cm/s)	(cm)	(cm^3/s)	(cm/s^2)	(cm)	(s^{-1})	(cm)	(cm)	(cm)			
(1)	(2)	(3)	(4)	(5)	(6)	(7)	(8)	(9)	(10)	(11)	(12)	(13)	(14)
3-11-1	90	0	5	2.37	111.9	52	0.299	43	30	26	69.7	154.8	941
3-11-2	90	0	5	2.42	114.4	28	0.299	46	33	38	76.7	152.5	959
3-11-3*	90	0	5	2.35	114.4	52	0.299	44	31	28	76.1	193.0	930
3-11-4*	90	0	5	2.42	114.4	102	0.299	43	30	28	75.7	151.1	958
3-12-1*	90	2.26	5	2.38	115.6	102	0.303	-	-	-	80.8	151.3	946
3-12-2	90	2.30	5	2.33	114.0	102	0.299	46	34	31	76.0	134.0	926
3-13-1	90	4.82	5	2.33	114.1	152	0.306	40	35	24	143.6	264.2	926
3-13-2	90	4.84	5	2.42	112.6	152	0.301	42	34	27	129.6	243.2	956
3-13-3	90	4.80	5	2.47	112.6	77	0.301	38	34	19	114.9	242.3	981
3-13-4*	90	4.81	5	2.43	112.3	40	0.301	36	30	19	76.3	190.0	966
3-13-5	90	4.80	5	2.37	114.3	302	0.301	-	-	33	132.5	246.8	939
3-14-1	90	10.30	5	2.38	111.4	152	0.293	-	-	-	-	-	946
3-14-2*	90	10.45	5	2.33	116.3	202	0.305	28	28	12	188.5	381.5	926
3-14-3	90	10.3	5	2.37	114.3	602	0.301	27	27	16	200.8	429.0	941
3-15-1	90	22.06	5	2.37	111.9	202	0.293	16	16	6	230.4	480.0	941
3-15-2	90	22.04	5	2.38	117.7	602	0.290	21	21	12	337.7	650.4	946
3-15-3	90	22.03	5	2.37	117.7	202	0.290	19	19	6	233.6	542.1	941
3-15-4*	90	22.26	5	2.33	117.7	102	0.290	-	-	-	168.0	-	926
3-15-5*	90	22.0	5	2.38	116.5	802	0.301	20	20	12	329.9	705.0	947
3-22-1	0	2.30	5	2.37	114.0	133	0.299	45	32	30	75.4	154.1	936
3-23-1*	0	4.78	5	2.32	114.1	183	0.306	43	35	34	76.2	211.9	921
3-23-2	0	4.80	5	2.35	115.3	333	0.296	45	37	29	88.0	203.2	931
3-23-3	0	4.78	5	2.37	115.3	183	0.296	45	35	30	90.6	195.3	936
3-23-4	0	4.73	5	2.33	115.3	108	0.296	47	37	33	74.1	163.4	926
3-24-1*	0	10.55	5	2.37	116.3	233	0.298	39	18	31	107.0	244.4	941
3-24-2	0	10.4	5	2.43	119.6	433	0.295	42	31	34	124.4	332.1	964
3-24-3	0	10.40	5	2.33	119.6	133	0.295	-	-	31	101.5	281.3	924
3-25-1	0	22.25	5	2.38	116.3	233	0.305	35	27	18	100.7	305.5	946
3-25-2	0	22.20	5	2.42	118.6	833	0.295	42	25	33	201.3	528.6	957
3-25-3*	0	22.20	5	2.33	118.6	433	0.295	45	23	33	178.1	451.0	928
3-25-4*	0	22.2	5	2.48	117.6	833	0.301	35	30	24	167.6	-	988
3-32-1*	45	2.30	5	2.32	114.0	123	0.299	43	32	30	70.0	142.6	916
3-33-1*	45	4.80	5	2.30	114.1	173	0.306	41	-	31	97.7	-	911
3-34-1	45	10.49	5	2.33	116.3	223	0.298	28	26	16	165.2	352.4	926
3-35-1*	45	22.10	5	2.33	111.9	223	0.293	16	16	4	195.1	469.2	926
3-35-2*	45	22.30	5	2.40	119.6	623	0.295	19	19	10	279.2	555.6	951
4-11-1*	90	0	5	3.62	68.1	52	0.298	39	28	26	49.0	98.7	1431
4-13-1*	90	4.60	5	3.52	67.2	152	0.298	38	35	27	77.2	136.2	1396
4-14-1*	90	10.0	5	3.60	67.4	402	0.288	27	26	16	125.6	236.8	1426
4-14-2	90	10.00	5	3.55	66.6	202	0.288	31	31	12	117.0	229.3	1406
4-14-3	90	10.00	5	3.67	66.6	102	0.288	26	26	26	81.2	214.5	1451
4-15-1*	90	21.70	5	3.60	67.2	202	0.297	17	17	5	145.5	345.9	1426
4-15-2*	90	22.0	5	3.78	74.4	202	0.313	17	17	10	219.0	392.8	1495
4-23-1	0	4.58	5	3.58	67.1	183	0.298	39	32	30	58.5	125.0	1421
4-24-1*	0	10.03	5	3.50	65.0	233	0.296	35	23	28	62.4	146.0	1386
4-24-2*	0	10.3	5	3.73	76.9	433	0.326	37	32	28	80.7	-	1480
4-25-1	0	21.80	5	3.58	67.2	233	0.297	33	25	14	59.6	185.7	1421
4-25-2*	0	22.00	5	3.73	74.4	633	0.313	34	20	25	104.2	354.3	1481
4-25-3	0	22.2	5	3.83	76.9	833	0.326	32	27	24	99.4	-	1518

Table 1. Results for Applications Example for a Perpendicular Current: Metropolitan Seattle Outfall at West Point

Current speed, u (cm/s) (1)	Froude number, $F = \frac{u^3}{b}$ (2)	Normalized dilution, $\frac{S_m q N}{b^{2/3}}$ (3)	Minimum dilution, S_m (4)	Height to top of wastefield, z_t (m) (5)	Height to level of minimum dilution, z_a (m) (6)	Wastefield thickness, h_a (m) (7)
0	0	0.97	80	31.5	21.4	22.7
10	0.13	1.04	86	34.5	23.8	26.6
20	1.05	1.69	139	31.2	21.5	26.1
30	3.53	2.18	180	25.6	15.6	23.8
40	8.37	2.60	214	22.1	13.0	22.1
50	16.3	2.97	245	19.8	11.8	19.8

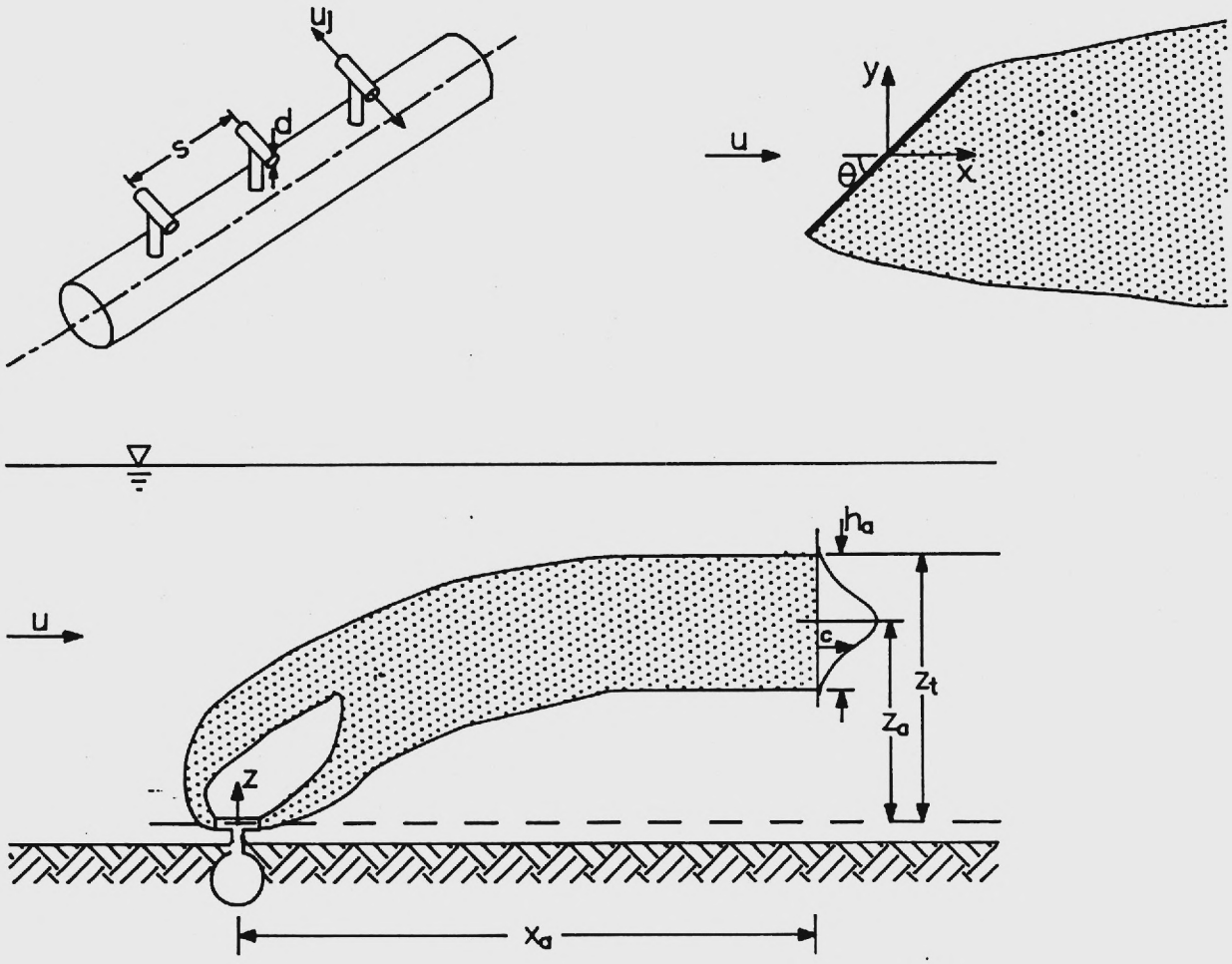

Figure 1. Definition Diagram

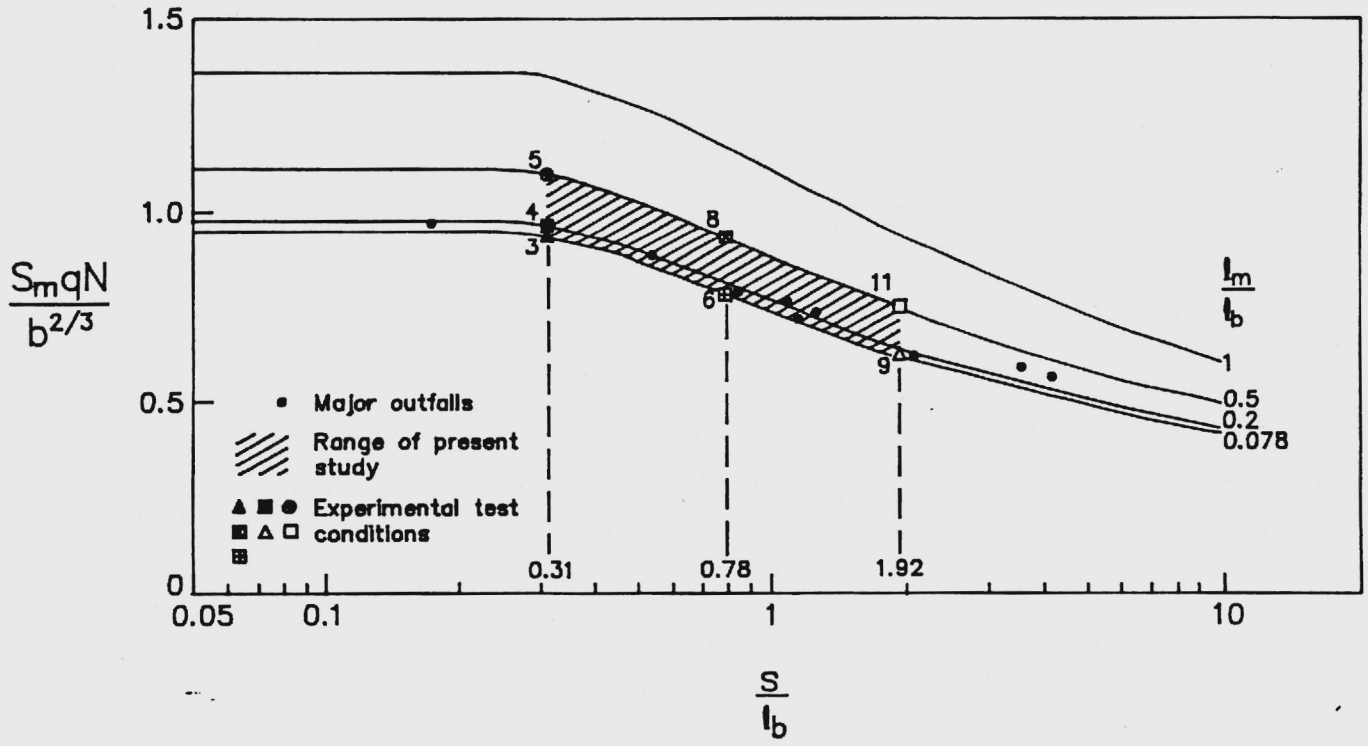

Figure 2. Numerical Predictions of Dilution in a Stagnant Ambient, from Wright et al. (1982). Shows Range of Present Study, Data Symbols, and Experimental Series Numbers

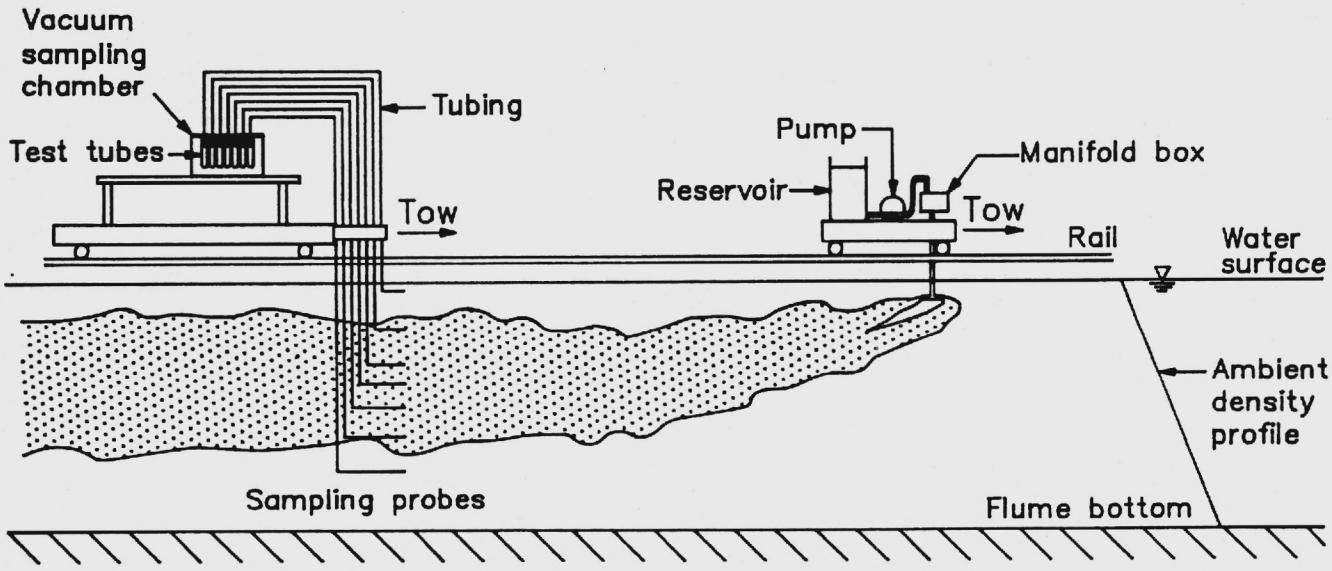

Figure 3. Experimental Configuration

a) F = 0

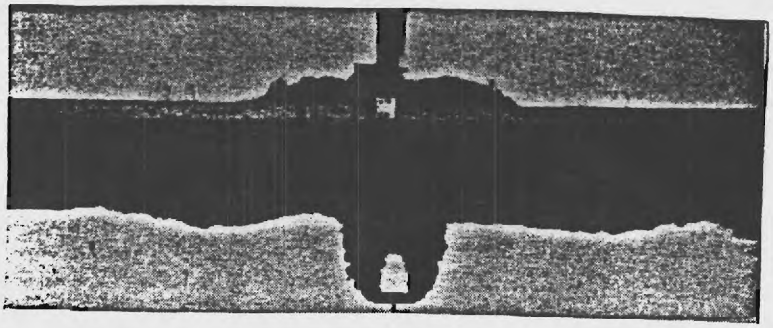

b) F = 0.1

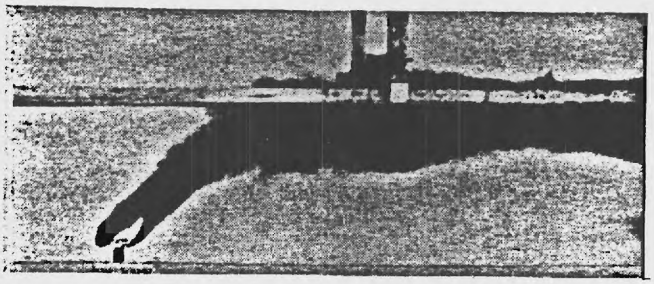

c) F = 1

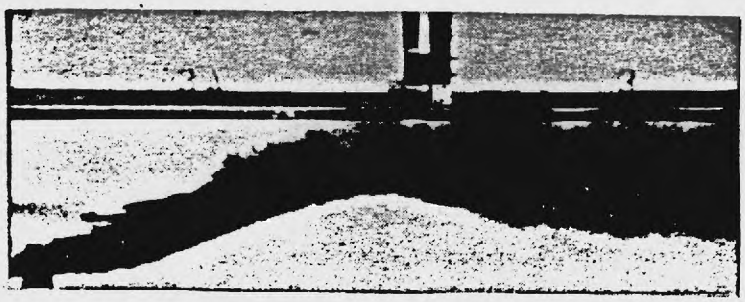

d) F = 10

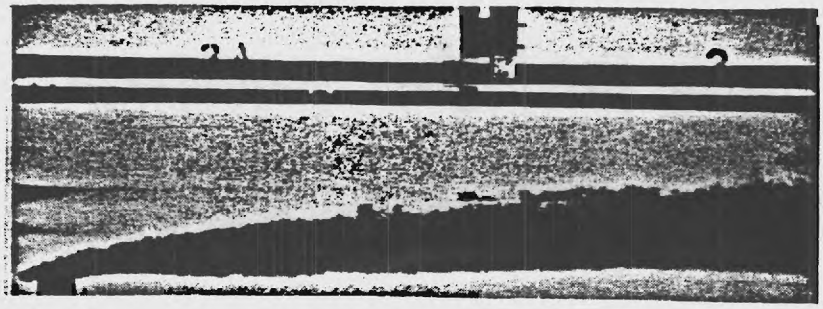

e) F = 100

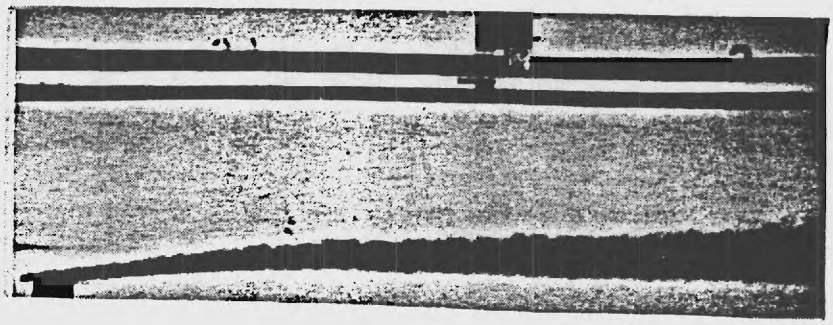

Figure 4. Photographs of Line Plume Conditions (series 3) in Perpendicular Currents

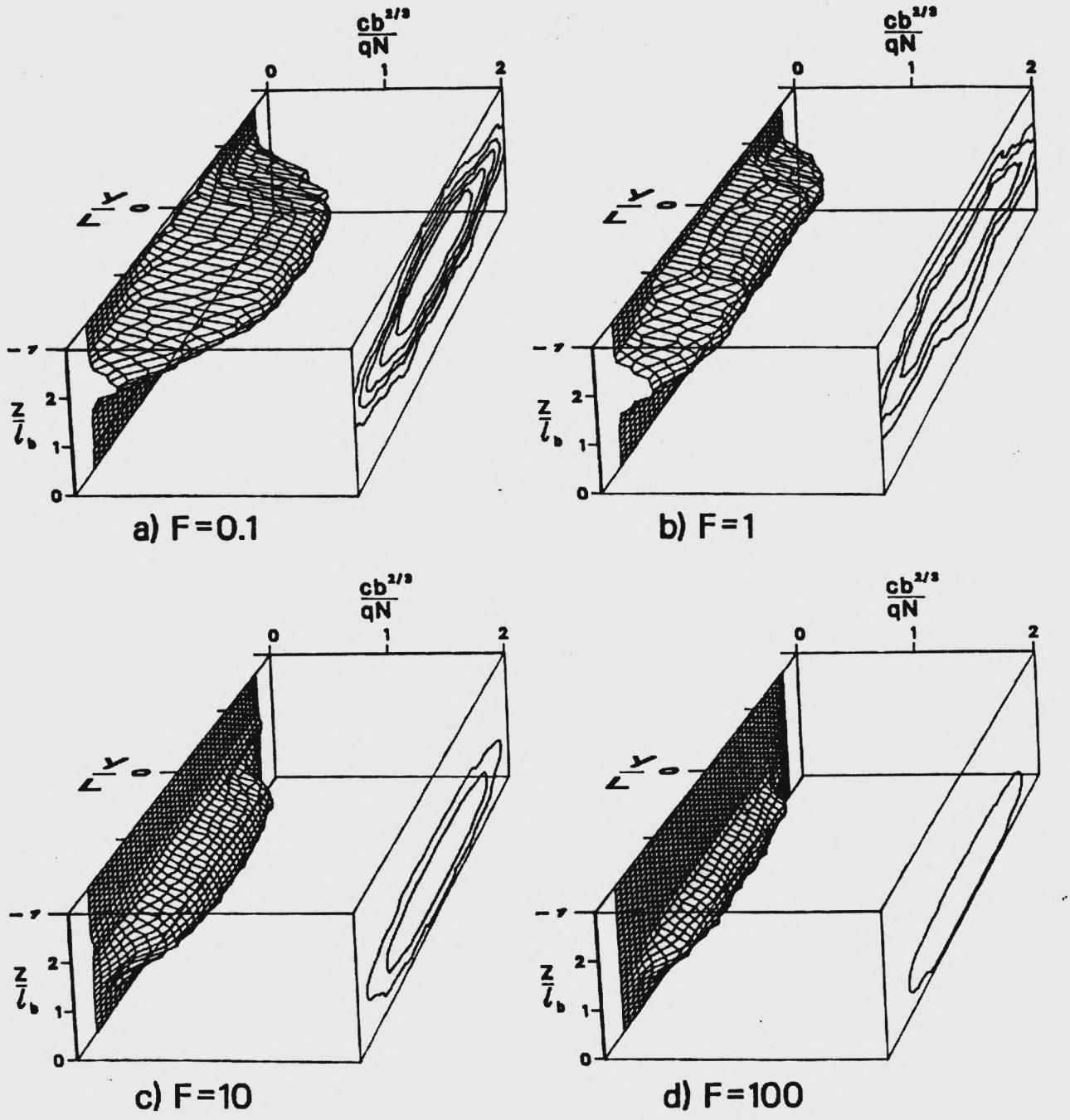

Figure 5. Normalized Concentration Profiles for Line Plume Conditions (series 3) in Perpendicular Currents

a) F = 0.1

b) F = 1

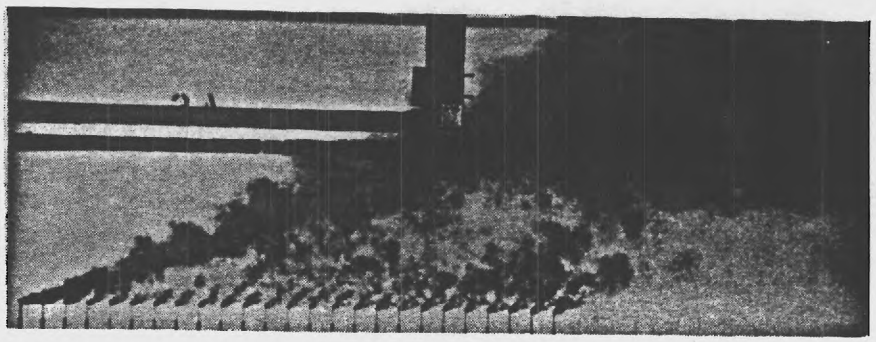

c) F = 10

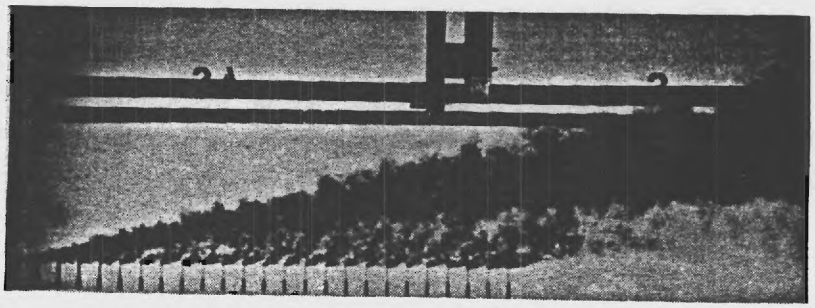

d) F = 100

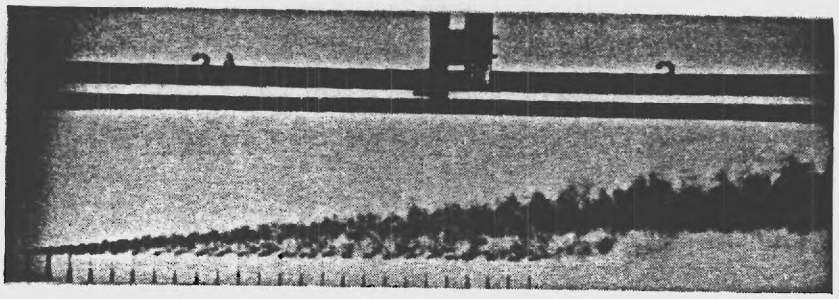

Figure 6. Photographs of Line Plume Conditions (Series 3) in Parallel Currents

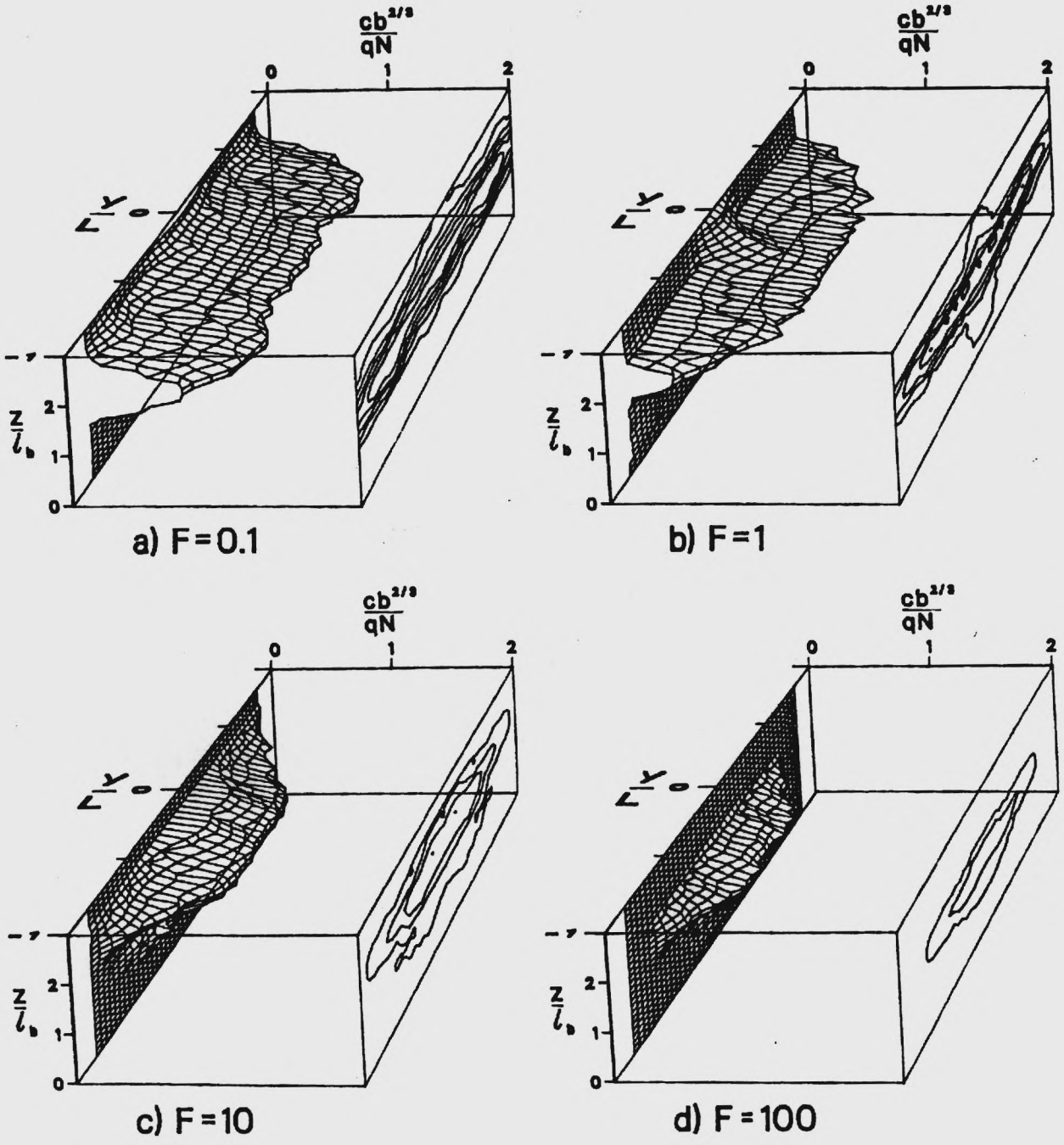

Figure 7. Normalized Concentration Profiles for Line Plume Conditions (Series 3) in Parallel Currents

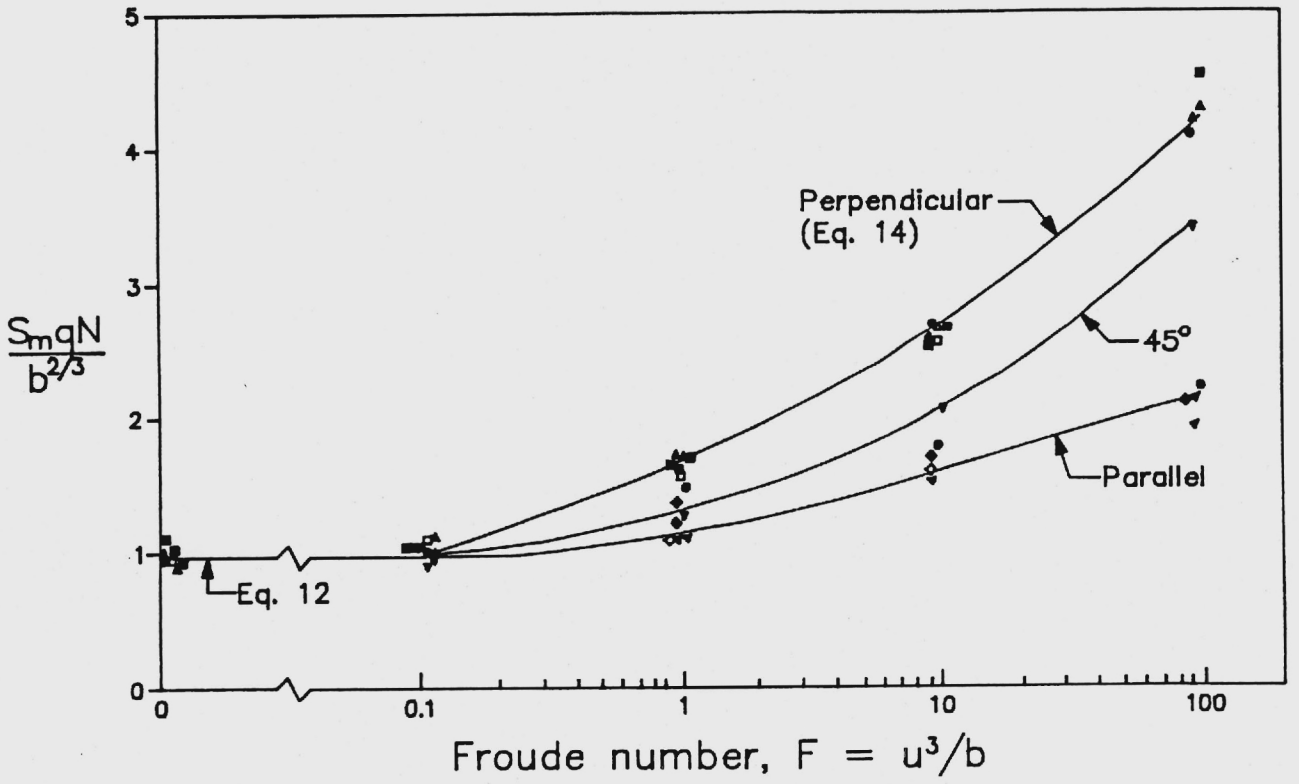

Figure 8. Asymptotic Minimum Dilutions for all Experiments. See Figure 2 for Symbol Definitions

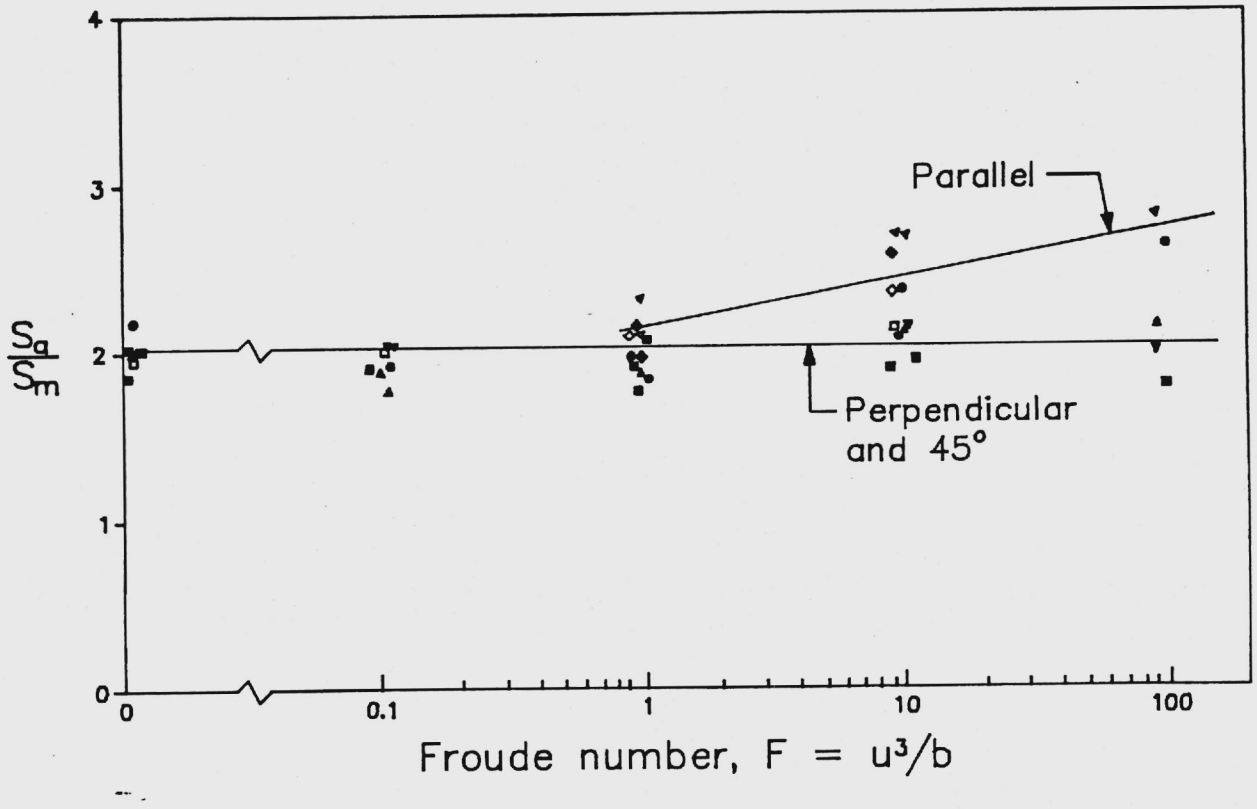

Figure 9. Spatial Average Dilutions for all Experiments. See Figure 2 for Symbol Definitions

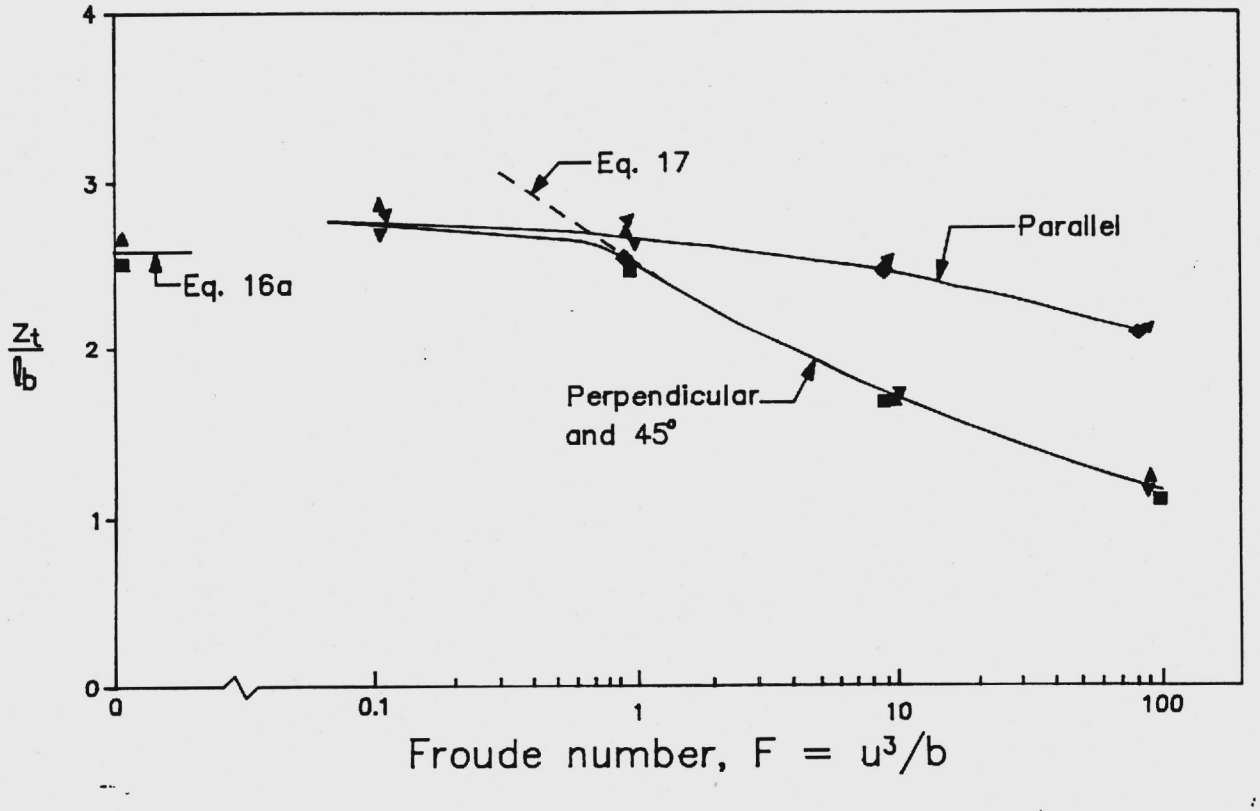

Figure 10. Height to Top of Established Wastefield for Line Plume Conditions (Series 3 and 4)

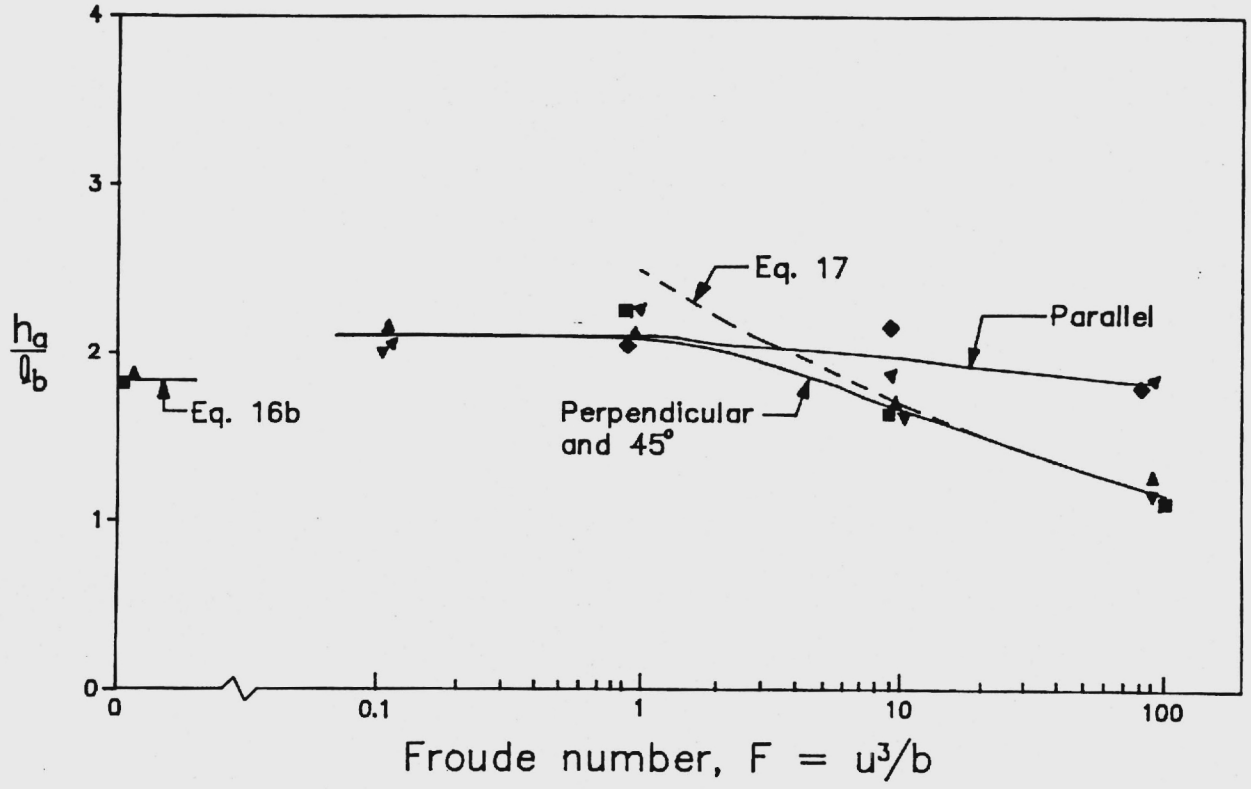

Figure 11. Thickness of Established Wastefield for Line Plume Conditions (Series 3 and 4)

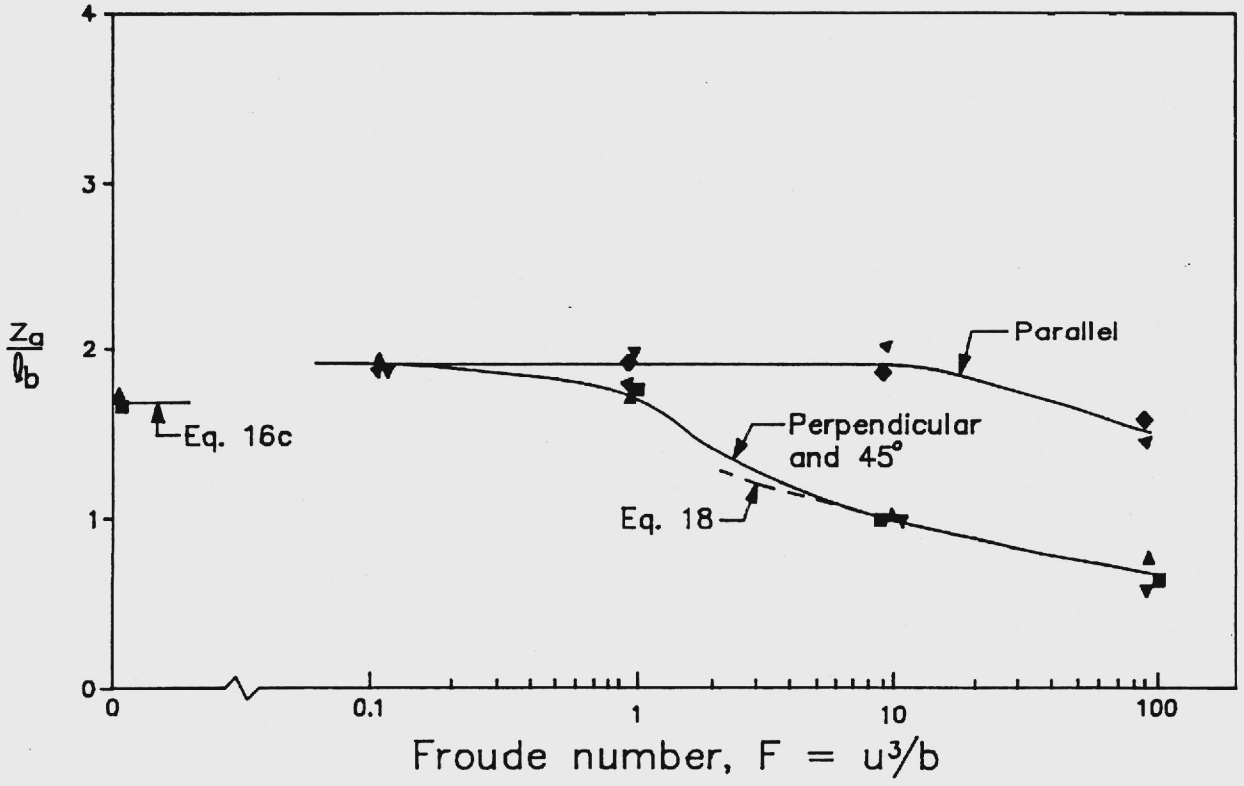

Figure 12. Height to Level of Minimum Dilution for Line Plume Conditions (Series 3 and 4)